

**Sedimentation in High-Arctic Lake, Linnévatnet, Svalbard:  
A Modern Process Study Using Sediment Traps**

An Honors Thesis  
Presented to  
The Faculty of the Department of Geology  
Bates College

in partial fulfillment of the requirements for the  
Degree of Bachelor of Science

by  
Megan Sarah Arnold

Lewiston, Maine  
April 6, 2009

**NOTE TO READER:**

The valley and many geographic features in and around the valley are named after the Swedish taxonomist, Carl von Linné. In this study I refer to these features by their Norwegian names, which combine Linné with the Norwegian noun. Thus, “Lake Linné” is Linnévatnet, “Cape Linné” is Kapp Linné, “Valley Linné” is Linnédalen, “Glacier Linné” is Linnébreen, and “River Linné” is Linnéelva.

## ABSTRACT

Linnévatnet is a High Arctic glacier-fed lake in Svalbard in which past climatic characteristics are recorded in laminated lake sediments that likely span the past 9,000 years. The laminae are comprised of annual terrigenous couplets consisting of distinct coarse summer and fine winter layers. Previous studies in similar proglacial lakes throughout the Arctic and alpine regions have determined that varves of this type may record an archive of past weather and climatic influences in the catchment area.

Sedimentation in Linnévatnet has been studied since 2003 using sediment traps and instruments deployed yearly and seasonally. The traps were deployed at five locations in the lake proximal and distal to the major inlet. Depending on the water depth at each location two to five traps were attached mooring lines.

In the sediment traps, the summer melt season sediment is represented by distinct coarse sediment events reflecting meltwater pulses, the timing of which are constrained by time lapse photography and loggers on the moorings. The first and coarsest (26 microns) grained sediment pulse was deposited on July 4 – 5, 2008, coinciding with peak snowmelt discharge. Subsequent events appear as finer (12 – 14 microns) graded laminae in the traps and are associated with similar high discharge events in mid-July. The fine winter layer (5 – 8 microns) coarsens slightly upward and reflects quiet winter sedimentation.

Sediment stratigraphy and grain size trends in 2007 – 2008 were compiled with sediment trap analyses back to 2003 to form a composite record to compare with lake bottom deposition as reflected in sediment cores recovered adjacent to the moorings. Thin sections of laminated sediments from the cores display complex summer layer stratigraphy with multiple sedimentation units as seen in the sediment traps. Correlation between distinct units in the thin sections and sediment traps was attempted to evaluate climatic and environmental conditions responsible deposition of recent varved sediments.

## ACKNOWLEDGMENTS

First, I want to express the greatest thanks to the Hughes Summer Research committee for funding my field work in Svalbard. Also, the project was funded by the National Science Foundation Office of Polar Programs.

Most importantly, to Mike Retelle, thank you! You are the inspiration that brought me to geology and to the Arctic. I have caught the most serious “Arctic Bug” and I don’t think it will ever go away. For your support, encouragement, confidence in me, funny stories, YouTube videos, Flying Fyooogie’s, visits to Coram, and everything else that makes you the most wonderful adviser in the whole wide world – Thank you!

Al Werner, thank you for your support over the past two years of working on Svalbard projects, I thoroughly enjoy your e-mails and interpretations. Steve Roof, I wish you could have been at Linné with us this summer, thank you for your support from a distance! To all of the Svalbard REUers, the field season was so enjoyable because of you guys, thank you for the team effort to get the projects done! And to Maya, my wonderful Polarbrakken roommate, for making sure I didn’t go out into the field when I was too tired.

Mama Janet Arnold, you deserve the upmost thanks for your patience through late night panic phone calls and editing thesis chapters. Dad, thanks for working the night shift so I could call on my way home from the lab. Catherine, your support and enthusiasm means the world to me!

As for the Batesies, Anne Mueller you are my guardian angel. Thank you for being there to see me through the hard times and to distract me when I needed it most. Thank you for working in the lab with me again, Hail the Sonicating Queen! Keegan Runnals, your assistance in the lab helped me out so very much, you are going to make a wonderful sediment geologist! Dana Oster, the other half of our unit, thank you for letting me live with you over February break, for hosting Desperate Housewives night, and for making working in a computer lab tolerable, for more reasons than the obvious!

To the Geology Department of Bates College, thank you for the four years of support and the past year of patience. To Geology class of 2009: Dana, Emily, Chris, Simon, Maura, and Mike, thanks for listening to all of my presentations about mud, and the Troll.

To my friends at Bates and home, thanks for the phone calls, the interest, the support, and the enthusiasm. Without any of you, this would not have worked out so well!



## TABLE OF CONTENTS

Note to Reader	ii
Abstract	iii
Acknowledgements	iv
Table of Contents	v
Table of Figures	vii
Table of Tables	ix
<b>1. Introduction</b>	<b>1</b>
1.1 Purpose Overview	2
1.2 Study Area	3
<i>Bathymetry</i>	9
<i>Bedrock</i>	12
1.3 Climate and Climate Change of the Arctic	14
<i>The Atmospheric Circulation Patterns</i>	14
<i>Climate Change in the Arctic</i>	17
<i>Climate of Svalbard</i>	21
1.4 Arctic Hydrology	23
<i>Snow</i>	23
<i>Snowmelt</i>	23
<i>Permafrost</i>	24
<i>Glacier Melt</i>	24
1.5 Glacial History of Svalbard	25
<i>Last Glacial Maximum</i>	26
<i>Deglaciation of Linnédalen</i>	28
<i>Holocene Glacial Fluctuations of Linnédalen</i>	28
1.6 Lacustrine Sediments	30
<i>Sediment Sources for Linnévatnet</i>	30
<i>Lake Stratification</i>	32
<i>Lake Inflow</i>	32
<i>Flow Dynamics</i>	34
<i>Sediment Deposition Characteristics</i>	37
1.7 Sediment Traps	37
1.8 Previous Work	41
<b>2. Methods</b>	<b>42</b>
2.1 Field Methods	43
<i>Mooring and Sediment Trap Design</i>	43
<i>Sediment Trap Collection</i>	49
<i>Sediment Core Collection</i>	51
<i>Weather and Environmental Data</i>	51
2.2 Laboratory Methods	59
<i>Splitting the Samples</i>	59
<i>Visual Stratigraphy</i>	61
<i>Sediment Flux &amp; Equivalent Thickness</i>	63

<i>Grain Size Analysis</i>	64
<i>Thin Section Preparation</i>	67
<b>3. Results</b>	<b>71</b>
3.1 Visual Stratigraphy	72
<i>Trap Description</i>	72
<i>Digital &amp; X-Ray Images</i>	72
<i>Core &amp; Thin Section Description</i>	72
3.2 Sediment Flux and Equivalent Thickness	76
3.3 Grain Size Analysis	79
<i>Mooring C: Year Long</i>	79
<i>Mooring C: Spring</i>	81
<i>Mooring D</i>	83
<i>Mooring E</i>	85
<i>Mooring F</i>	87
<i>Mooring G</i>	89
3.4 Weather and Environmental Data in Linnédalen	91
<i>Air Temperature</i>	91
<i>Precipitation</i>	91
<i>Solar Radiation</i>	94
<i>Snow Tree</i>	98
<i>Stream Temperature</i>	100
<i>Intervalometer</i>	102
<i>Mooring C Temperature Loggers</i>	104
<i>Mooring C Spring Turbidity</i>	106
<b>4. Discussion</b>	<b>108</b>
4.1 Interpretations of Grain Size Analysis	109
<i>Fall Event</i>	109
<i>First Spring Sediment Event</i>	110
<i>Minor Events</i>	117
<i>Second Major Event</i>	117
4.2 Sediment Flux, 2007 – 2008	122
4.3 Comparison of Sediment from Previous Years	124
4.4 Comparison of Weather from 2004 – 2008	127
4.5 Comparison of Lake Bottom Deposition from 2004 – 2008	131
<b>5. Conclusions</b>	<b>135</b>
<b>6. References</b>	<b>139</b>
<b>7. Appendices</b>	<b>142</b>

## TABLE OF FIGURES

1.1	Map of the Arctic Circle.	5
1.2	Nasa Landsat image of Svalbard.	6
1.3	Map of study site.	7
1.4	Permafrost thickness of study area.	8
1.5	Bathymetric map of Linnévatnet.	10
1.6	Map of study area noting sources of inflow.	11
1.7	Bedrock map of study area.	13
1.8	Plot of AO and NAO.	16
1.9	Effects of AO phases.	16
1.10	Annual mean surface temperature anomaly plot.	19
1.11	Extended AO index plot.	20
1.12	Temperature and precipitation plot for Longyearbyen.	22
1.13	LGM extent of Barents Sea Ice Sheet.	27
1.14	Oblique aerial photograph of study area.	29
1.15	Sediment sources for Linnévatnet.	31
1.16	Thermal lake stratification diagram.	33
1.17	Inflow density currents diagram.	33
1.18	Fine grained sediment distribution in a glacier-fed lake diagram.	35
1.19	Underflow or turbidity current deposition in a glacier-fed lake diagram.	35
1.20	Sediment distribution and sediment isopach diagrams.	36
1.21	Sediment trap models.	39
1.22	Sediment trap model used in the study.	40
2.1	Bathymetric map of Linnévatnet with mooring locations.	45
2.2	Diagram of a mooring line.	46
2.3	Images of two different sediment traps.	48
2.4	Illustration of mooring collection.	50
2.5	Map of instrument locations.	54
2.6	Photograph of the Onset HOBO weather station.	55
2.7	Photographs of the intervalometer.	56
2.8	Photograph of the plume camera and an image the plume camera recorded.	57
2.9	Photograph of the snow tree.	58
2.10	Photographs of splitting device.	60
2.11	Photographs of sample splitting.	60
2.12	Photograph of split sample.	62
2.13	Diagram of sub-sample dimensions.	65
2.14	Photograph of Beckman Coulter LS 13 320.	66
2.15	Photographs depicting thin section liquid nitrogen submersion	70
2.16	Photographs depicting epoxy impregnation.	70
3.1	Digital and X-ray imagery of traps C4 and D4.	73
3.2	Digital image of core C2.	74
3.3	Digital scan of thin section from core C2.	75
3.4	Plot of sediment flux for traps in 2007 – 2008.	78

3.5 Mooring C, Year-Long grain size analysis.	80
3.6 Mooring C, Spring grain size analysis.	82
3.7 Mooring D grain size analysis.	84
3.8 Mooring E grain size analysis.	86
3.9 Mooring F grain size analysis.	88
3.10 Mooring G grain size analysis.	90
3.11 Air temperature and precipitation plot.	93
3.12 Solar radiation plot.	95
3.13 Maximum solar radiation, temperature, and precipitation plot.	96
3.14 Snow tree plot.	99
3.15 Stream temperature plot.	101
3.16 The intervalometer plot.	103
3.17 Mooring C logger temperatures plot.	105
3.18 Troll turbidity and temperature plot.	107
4.1 Fall sediment event.	112
4.2 1 <sup>st</sup> Spring sediment event.	113
4.3 Plume camera images for 1 <sup>st</sup> spring sediment event.	114
4.4 Lake stratification.	115
4.5 Stratified inflows.	115
4.6 Delay of stream discharge.	116
4.7 2 <sup>nd</sup> spring sediment event.	119
4.8 Homopycnal flow.	120
4.9 Plume camera images for 1 <sup>st</sup> spring sediment event.	121
4.10 Comparison of SC2 and SC3.	123
4.11 Composite graph of sedimentation 2004 – 2008.	126
4.12 Comparison of composite with thin section.	133

## TABLE OF TABLES

2.1 Mooring deployment, retrieval, and duration.	47
2.2 Mass of the components for the epoxy.	68
3.1 Sediment flux and lake bottom deposition.	76
3.2 Maximum values for solar radiation, air temperature, and precipitation.	97
4.1 Sediment flux at Mooring C 2004 – 2008.	124
4.2 Average monthly air temperature.	128
4.3 Average monthly solar radiation.	129
4.4 Average monthly precipitation.	130
4.5 Lake bottom deposition.	131
4.6 Thickness of laminae in thin section.	132
4.7 Composite trap accumulation.	134

**CHAPTER ONE**

**INTRODUCTION**



## **1.1 – Purpose & Overview**

With the prognosis of climate change throughout the next century due to the current warming trend, it is critical to study current environmental systems to understand the impacts of recent climate change (IPCC, 2007). Modern climate processes are influencing the present environmental systems in the Arctic. The purpose of this study is to monitor modern sedimentation processes in Linnévatnet, a High Arctic lake. The sediment record is used as a proxy for climate indicators.

Linnévatnet is a glacier-fed lake in Svalbard in which past climatic characteristics are recorded in laminated lake sediments that likely span the past 9,000 years. The laminae are comprised of annual couplets which consist of two distinct seasonal layers, a summer and a winter. Previous studies in similar proglacial lakes throughout the Arctic and alpine regions have determined that varves indicate weather and climate influences in the catchment area (Leeman & Niessen, 1994, Mangerud & Svendsen, 1990, Snyder et al, 2000,).

Svalbard Research Experience for Undergraduates (REU), funded by the National Science Foundation, has studied glaciers, melt-water streams, and sedimentation in lakes in relation to climate change (Werner, 2007). Four students have previously analyzed sedimentation using sediment traps deployed yearly and seasonally. In these previous studies, trap stratigraphy, composition, and grain size were evaluated to compare sedimentation records with local weather data and other watershed parameters (McKay, 2004; Motley, 2006; Roop, 2007; and Cobin, 2008).

This present study is a continuation of the project and focuses on the modern processes of sedimentation in Linnévatnet to determine if there is a relationship between

sedimentation and climate-weather variables. This study will compile all available data from the five years of the REU project to date to provide a complete record of sediment trap stratigraphy, grain size, and weather data. Sediment cores were collected for analysis of five years of laminae thickness with 5 years of sediment trap data to determine the relationships of trap accumulation, sediment deposition, and meteorological data.

## **1.2 - Study Area:**

Svalbard is an archipelago located within the Arctic Circle between 74° and 81° north and 10° and 35° east (Figure 1.1). Kapp Linné is a small cape on the west coast of Spitsbergen, the largest island in the archipelago (Figure 1.2). The cape is situated where Isfjorden, the major fjord of Spitsbergen, flows into the Atlantic Ocean. Isfjord Radio is a small radio relay station located on Kapp Linné that is used for tourism and scientific expeditions. Linnévatnet is approximately 5 kilometers east of Isfjord Radio.

Linnévatnet is 4.7 kilometers in length and 1.3 kilometers in width with a deep hole at 35 meters depth (Bøyum and Kjensmo, 1978). Linnévatnet is oriented along a north-south axis, bounded on the east and west by two mountains (Figure 1.3). The mountains, which protect the lake from easterly or westerly winds, permit the southerly winds blowing down the valley Linnédalen to “have a strong effect on the lake surface” (Bøyum and Kjensmo, 1978). However, the lake is covered with ice from approximately September to July (Snyder et al., 2000) and thus the winds only affect the lake in the summer months.



The catchment basin is approximately 27 km<sup>2</sup> and 6.3% of the area is glaciated (Snyder et al., 2000). The primary inlet, Linnéelva, feeds into the south end of the lake. Linnéelva is a meltwater stream fed by a glacier, Linnébreen, which is located six kilometers south of Linnévatnet. From the north end, Linnévatnet drains into Isfjorden, a fjord that merges in the North Atlantic Ocean.

Svalbard is an area within the zone of continuous permafrost. Permafrost terrain features frequent the landscapes that are not glaciated with thicknesses up to 450 meters in the highland (Figure 1.4). The coastal areas have thicknesses ranging from 10 – 40 meters. Linnévatnet is located in an area with thicknesses ranging from 225 – 275 meters.



Figure 1.1: Map of the Arctic Circle. Thick blue circle outlines Svalbard. Blue dashed line denotes the 66°N latitude of the Circle, red line marks the 10°C isotherm in July, and green line marks treeline. From The Perry-Castañeda Library Map Collection: Maps of Polar Regions and Oceans. (<http://www.lib.utexas.edu/maps/polar.html>)



Figure 1.2: A NASA Landsat image of Svalbard. Red square notes the peninsula with Kapp Linné, Isfjord Radio, and Linnévatnet. The yellow “L” notes Longyearbyen, the most populated town in Svalbard. The large fjord north of the study site and Longyearbyen is Isfjorden.



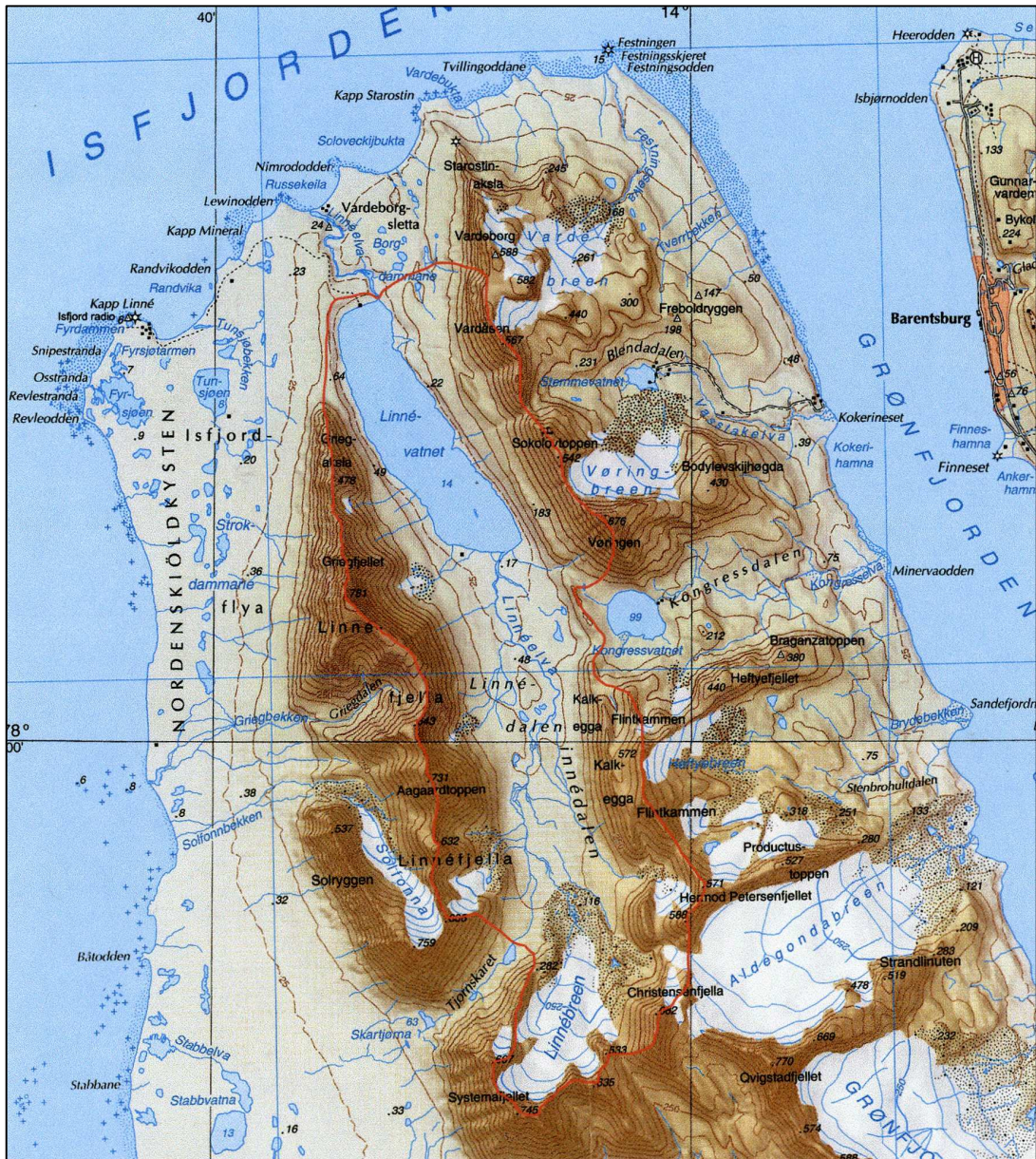


Figure 1.3: A 2004 Norsk Polar Institute map of the study region showing Linnévatnet, Linnéelva, and Linnébreen. The red line highlights the Linnévatnet watershed which includes Linnébreen. Please note the elevation of Linnévatnet is 12 meters opposed to 14 meters on map (Svendsen et al., 1989). From Motley, 2006.

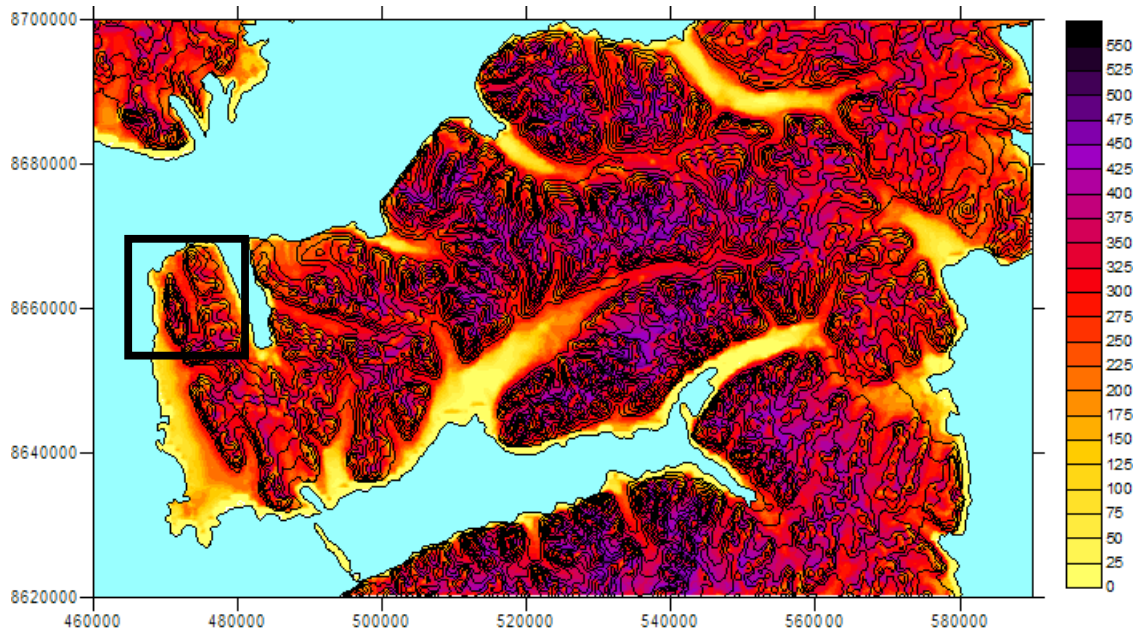


Figure 1.4: Permafrost thickness in the region around study area (outline by black box). The color scale notes thickness with yellow as shallow (0-125 meters) progressing to purple as deep (400-550). The permafrost in the study area is approximately 250 meters to 325 meters thick. From Ingolfsson, 2006.

### *1.2.1 Bathymetry*

The bathymetry of the lake bottom is divided into three basins: “west basin,” “east basin,” and “main basin” (Figure 1.5). The main basin is the largest and contains the maximum lake depth of 35 meters. The east and west basins are located at the south end of the lake. The east basin is the next largest and is fed by the major inlet, Linnéelva which carries turbid meltwater from Linnébreen. The depths in the East basin reach 15 meters. A bathymetric rise of 4 meters depth divides the east and west basins. The west basin is fed by a small stream flowing from a previously glaciated cirque which now contains a thin perennial snowpack (Figure 1.6). The inlet is an insignificant sediment source compared to Linnéelva. The maximum depth in the west basin is 15 meters. The south end of the lake receives the majority of inflowing water but there are several smaller inlets around the lake.



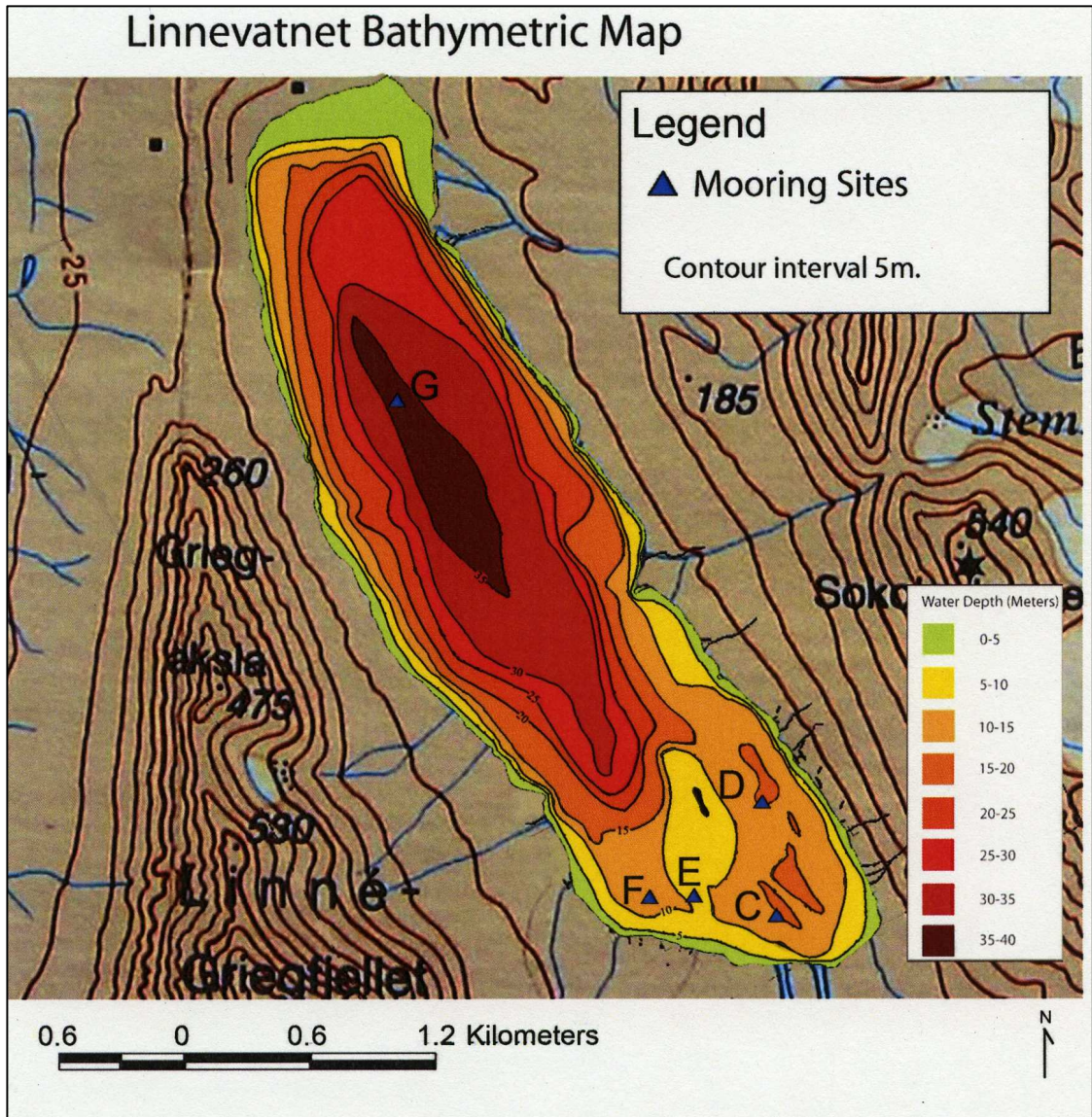


Figure 1.5: Bathymetric map of Linnévatnet. The dark red marks the deep basin and the light orange marks the east and west basins. From Leon, 2007.

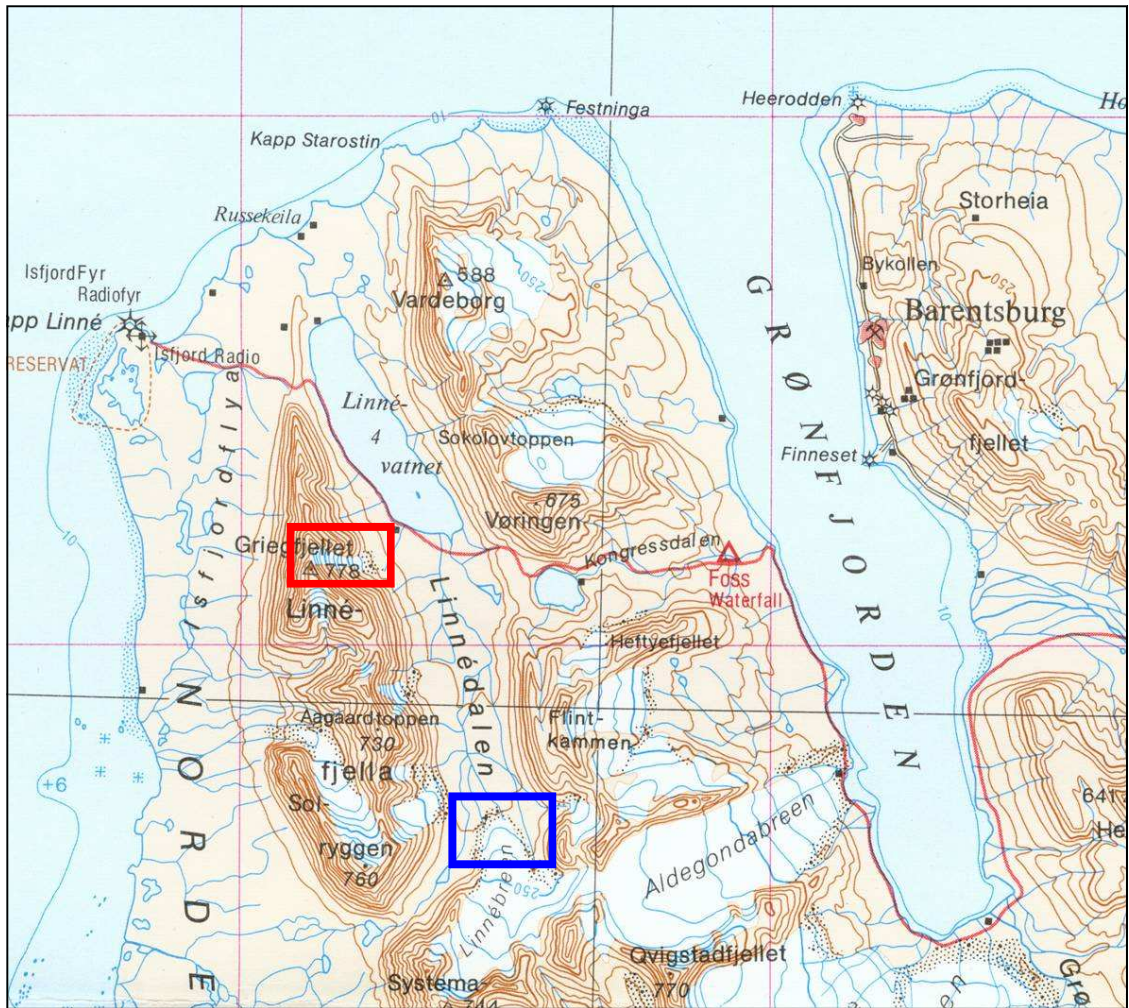


Figure 1.6: A modification of the 1936 Norsk Polar Institute map of Linnédalen. The red square outlines cirque glaciated during the Little Ice Age which fed a stream into Linnévatnet. The blue square notes the LIA extent of Linnébreen. Refer to figure 1.3 for the moraines in 2004.



### *1.2.2 Bedrock*

Linnévatnet is situated in the catchment along the north-south strike of the bedrock (Figure 1.7). The lake itself predominantly overlies a Carboniferous sandstone unit. The valley is bounded to the west by Precambrian metasediments of the Hecla Hoek formation and to the east by Carboniferous limestones and gypsum and Mesozoic shales, siltstones, and cherts (Hjelle, et al., 1986). The bedrock of Linnédalen contributes to the lacustrine sediments in Linnévatnet.

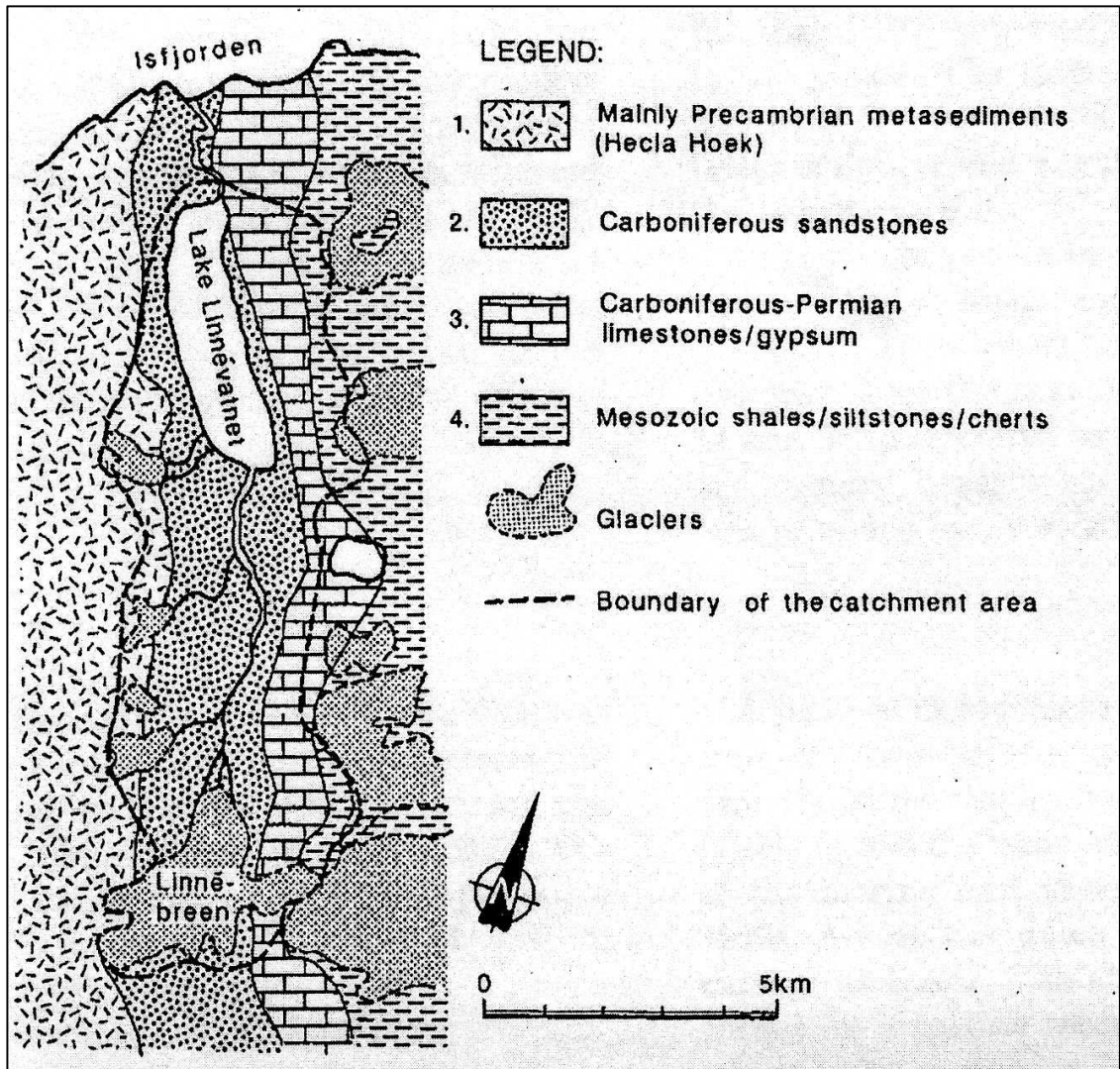


Figure 1.7: Bedrock map of Linnévatnet. Note that the Linnévatnet long axis follows the strike of the bedrock. From Svendsen, 1989.

### **1.3 – Climate and Climate Change of the Arctic**

The Arctic is commonly defined as the land above latitude 66 °N – the Arctic Circle limit. Arctic climate varies with the environment; for example, open tundra experiences midwinter winds approximately one-half greater than subarctic open forest (Rouse, 1993). The High Arctic is characterized as a polar desert due to low precipitation – less than 4 mm of water vapor annually. The High Arctic receives less than half of the annual 200 – 400 mm precipitation at lower polar latitudes (Rouse, 1993).

#### *1.3.1 The Atmospheric Circulation Patterns*

Two of the forces that determine the Arctic climate are the atmospheric pressure patterns known as the North Atlantic Oscillation (NAO) and the Arctic Oscillation (AO). The North Atlantic Oscillation describes a positive relationship between the Icelandic Low and the Azores High (Serreze, et al., 2000). A positive NAO describes strengthening of the Icelandic Low and Azores High and negative temperature anomalies over Greenland and eastern Canada. The positive NAO also permits more west to southwesterly winds carrying warm and moist air to Scandinavia (Serreze, et al., 2000). A negative NAO phase describes opposite conditions – weakening of the Icelandic Low and Azores High, positive temperature anomalies in Greenland and Canada, cool and dry northwesterly winds to Scandinavia.

The Arctic Oscillation is greatly influenced by the NAO (Figure 1.8). The positive AO expresses positive sea level pressure (SLP) anomalies over the Arctic which are related to higher temperatures over Siberia and lower temperatures over the Labrador Sea, and Southern Greenland (Serreze, et al., 2000). The negative AO is the opposite

with negative SLP and lower temperatures over Siberia and higher over the Labrador Sea and Southern Greenland (Figure 1.9).

Positive phases of the NAO and AO permit an increase in cold-season cyclone frequency (Serreze, et al., 2000). The AO and NAO have tended to stay positive since the 1970's; currently 2007 and 2008 are strongly positive but with less strength than the 1990's regime.

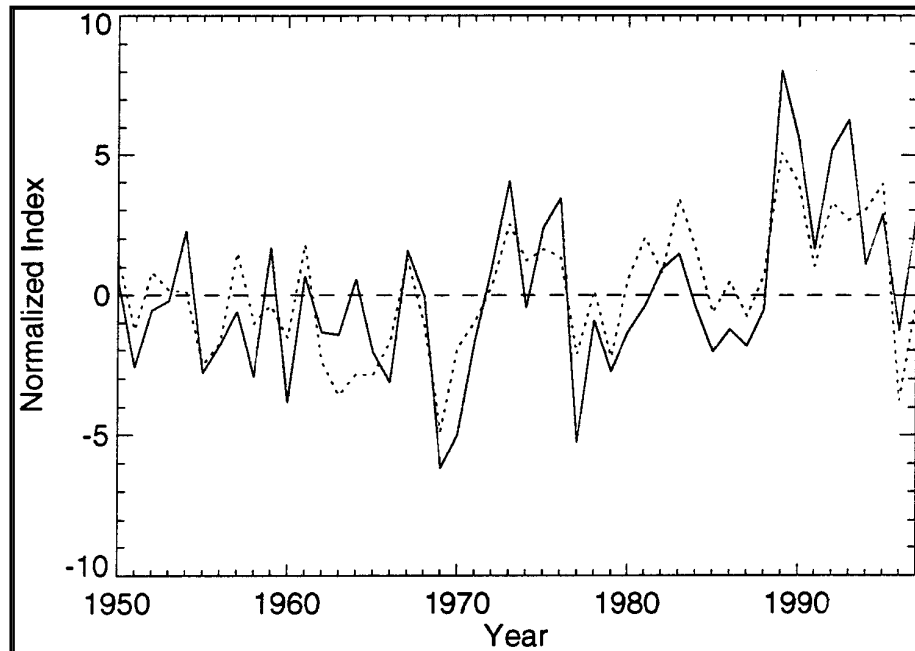


Figure 1.8: The AO (solid line) and NAO (dotted line) relationship. The two circulation patterns correspond. From Serreze, et al., 2000.

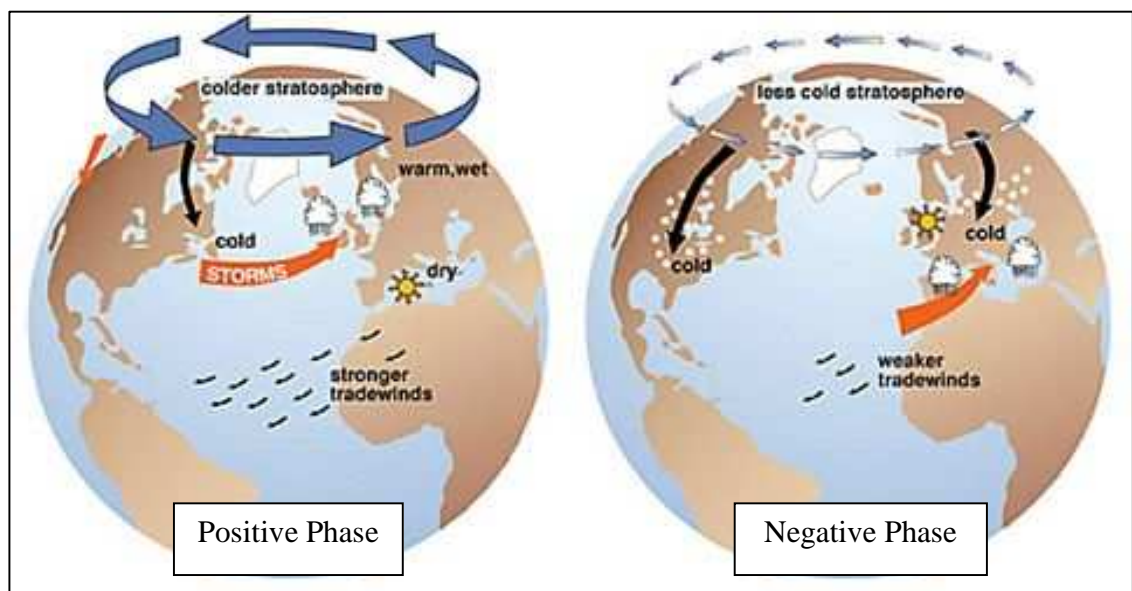


Figure 1.9: The effects of the AO positive phase and negative phase. From the NSIDC Arctic Climatology and Meteorology Primer, attributed to G. Holloway, Bedford Institute of Ocean Sciences (<http://nsidc.org/arcticmet/>)

### *1.3.2 Climate Change in the Arctic*

Due to the high latitude and extreme amounts of solar radiation, the Arctic is particularly sensitive to climatic changes amplified by positive feedbacks such as surface albedo and atmospheric circulation. Large areas of the Arctic are covered by snow and/or ice which reflect light and solar radiation. The albedo feedback is positive when snow or sea ice decreases in area allowing more solar radiation absorption which leads to more melting (Overpeck et al., 1997).

The climate of the Arctic has varied throughout the past several centuries. The 17<sup>th</sup> century is known for the cool periods which initiated the Little Ice Age (LIA), a period of glacial advance in the Arctic and alpine regions. The 18<sup>th</sup> century temperatures were almost as warm as late 20<sup>th</sup> century temperatures (Overpeck et al., 1997). However, great cooling occurred in the 19<sup>th</sup> century which marked the coldest Little Ice Age temperatures. Temperatures warmed 1 ° to 3 °C locally throughout the 20<sup>th</sup> century, ending the LIA (Overpeck et al., 1997).

The National Snow and Ice Data Center describes the Arctic as “showing signs of rapid change” including warming of air over the central Arctic Ocean and decreases in sea ice and snow extent. Since 1900, mean annual surface air temperature has been increasing and currently, autumn temperatures are 5 °C above normal, a new record (Figure 1.10). Autumn sea ice extent has been decreasing (The Arctic Report Card). September 2007 marked a record low for sea ice extent and September 2008 experienced the next minimum. The extended winter AO index describes 1950-1980 as negative phases with a consistent positive phase in the 1970's (Figure 1.11). However, the 1990's

describe a decade of very strong positive AO. The years since have been less positive and weakly negative until 2007 and 2008 when the AO returned to a strong positive.

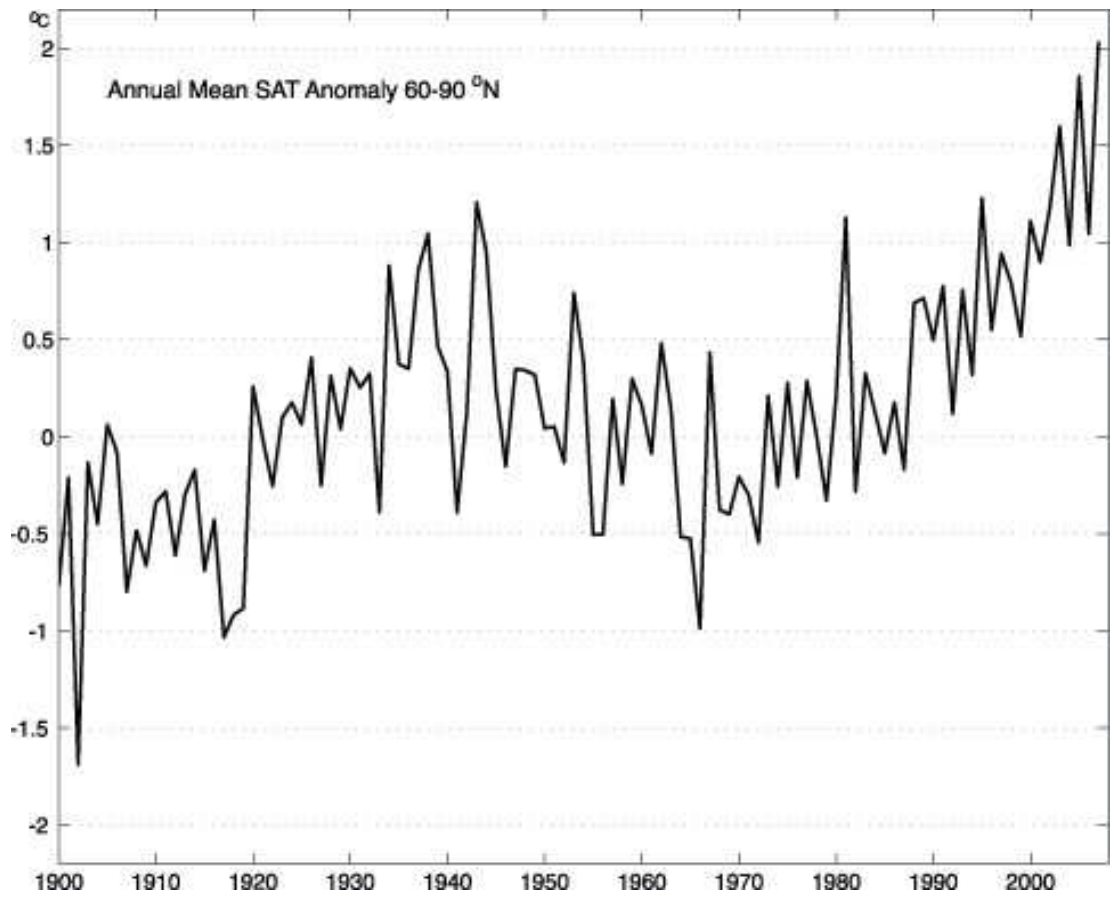


Figure 1.10: Annual mean surface air temperature anomaly from 1900 to 2008. Note the general increasing temperature trend. From the Arctic Report Card, 2008.



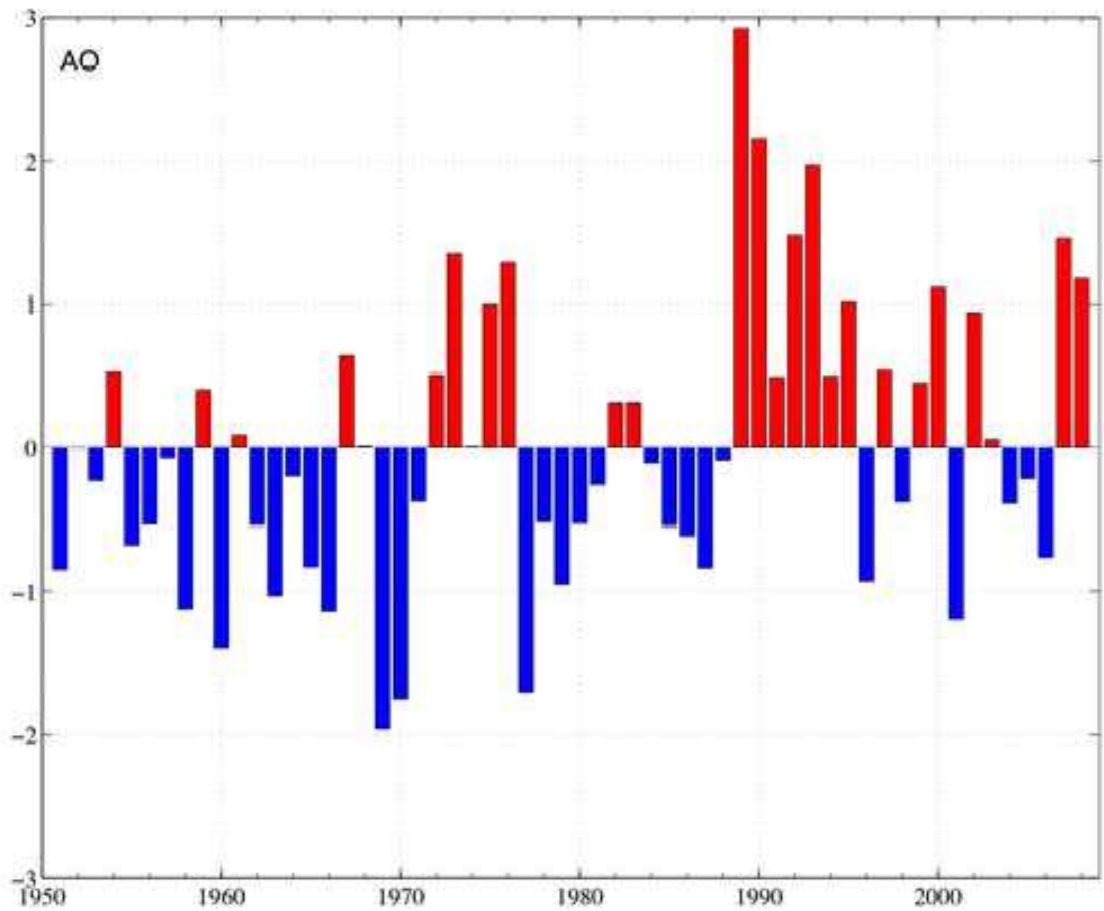


Figure 1.11: Extended winter AO index from 1950 – 2008. Red bars are positive and blue bars are negative. Note the strong positive regime in the 1990's. From the Arctic Report Card, 2008.

### *1.3.3 Climate of Svalbard*

Svalbard is a polar desert; the climate is described as arctic. The mean annual temperature at sea level is  $-6^{\circ}\text{C}$  and  $-15.2^{\circ}\text{C}$  in the high mountains. Coastal areas accumulate the most precipitation of approximately 400 – 600 millimeters w.e. (water equivalency) per year. Inland and mountain regions accumulate 200 mm w.e. per year (Ingolfsson, 2006). Snow is the dominant type of precipitation, however due to strong winds the measured values are likely an underestimation.

The largest continuous meteorological record in Svalbard comes from Longyearbyen. This large settlement provides a century-long record of air temperature and precipitation accumulation (Figure 1.12). Summer air temperature in Longyearbyen remains consistent throughout the record varying between average values of  $3^{\circ}$  –  $6^{\circ}\text{C}$ . However, winter temperatures have experienced great variability throughout the 20<sup>th</sup> century. Temperatures range from a low of  $-20^{\circ}\text{C}$  to a high of  $-10^{\circ}\text{C}$ . Since Longyearbyen is approximately 50 kilometers inland, the precipitation fluctuates between a low of 125 mm and a high of 250 mm per year (Ingolfsson, 2006).

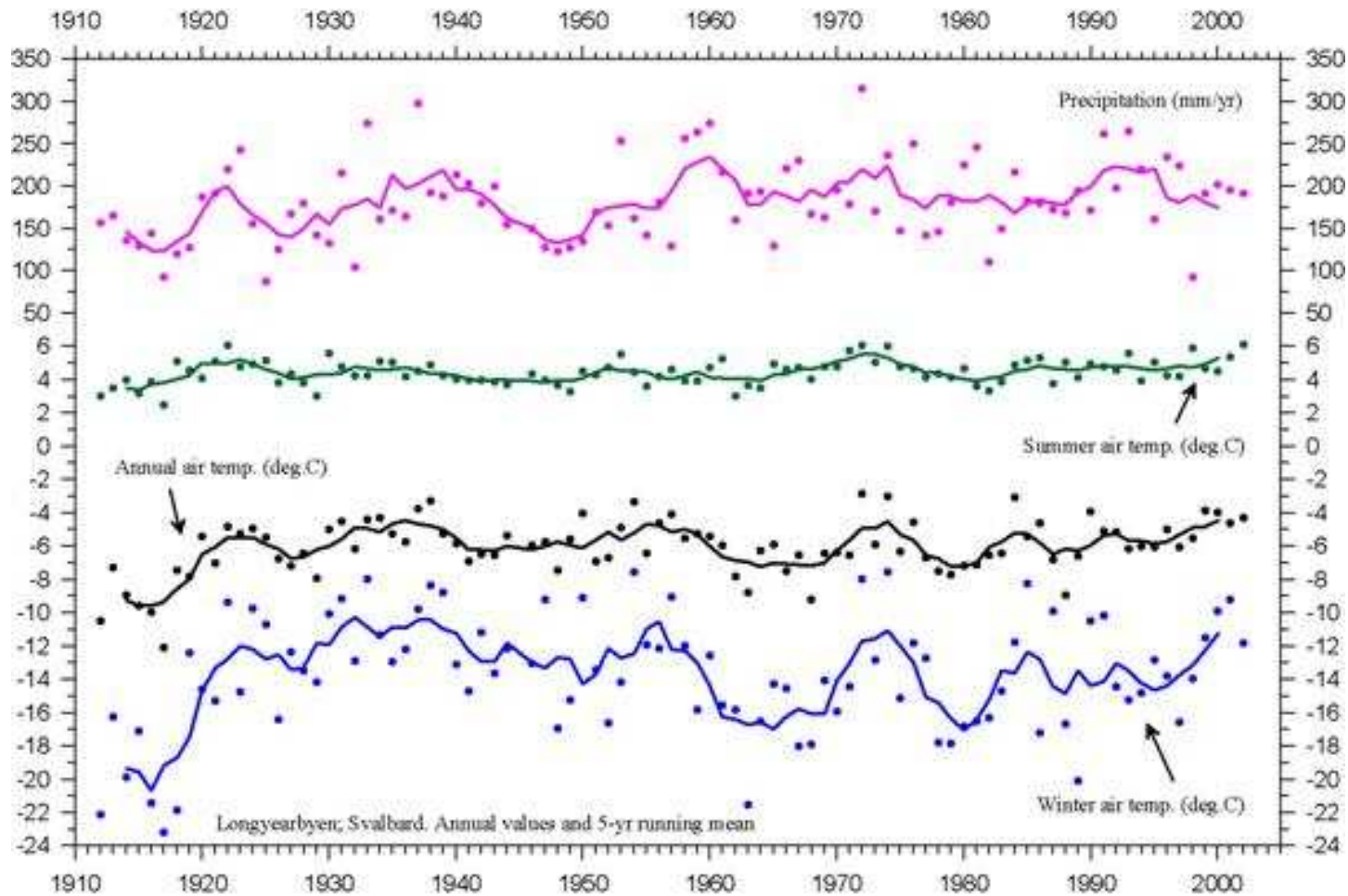


Figure 1.12: Weather temperature data from Longyearbyen collected since 1910 to the present. Y-axis is temperature °C and accumulation mm. Note the consistency of summer air temperature throughout and the high variability of winter air temperature. Data by Ole Humlum in Ingolfsson, 2006.

## **1.4 – Arctic Hydrology**

The distinctly seasonal climate of the Arctic drives a unique hydrological system throughout the region. Due to the amount of light received throughout the year, the hydrological cycle is greatly reduced to a much shorter time period than in temperate regions (Woo, 1993). The circulation of water throughout the Arctic is determined by snow, ice, and frozen ground.

### *1.4.1 Snow*

Snow is the dominant type of precipitation in the Arctic. Often, accumulation measurements underestimate snowfall due to the difficulty of catching blowing snow. The snow can actually hold up to 130 – 300 % more water content than measured (Woo, 1993). High Arctic snow temperatures can reach -15 °C and is much denser than temperate snow. Due to lack of vegetation in the Arctic, wind greatly redistributes snow (Woo, 1993). The topography controls the distribution of snow, compressing the snow into valleys, gullies, and depressions (Woo, 1993; Kane et. al, 1992). Snow accumulation can represent 60 – 80% of the annual precipitation.

### *1.4.2 Snowmelt*

Snowmelt is the dominant hydrological event of the year (Kane et. al, 1993). In the High Arctic, the snowmelt events usually coincide with the greatest amount of solar radiation. As the melt season begins, albedo decreases with the decreasing snow coverage. This leads to more heat absorption by the bare ground (Kane et. al, 1993), accelerating more melt and facilitating heating of the active layer.

When the snowmelt events begin in June, the bottom snow and permafrost surface temperatures are less than 0° C. As the first surface snow begins to melt, it percolates

into the underlying layers and refreezes (Kane et. al, 1992). This cycle continues until the snow is saturated and begins to flow down slope. Most snow in the High Arctic is drifted into valleys and depressions, thus the amount of snow accumulated in these regions may delay streamflow initiation by several days (Woo, 1993). The deep snow retains meltwater and water movement is contained within the snowpack in channels or ponds. When the channels coalesce into a drainage network, water will then flow from the snowpack and out of the valley (Woo, 1993). There are some snow banks that retain snow well into the season and these deliver meltwater continuously throughout the melt season.

#### *1.4.3 Permafrost*

Permafrost is a zone of perpetually frozen soil and subsurface. The uppermost meter is the only subsurface layer that melts; this is called the “active layer.” The active layer thaws during or after the snowmelt. The maximum thaw depth occurs in well-drained hill slopes (Kane, et. al, 1992). All water flowing on the ground down slopes travels through the active permafrost layer seasonally. As surface temperatures cool, the active layer freezes from the surface downward. The water contained in the warmer soil moves from warm temperatures toward the colder freezing front (Woo, 1993). Although most of the permafrost is frozen, there may be subpermafrost water flows that result in springs or seepage into lakes (Woo, 1993).

#### *1.4.4 Glacier Melt*

During the winter with low temperatures glaciers accumulate mass through snowfall, avalanches, or snow drifting. The melt season is initiated by energy from increased solar radiation that causes the surficial snow and firn melt (Woo, 1993).

Runoff responds to heat energy as opposed to rainfall, therefore more melt occurs in years with warm and dry conditions. Melt can be diurnal, responding to daily fluctuations of solar radiation; peak flows occur in early afternoon (Woo, 1993). Meltwater runoff can flow supraglacial, englacial, or subglacial. Supraglacial flows can often be a slushflow, mixture of water and snow, early in the season. As more water runoff flows down glacier, erosion of the ice surface creates channels within the ice. Fissures, crevasses, or moulins provide supraglacial flows to have a significant impact on englacial and subglacial flows.

The elevation at which snow and firn are retained after a melt season marks the equilibrium line of accumulation (ELA) (Bennett & Glasser, 1996). The ELA migrates up-glacier or down-glacier depending the snowline of that season. The state of a glacier can be assessed quantitatively through mass balance – the amount of snow retained minus the amount melted (Bennett & Glasser, 1996). When a glacier has retained more accumulation than the volume of melt, the glacier experiences a positive mass balance. However when the volume of melt exceeds the volume of accumulation retention, the glacier experiences a negative mass balance.

### **1.5 – Glacial History of Svalbard**

The Svalbard archipelago is dominated by ice mass in the form of glaciers and ice caps which cover approximately 60% of the landscape (Ingolfsson, 2006). Glaciers are controlled by precipitation; areas such as central Spitsbergen have smaller glaciers due to the dry climate. The ELA reflects the climatic conditions by lowering along the humid

coastal glaciers and rising in the dry mountains. Non-glaciated landscape describes past glaciations as larger and more extensive.

#### *1.5.1 Last Glacial Maximum*

Svalbard has experienced a number of glacial advances throughout the Late Cenozoic, the greatest of which is known as the Last Glacial Maximum (LGM). The landscape is marked by raised marine terraces; in Linnédalen such a feature reaches 87 meters above sea level (Mangerud & Svendsen, 1990). The terraces appear at higher elevations following an eastward trend (Siegert et. al, 2002) indicating significant isostatic loading was centered over the Barents Sea (Figure 1.13) (Svendsen et. al, 2004).

Isfjorden was glaciated during the Late Weichselian and Linnédalen held a tributary glacier feeding into the fjord glacier (Mangerud & Svendsen, 1990). The Linnédalen tributary scoured pre-existing sediments. All marine sediments in Linnévatnet postdate 12,500 BP. Mangerud and Svendsen, 1990, conclude that the Late Weichselian glaciation in this region lasted approximately from 17,500 to 12,500 BP.



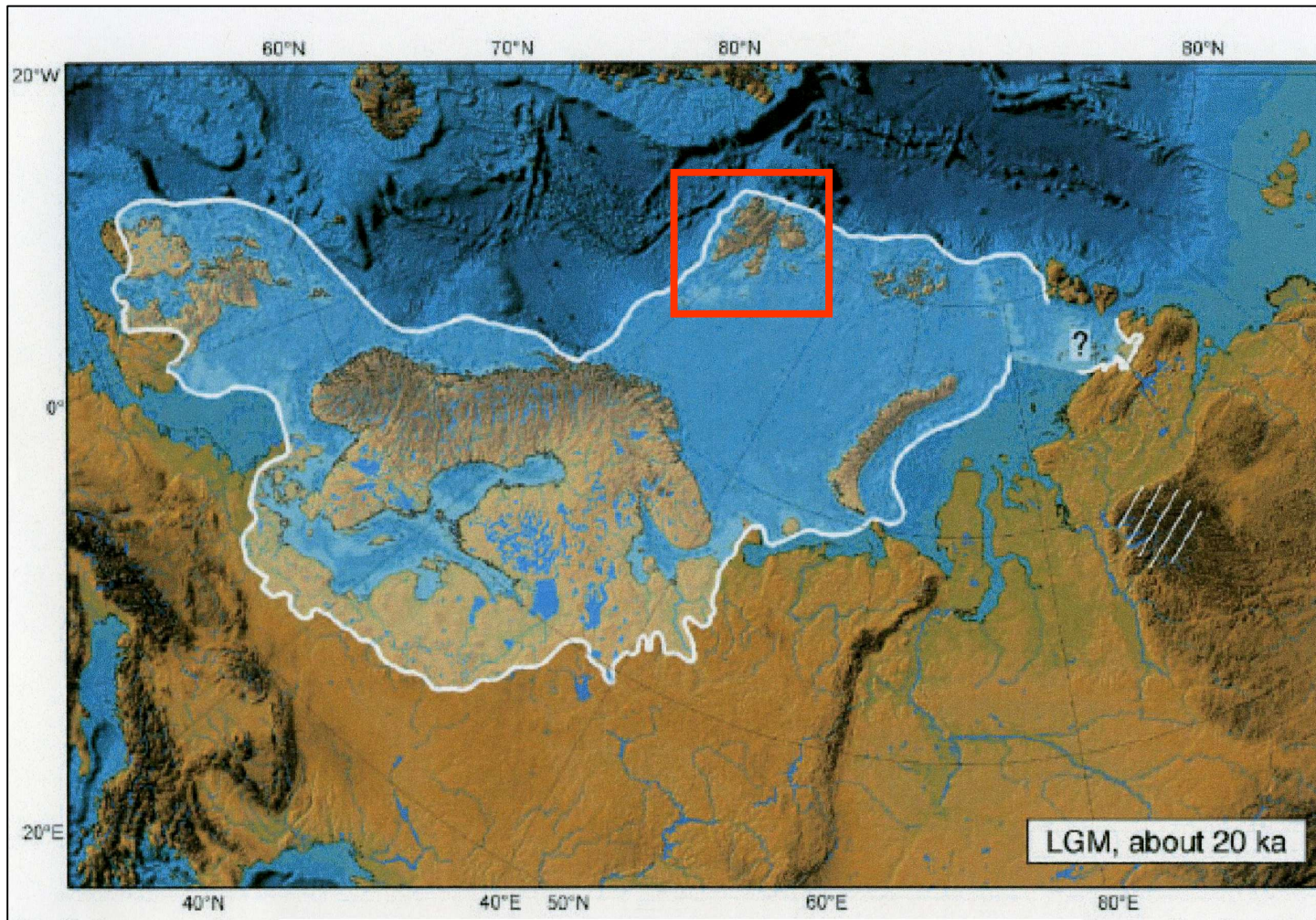


Figure 1.13: The extent of the Barents Sea Ice Sheet during the LGM approximately 20 ka. Note Svalbard is contained in the top center of the ice sheet, marked by red square. From Svendsen et. al, 2004.



### *1.5.2 Deglaciation of Linnédalen*

Deglaciation of Western Spitsbergen began approximately 13,000 years before present. Radiocarbon aged marine fossils contained in marine sediments indicate that Linnévatnet was filled with sea water at 12,500 kya which suggests the valley was deglaciated (Mangerud and Svendsen, 1990). Due to isostatic depression, Linnédalen was a fjord and beaches were deposited as isostatic rebound progressed. At approximately 9,600 years ago, uplift and subsequent longshore transport of marine sediment created a prominent marine terrace that isolated Linnévatnet into a freshwater lake (Snyder, et. al, 2000). Radiocarbon evidence from paired mollusks contained within the youngest marine sediment is consistent with the age of Linnévatnet isolation (Snyder, et al., 2000).

### *1.5.3 Holocene Glacial Fluctuations of Linnédalen*

In the early to mid-Holocene, the climate in Svalbard was warm and Linnédalen was ice free. At approximately 4-5,000 years ago, Linnébreen began to form as a small valley glacier (Svendsen and Mangerud, 1997). A cirque in the mountains at the southwest corner of Linnévatnet was deglaciated prior to the isolation of the lake until the Little Ice Age (Snyder et al., 2000). Glacier advance around the world in historical times suggests a small glacial period from about 1600-1900 C.E. known as the Little Ice Age (LIA). An ice-cored moraine approximately 2 km down valley of Linnébreen indicates the furthest ice extent of the valley glacier during the LIA. A 1936 oblique aerial photograph (Figure 1.14) depicts the terminus of Linnébreen close to the moraine.



Figure 1.14: An oblique aerial photograph of Linnédalen facing south. Upvalley, Linnébreen appears to sit at the LIA moraine (noted by blue box). Also refer to Figure 1.6 for another view of the LIA moraine. Photo courtesy of the Norsk Polar Institute.

## **1.6 – Lacustrine Sediments**

### *1.6.1 Sediment Sources for Linnévatnet*

Linnéelva is the main source of sedimentation in Linnévatnet. The drainage basin for Linnéelva is 27 km<sup>2</sup> (Synder et. al, 2000). The braided river flows from Linnébreen over bedrock, through permafrost, and gullies draining into Linnévatnet. The turbid river receives and carries suspended sediments to the lake.

Smaller sources include two alluvial fans at the southern end of Linnévatnet and small meltwater streams from the mountain sides (Figure 1.15). The large alluvial fan at the southeast corner of Linnévatnet contributes snowmelt and groundwater flow to the lake and Linnéelva (Snyder et al., 2000). The smaller fan to the southwest carried meltwater from the previously glaciated late Holocene cirque (Snyder et al., 2000). The stream currently carries meltwater from a perennial snowpack.



### *1.6.2 Lake Stratification*

The water column in lakes can be divided by several parameters such as density, temperature, or salinity. For the purpose of the study, temperature will be discussed and density can be inferred since temperature is the prominent variable in density. The vertical temperature water column is created by solar heating and heat transfer within the water (Smith and Ashley, 1985). Top water and bottom water can stratify based on large differences in temperature (Figure 1.16). The boundary between these two units is known as the thermocline and the zone of temperature increase is known as the metalimnion. The thermocline separates the epilimnion – upper water from the hypolimnion – bottom water.

### *1.6.3 Lake inflow*

Relative density between lake water and inflowing water determines how the inlet enters the lake column. The density of both waters may be controlled by temperature, dissolved ion concentration, and suspended sediment concentration (Smith and Ashley, 1985). The behavior of inflowing water is described as overflow, interflow, underflow, or homopycnal flow (Figure 1.17). If the density of the inflowing water is less than the lake water, it will flow over the water column as an overflow. These are seen from the surface as a distinct sediment plume. If the inlet is more dense it will plunge under the water column and flow along the bottom of the lake. Interflows can occur if the inflowing water is more dense than the surface water but less dense than the bottom water. A homopycnal flow occurs when the water column density and the inflow density are the same. The two waters will mix and the inflow will spread evenly throughout the column.

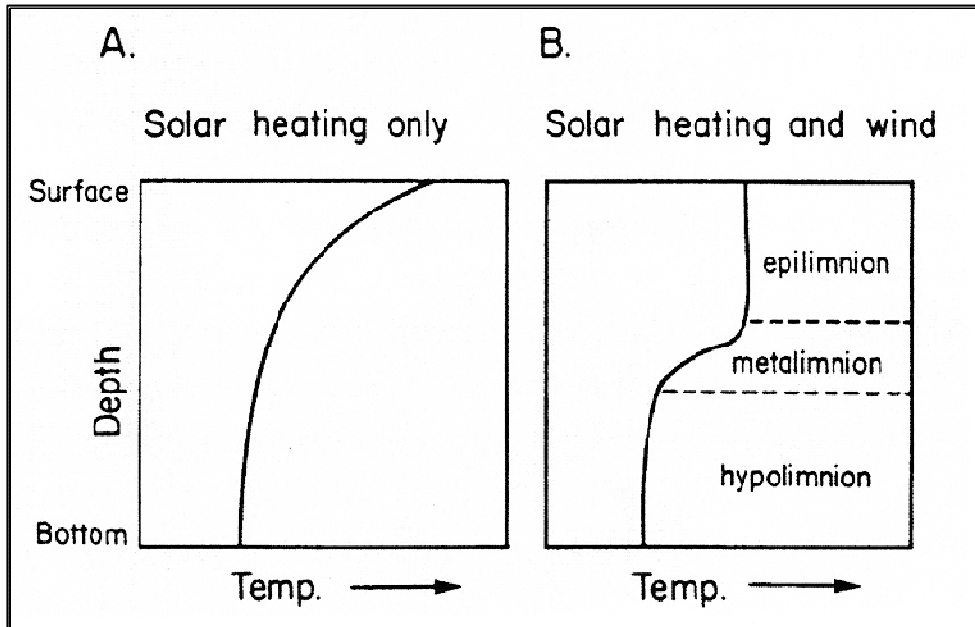


Figure 1.16: Stratification of the water column by solar heating only in A and solar heating with wind in B. The temperature change in the metalimnion marks the thermocline. From Smith and Ashley, 1985.

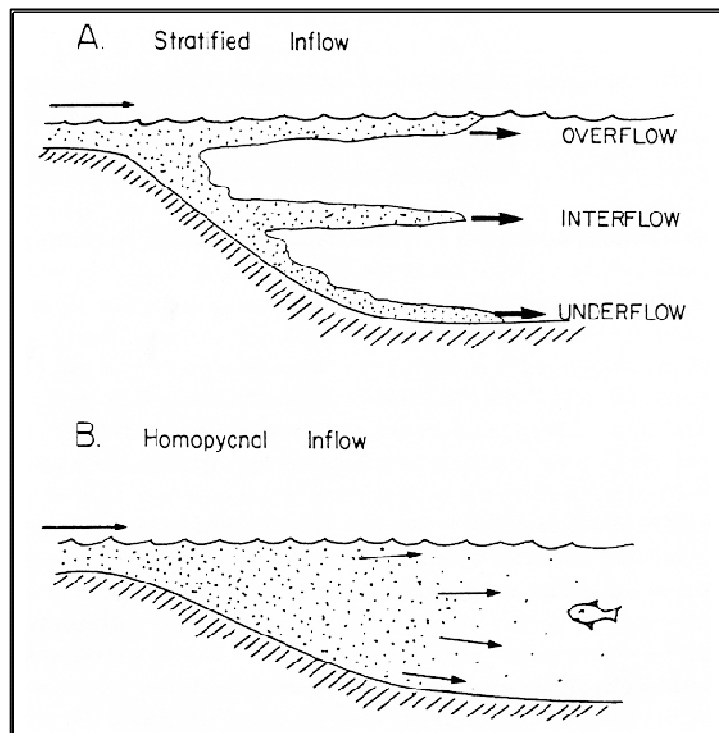


Figure 1.17: Description of the four inflows which depend on the relative density between inflowing water and the lake column. The dotted regions mark the turbid inflowing water. From Smith and Ashley, 1985.

#### *1.6.4 Flow Dynamics*

The distribution of inflowing water is affected by wind, waves, and gravity. Wind and wave direction greatly influence the distribution pattern as they dictate the overflow plume orientation. The Coriolis effect deflects moving water and the suspended sediment plume to the right of the inlet (Figure 1.18 & Figure 1.19) (Smith and Ashley, 1985). The range of suspended sediment grain size is influenced by these parameters. Finer grained sediment will travel farther than the coarser grained and subsequently deposit on the lake floor (Figures 1.18 & 1.19) (Smith and Ashley, 1985). The sediment thickness of the lake floor decreases further from the inlet. The depositing particles decrease in size with distance. The Coriolis effect on Linnévatnet is described in Figure 1.20 with the thickest sediment on following the east side of the lake.

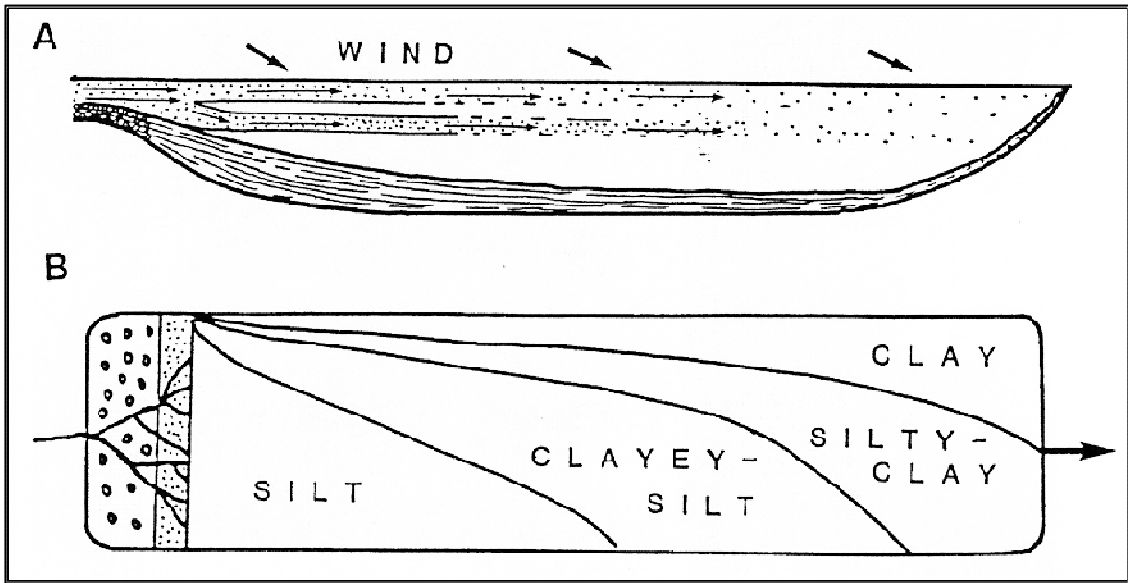


Figure 1.18: Influence of wind, waves, and the Coriolis Effect on sediment plume. The plume turns to the right of the inlet and grain size distribution separates coarse (proximal) from fine (distal). From Smith and Ashley, 1985.

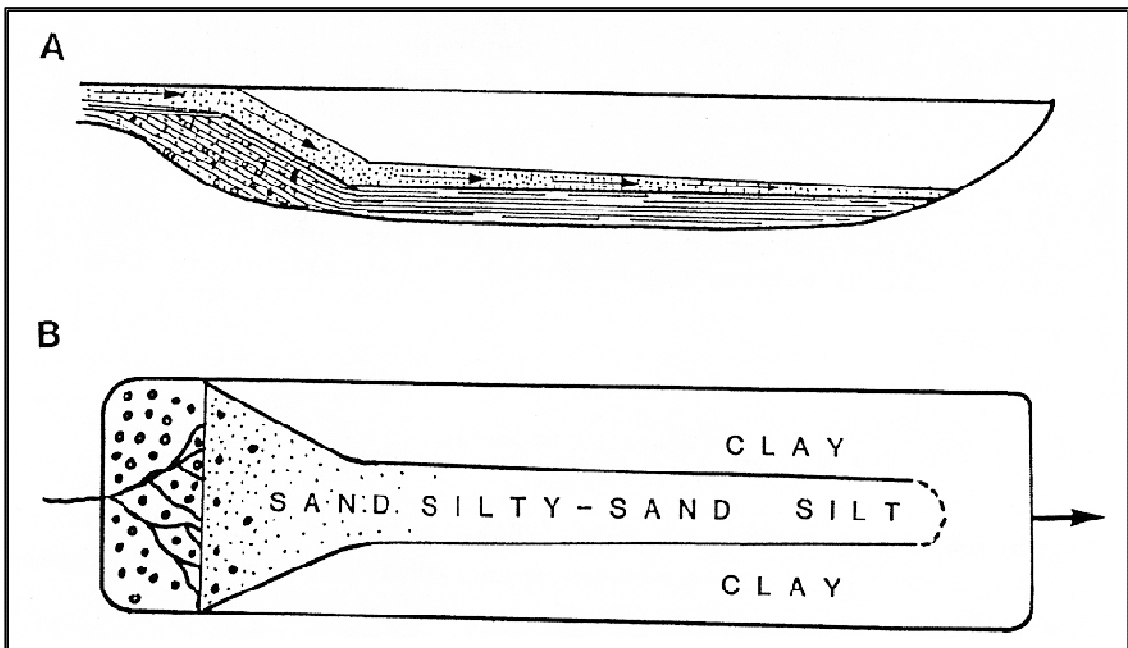


Figure 1.19: Distribution of sediment grain size from a sediment underflow. Sediment thickness decreases with distance from the inlet (A). Coarse grains are proximal to inlet and fine grains are distal (B). From Smith and Ashley, 1985.



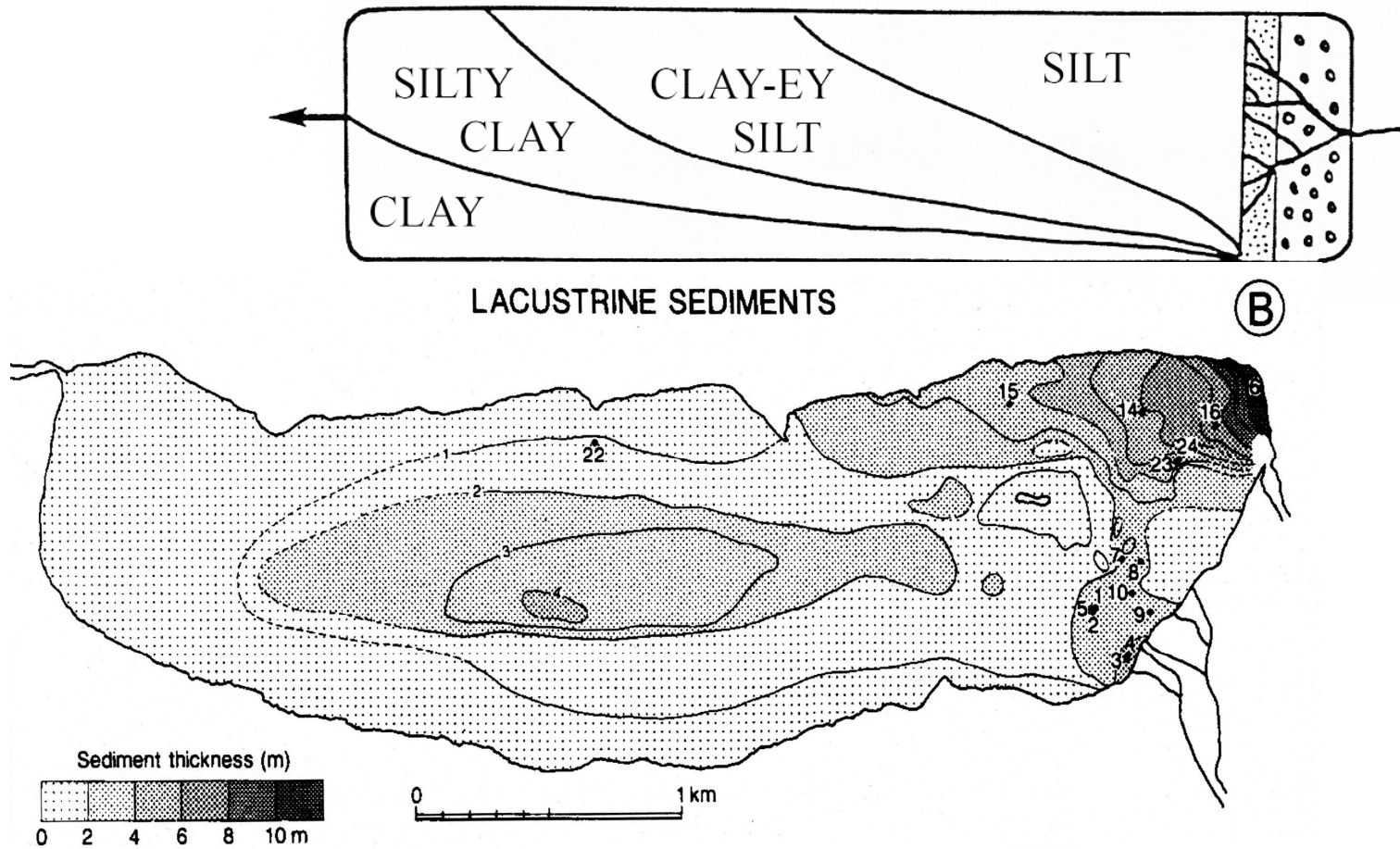


Figure 1.20: Comparison of the Coriolis effect (A) and the lacustrine sediment thickness in Linnévatnet (B). The sediment thickness is deeper at the southern end of the lake near the Linnéelva inlet. Note the contour of the thickness grades to the east side of the basin – this is the Coriolis effect on the sediment deposition. The sediment grain size likely follows the deposition pattern in Figure A. Figure A is modified from Smith and Ashley, 1985. Figure B is from Svendsen et al., 1989.

### *1.6.5 Sediment Deposition Characteristics*

Due to the lack of biota in Linnévatnet, there is very little bioturbation of the deposited lacustrine sediment. A unique characteristic of preserved sediment in Arctic lakes is called a varve. Varves are annually laminated sediment couplets that alternate light and dark laminae. Varves can be divided into two layers – a layer of summer deposition and a layer of winter deposition (Sturm, 1979). The summer layer tends to be coarser silt particles and winter layers tend to be finer clay sediments (Smith and Ashley, 1985). The silt layer may grade to the clay layer, however the contact between two couplets at the clay-silt boundary is very sharp (Smith and Ashley, 1985).

Since varves are deposited annually, they can be counted back through time like tree rings. Thickness and grain size of layers can be indicative of the depositional environment such as precipitation, runoff, and temperature (Leemann & Niessen, 1994).

### **1.7 – Sediment Traps**






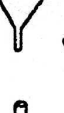
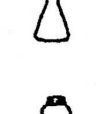

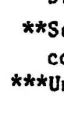
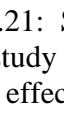



Sediment traps are a useful tool to understand and quantify suspended sediment fluxes in lakes. They have been used for many years to capture in situ particles. There are many different types of sediment traps which result in varying amounts of efficiency. Gardner, 1980, tested many different models for trap efficiency (Figure 1.21). The most efficient model, with 71% and 90% efficiency for two tests, is a funnel with a baffle attached to the top.

This project utilizes simple plastic funnels for sediment capture attached to polycarbonate tubing for sediment accumulation (Figure 1.22). The bottom of the tubes are either plugged with a rubber stopper or sealed with electrical tape. Attached to the

top of each trap are one centimeter height baffles with a one centimeter square grid. The baffles serve to protect the sediment from possible bioturbation and to also facilitate sediment capture. The funnel-baffle system has been used for several years on the project. Year-to-year results will be well-correlated with the consistent system of sediment capture.

## Series III flume conditions and trap efficiencies

Experiment No.	8*	9	10**	Fish Tank
Time (hrs.)	10.8	11.3	17.3	17.3 hrs.
Velocity (cm/sec)	4.3	4.0	4.0	0
Flow Depth (cm)	14.3	14.8	14.8	24.2
Initial Conc. (mg/l)	34.4	31.2	82.4	46.1
Final Conc. (mg/l)	18.5	17.8	36.2	5.4

TRAP	EFFICIENCY			
	1	64%		
	2	67%		
	3	59%		
	4	60%		
	5	56%		
$\bar{E}$ 1-5		60%		
		44%	60%	
		65%	84%	82%
		71%	90%	
		136%	80%	81%
		62%		94%
		>264%***	550%	322%
			60%	
			65%	
				554%
				743%
				896%
				231%

\*A clockwise rotation of 180°, 45° and 135° was made on all traps at 3.0, 5.3 and 9.2 hours into the experiment.

\*\*Sediment which was mostly between 2-62 $\mu$ m was added to increase initial concentration.

\*\*\*Unknown amount lost during filtration.

Figure 1.21: Sediment trap models and their respective efficiencies. The model selected for this study is highlighted with the dashed blue box. The efficiencies are 71% and 90%, the most effective design in the study by Gardner (1980). Modified from Gardner, 1980.



Figure 1.22: Image of the sediment trap model used. The blue funnel is used to capture the sediment and the tubing collects the accumulation. The white baffle is a 1 cm<sup>2</sup> grid and protects the sediment from bioturbation.

## **1.8 – Previous Work**

The Svalbard REU has been conducting this project for five years. Nick McKay studied the 2003-2004 sediment year, Brookes Motley 2004-2005, Heidi Roop 2005-2006, Patrice Cobin 2006-2007. Each student studied the sediment traps for stratigraphy, grain size, and correlated the trap data to meteorological data from a nearby weather station. Leon, 2006, analyzed the laminated sediments for climate change. Other students have studied the valley for sediment provenance and many have studied the glacier for summer ablation. All of the information collected by the REU students pertains to this individual project.

## CHAPTER TWO

## METHODS



Twenty two sediment traps and three cores were retrieved and collected in the summer of 2008. The sediment traps were analyzed for visual stratigraphy with digital photos and X-rays and were analyzed for grain size using a Beckman Coulter LS 13 320 laser diffraction particle size analyzer system. The following methods describe in detail field and laboratory collection and analysis.

## **2.1 – Field Methods**

### *2.1.1 – Mooring and Sediment Trap Design*

The sites for sediment studies in Linnévatnet are the bathymetric depressions, i.e. the basins (Figure 2.1). Moorings with sediment traps and temperature loggers were deployed in the basins and on the bathymetric high separating the two proximal basins. The East Basin is the location for the most proximal site to the major inlet. Mooring C is 0.4 kilometers from the Linnéelva delta front in a depth of approximately 15 meters. Mooring D is located north of C about 1,000 meters from the inlet. The mooring is situated in 15 meters of water. Mooring E sits on a bathymetric rise which separates the East and West Basins. Mooring E is 700 meters from the major inlet in about 5 meters of water. Mooring F is located in the West Basin in 10 meters of water approximately 1,000 meters away from Linnéelva. Mooring G is the most distal site located 3,300 meters north of the delta. The mooring is situated in the deepest basin in Linnévatnet at approximately 35 meters of water.

Each mooring consists of a buoy attached to a rock anchor with a nylon line (Figure 2.2). The buoy is used to keep the line taught and is situated 1-2 meters below the water surface to prevent influence from wind and winter lake ice. Sediment traps and temperature loggers are attached to the mooring line. The number of traps per line



depends on the water depth. Moorings C, D, E, F, and G, have 4, 4, 2, 3, and 5 traps attached respectively. The deepest trap is always situated 1 meter above the lake bottom.

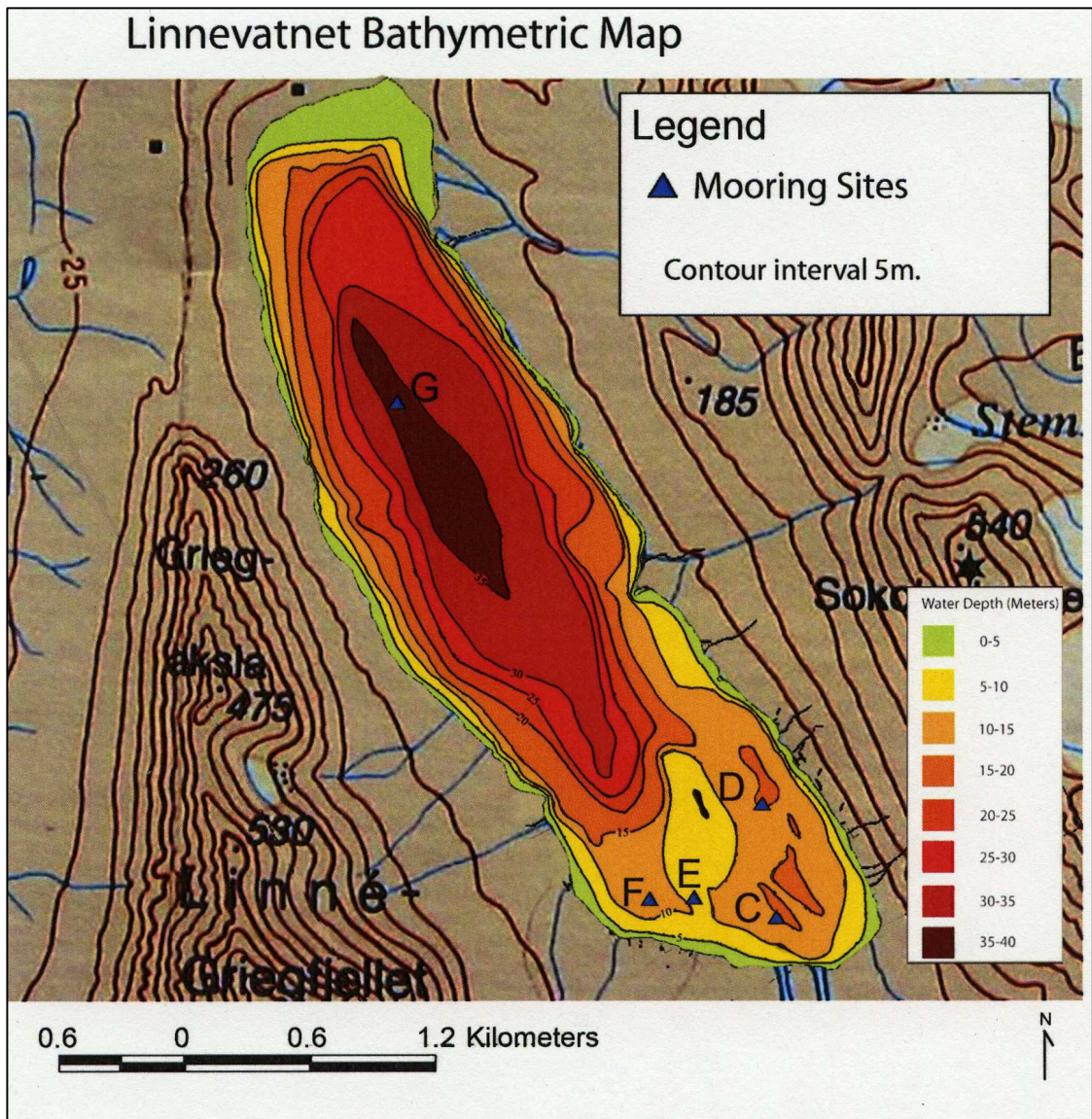


Figure 2.1: Bathymetric map of Linnévatnet. The triangles mark the mooring sites. Mooring C is the most proximal to the inlet. From Leon, 2006.

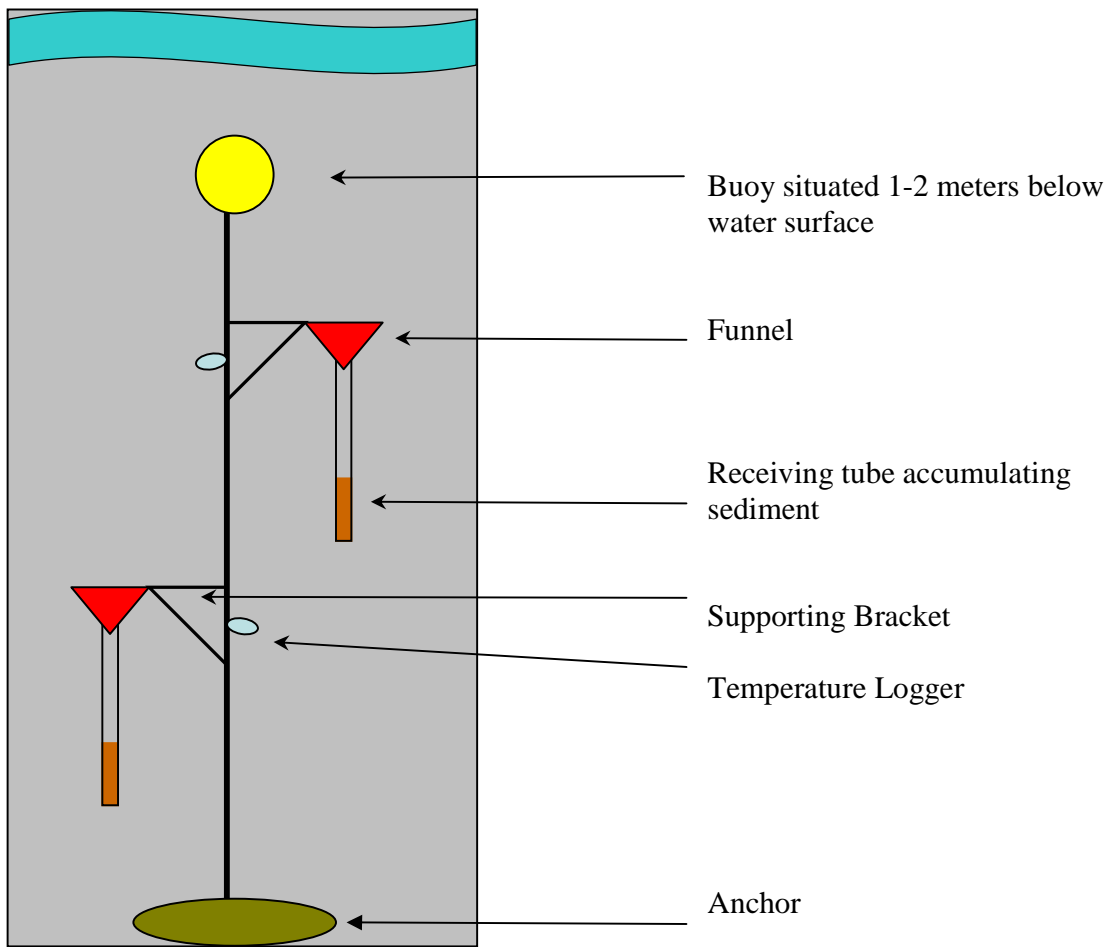


Figure 2.2: Diagram of a mooring. The number of traps depends on the water depth at the mooring site. Note the diagram is not to scale.

The sediment trap design utilizes a funnel to collect suspended sediment with the spout inserted into a polycarbonate receiving tube which is attached for sediment accumulation (Figure 2.3). The inner diameter of the receiving tube is 1.58 cm. The bottom of the tube is plugged with a rubber stopper to prevent leakage. A 1 cm<sup>2</sup> baffling is attached to the top of the funnel to protect sediment from resuspension and to facilitate sediment capture. The traps are attached to the mooring line with a plastic bracket. The bracket provides the necessary support to keep the trap vertical.

The traps designated “Year-Long” were deployed at each mooring July 26, 2007 and were retrieved between July 22 and August 1, 2008 (Table 2.1). The year-long traps use funnels with a diameter of 12.1 centimeters. “Spring Traps” were deployed at Mooring C on April 13, 2008 through lake ice and were recovered July 22, 2008. The spring traps use funnels which have a diameter of 17.4 cm. The larger diameter provides a magnification of sediment accumulation to describe the spring sedimentation events.

<u>Moorings</u>	<u>Deployed</u>	<u>Retrieved</u>	<u>Duration (days)</u>
Year-Long C	26-Jul-07	22-Jul-08	362
Year-Long D	26-Jul-07	28-Jul-08	368
Year-Long E	26-Jul-07	28-Jul-08	368
Year-Long F	26-Jul-07	28-Jul-08	368
Year-Long G	26-Jul-07	1-Aug-08	371
Spring C	13-Apr-08	22-Jul-08	100

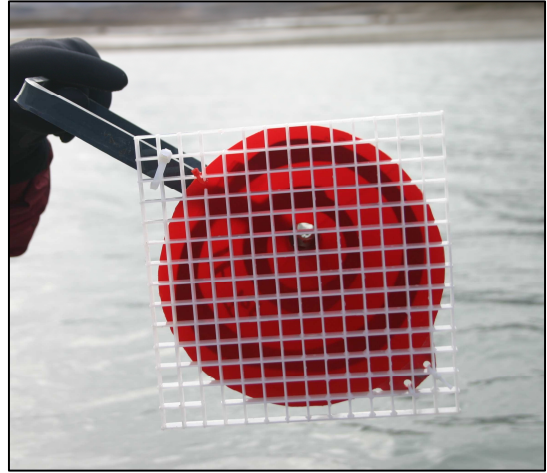


Figure 2.3: Image on the left is the year-long sediment trap complete with funnel, bracket, and receiving tube. Image on the right is the complete spring trap (From Motley, 2006).

### *2.1.2 – Sediment Trap Collection*

To retrieve the moorings and to collect the traps, GPS was used to locate the mooring sites. Once the buoy was sighted, a chain was lowered and wrapped under the buoy to pull the mooring line and anchor out of the water. A boom and pulley attached to the boat facilitated the retrieval (Figure 2.4). As each trap neared the pulley, it was detached from the line.

As each set of sediment traps was collected, they sat in a protected hut in the field to permit the suspended sediment to settle. The following day the stratigraphy was logged and marked on the tube prior to disassembling the funnel from the tube. The receiving tubes were sealed and carried by hand to the research station. At Isfjord Radio the water was siphoned out, the tube was cut to approximately 2 cm above the sediment, and the sediment was set next to indoor heater and allowed to almost dry. A paper towel was used several times to remove the excess water from each trap as it dried out. For transportation, a finger from a latex glove was stuffed with paper towel as absorbent packing and then inserted into the trap to protect the sediment from slumping or shifting.



Figure 2.4: The image illustrates the retrieval of the mooring. The pulley assists with the hauling of the mooring and the traps are removed from the line before reaching the pulley. From Cobin, 2008.



### *2.1.3 – Sediment Core Collection*

Three cores were collected in August 2008. Two cores were recovered adjacent to Mooring C and one near Mooring D. A Universal surface corer was lowered with a percussion hammer from the side of a zodiac. A calm day was necessary since the boat needed to hold position. Once the corer hit the lake bottom, the percussion hammer was lifted up and down to pound the corer deeper into the sediment. When the core tube appeared to have reached significant depth, the device was slowly pulled up. The corer was hauled up smoothly and before the tube had reached the surface, a plastic cap was placed on the bottom, to prevent loss of sediment.

Once the core tube was removed from the coring device, another plastic cap was placed on the top and the tube was carried back to Isfjord Radio. At the station, water was siphoned and the core tube was cut to 5 – 10 centimeters above the sediment. As the sediment dried, water accumulation was siphoned. For travel packaging, a thin plastic sheet was placed over the sediment and absorbent paper towels were tightly packed on top.

### *2.1.4 – Weather and Environmental Data*

An Onset HOBO weather station is located approximately a kilometer south of the lake in Linnédalen (Figures 2.5 and 2.6). This station measures precipitation, wind speed and direction, air temperature, ground temperature, and solar radiation upwards and downwards. The measurements were recorded in thirty minute intervals since July 2007. The most pertinent meteorological data to this study are precipitation and air temperature since these parameters greatly affect glacial melt and stream discharge.

In the lake, a network of Onset Water Temp Pro loggers is arrayed on the mooring lines. Each mooring has a temperature logger with the sediment trap as well as a logger on the rock anchor. The spring trap mooring at C had temperature loggers at every meter of depth, thus 14 temperature loggers on one line. The loggers recorded water temperature every thirty minutes since July 2007 and the Mooring C spring traps since April 2008.

Mooring C was also the location for the In-Situ Inc. 9000 Pro XP/e Troll (Figure 2.5). This instrument was situated 1 meter above the lake floor. The Troll measured temperature, turbidity, conductivity, and depth every two minutes since April 2008 and was retrieved July 22, 2008.

The intervalometer was deployed at Mooring C as well, approximately 1 meter above the lake bottom (Figures 2.5 and 2.7). This instrument is similar in design to a sediment trap with a 10 cm funnel attached to a receiving tube and covered with a 1 cm<sup>2</sup> baffle. However, the intervalometer measures sediment accumulation through light transmission utilizing an inverting Schmitt trigger. When the light source and receivers are in “sight” of each other, the switch is off; when the LED lights and receivers are blocked, the switch turns on. As the sediment settles into the receiving tube, LED lights are blocked from the receivers, turning the switch on, and subsequently increasing voltage. The sediment accumulates in the bottom of the receiving tube and covers the sensors as it increases in vertical thickness; thus voltage increases throughout time.

Onset Optic Stowaway temperature loggers (Figure 2.5) were deployed at two locations in Linnéelva. The “lower-stage” was approximately 75 meters south of the lake. The “mid-stage” was approximately half-way between Linnévatnet and

Linnébreen. The loggers were attached to a rock and placed in the deepest part of the river. They recorded water temperature every thirty minutes since July 2007.

An automated time lapse camera was installed along the eastern side of the valley (Figures 2.5 and 2.8) in 2006 and has been downloaded several times a year since then. The camera faced SSW (N78 02.220, E13 52.319) overlooking the south end of Linnévatnet, where Linnéelva empties into the lake. The camera recorded images twice a day, at 11:00 am and 4:00 pm, in the fall and spring. These images provide a visual record of activity with lake ice, stream ice, and snow melt.

A snow depth device was deployed at the mid-stage stream location (Figures 2.5 and 2.9). This device was a snow “tree” – a two-by-four stand with four rungs at 7 cm, 15 cm, 30 cm, and 45 cm above the ground. Attached to each rung was an Onset HOBO light intensity logger. Each logger measured light intensity at 30 minute intervals from July 2007 to July 2008. The loggers recorded when the light intensity dropped to 0, which indicated either nightfall or when the logger was covered by snow. After the period of minimal light intensity, the loggers showed a dramatic increase in intensity which indicated that the snow had melted enough to expose the logger. This device provides a record of snow depth of up to 45 cm.

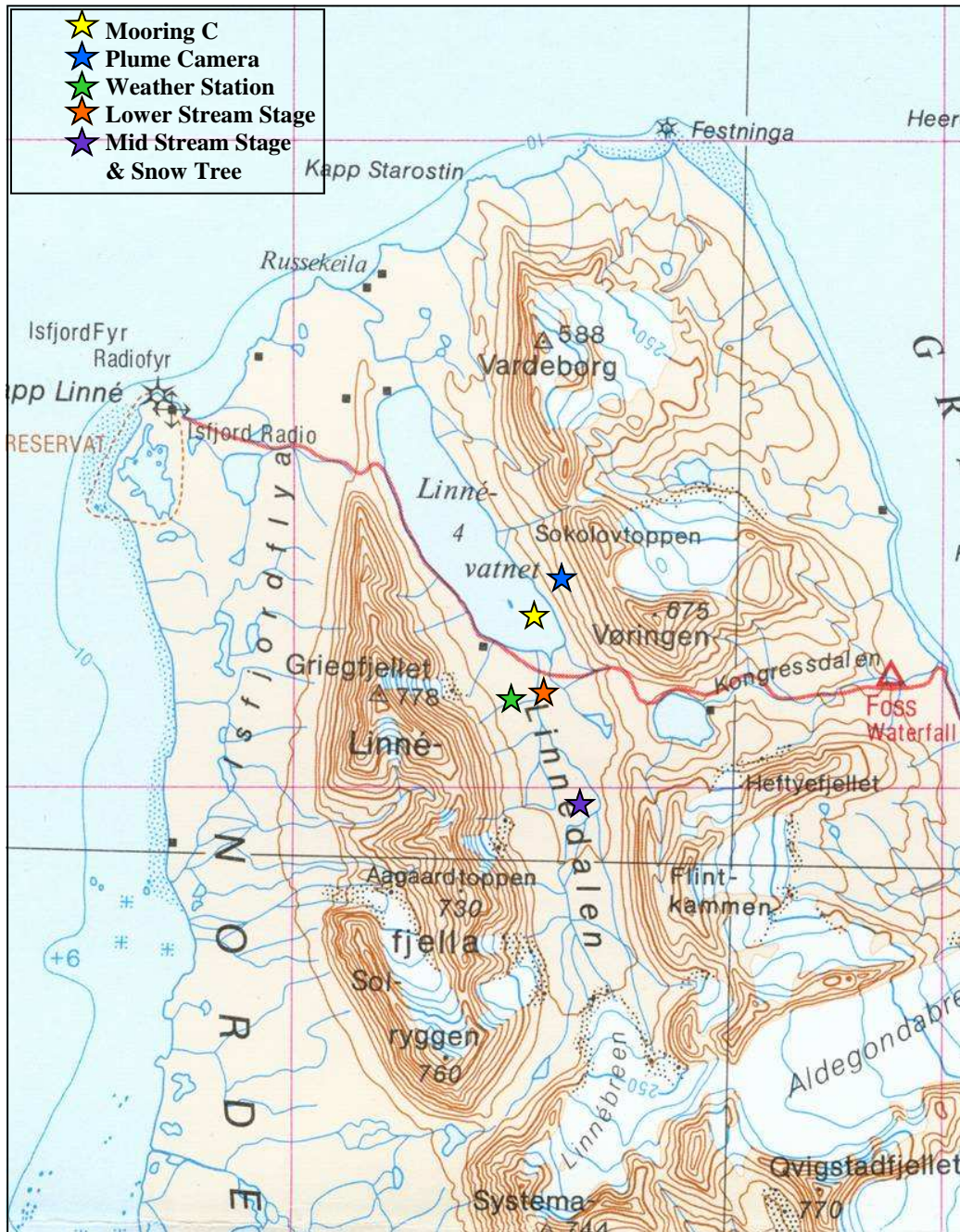


Figure 2.5: The locations of environmental and weather instruments. The legend is in the top left corner. Modified from Norsk Polar Institute, 1936.

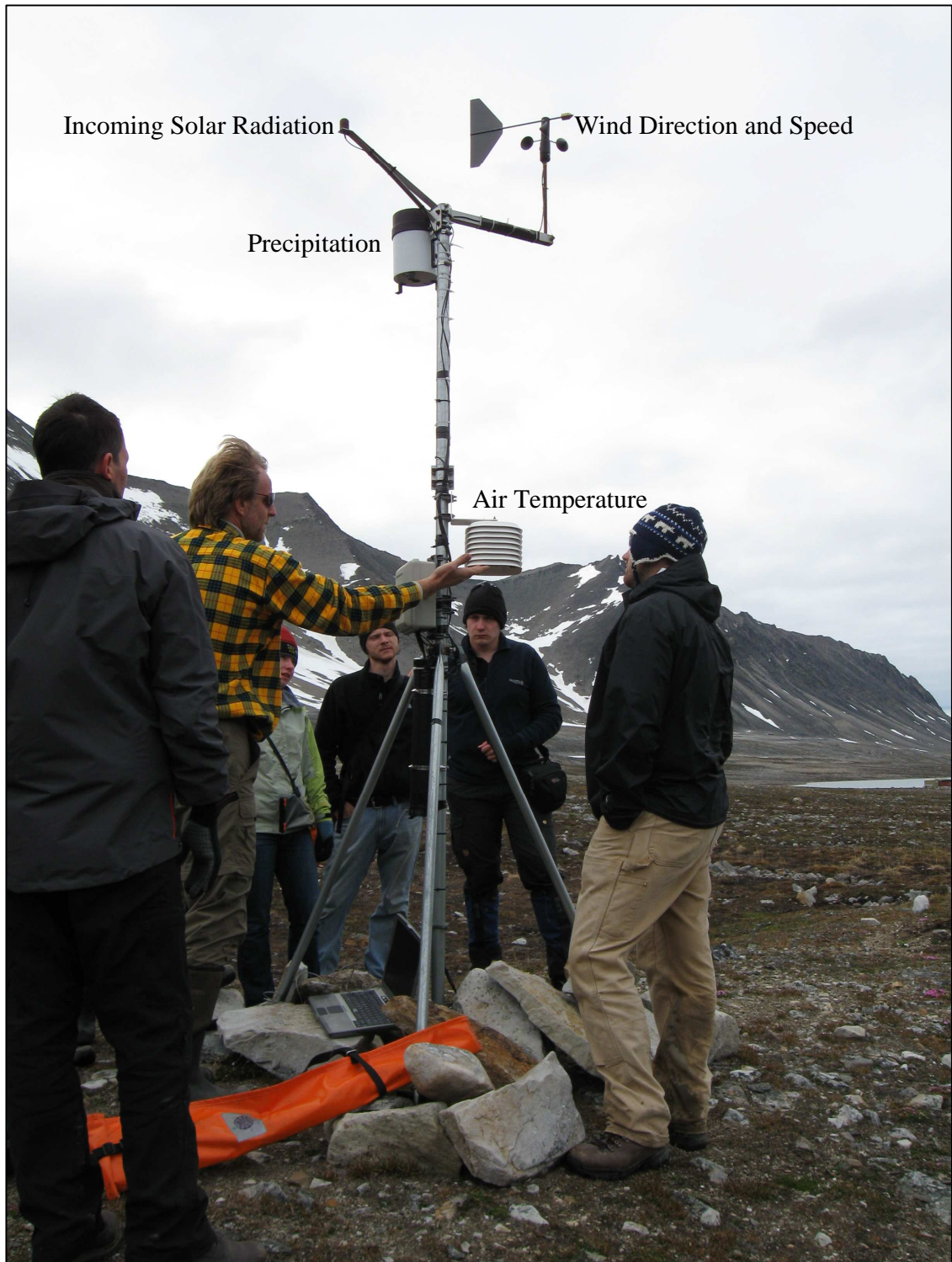


Figure 2.6: The Onset HOBO weather station.



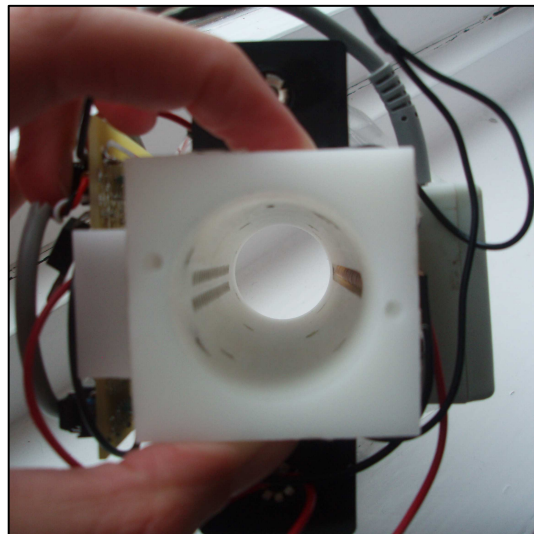
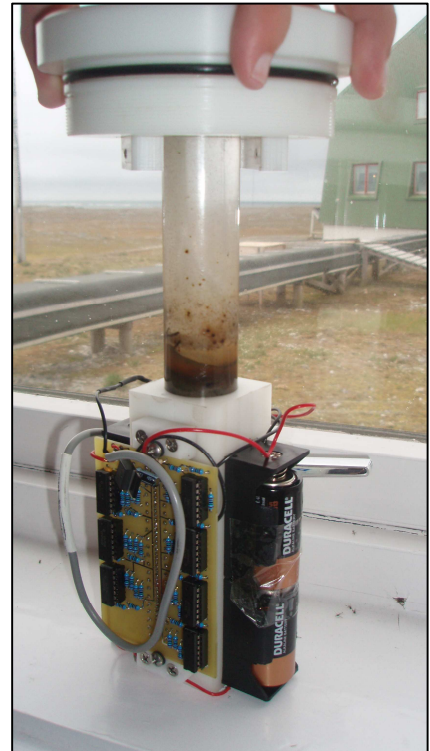


Figure 2.7: The intervalometer is like a sediment trap with a funnel, baffle, and receiving tube (top left). The receiving tube is held within casing with LED lights (top right). The bottom image shows the LED lights and receivers which measure sediment thickness.



Figure 2.8: The automated time lapse camera is encased in the white plastic box for protection (top image). The bottom image shows the view from the camera in one of the daily photos.



Figure 2.9: The snow tree consists of a two by four stand with rungs attached. The loggers are at 7 cm, 15 cm, 30 cm, and 45 cm from the bottom to the top.



## **2.2 – Laboratory Methods**

### *2.2.1 – Splitting the Samples*

The 22 sediment trap samples and the three cores were split open at Mount Holyoke College. The device used to split the trap samples and cores was designed and operated by Thomas Liimatainen of Mt. Holyoke College. This device was designed to split each sample with minimal sediment disturbance. The device utilized a handmade circular blade on a router that was attached to a sliding bar (Figure 2.10). The sediment samples were locked into a rail prior to splitting (Figure 2.11). Each sample had a piece of paper towel atop the sediment to block any polycarbonate debris from blowing into the sample. A cut was made on the sample tube by sliding the router rail past the sample. The smooth and even cut was just deep enough to reach the sediment. A thin aluminum sheet was inserted through the cut into the sample and the sample was rotated 180°. The second cut was made by sliding the router rail across the sample again and the sheet was pushed through to the second cut. The sheet evenly split the sample into two halves and prevented leakage. The sample was then plugged, taped, and sealed for transportation Bates College.

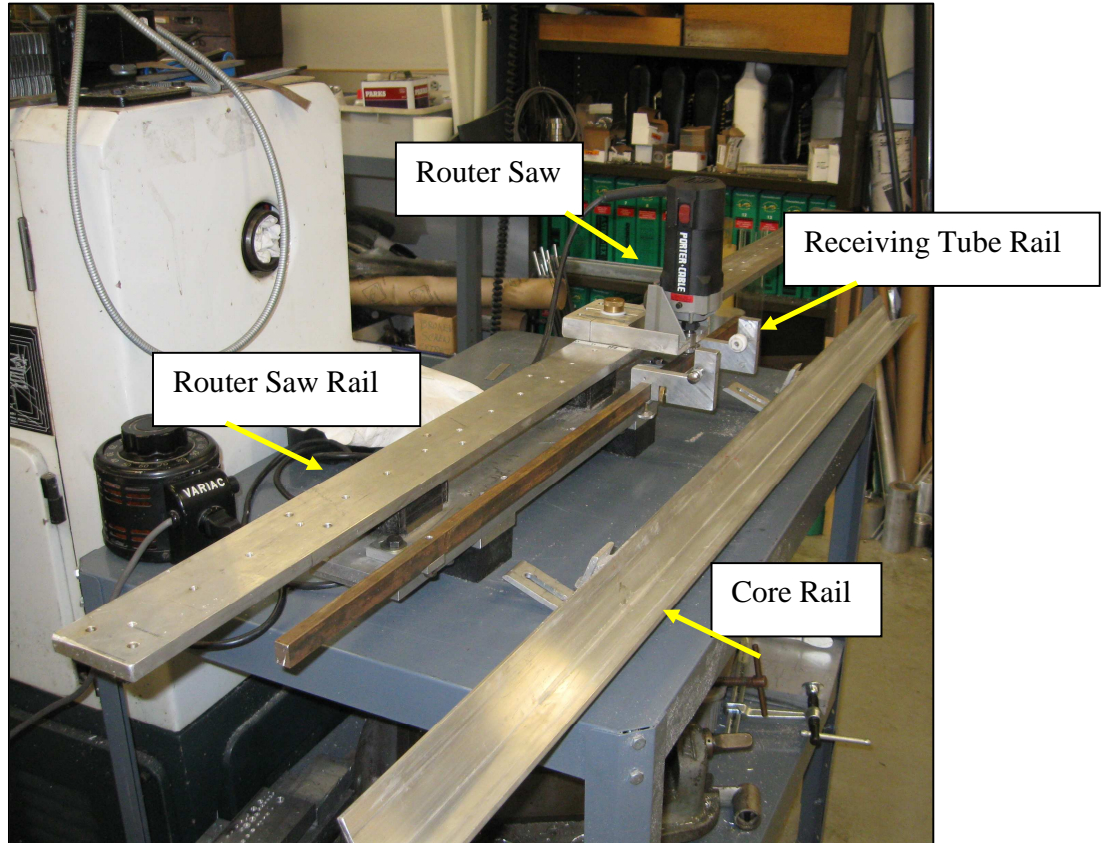


Figure 2.10: The receiving tube and core splitting device.

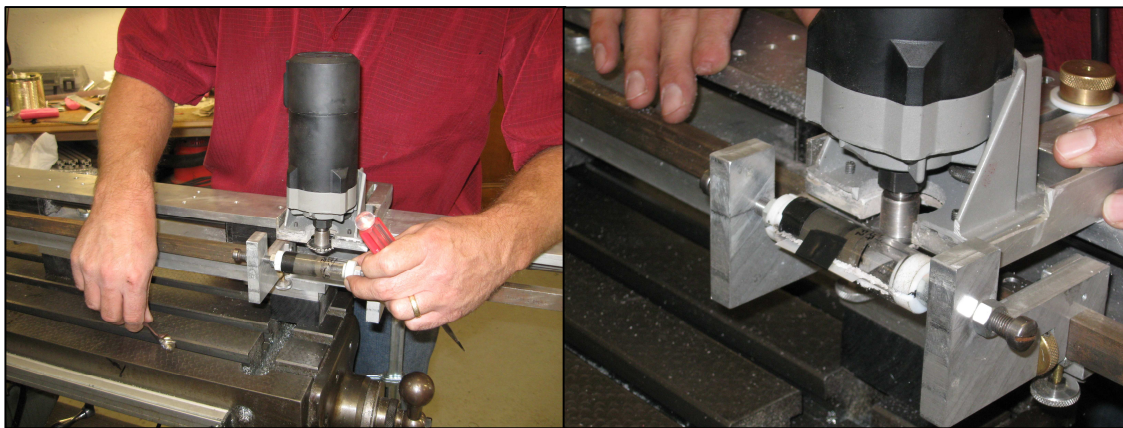


Figure 2.11: Cutting a sediment trap sample. The figure on the left depicts Thomas Liimatainen setting up the saw and sample. The image on the right shows the first cut with the aluminum sheet inside.

### *2.2.2 – Visual Stratigraphy*

Two methods were used to record visual stratigraphy of the samples after splitting the traps and core tubes. First, digital photos of the trap and core samples were captured with a Canon 590A camera. Each sample was accompanied with a Munsell Soil Color chart as a color key (Figure 2.12). The traps and cores were logged for sediment thickness and color. The second set of visual stratigraphy was X-ray images. One half of the bottom two samples from Moorings C and D and three U-channels of the upper 10-12 cm of the sediment cores were X-rayed at the Mt. Holyoke Health Center. The X-rays were captured using Kodak film in film canisters designed for fine bones which yield a high resolution. Each sample was exposed to 3 mA, 30 to 45 kV from 3-5 seconds. The energy and exposure times depended on the density of the sediment. The X-ray images described the sediment visually for density. The lighter regions were finer grained and the darker regions were coarser grained. The X-rays were particularly useful when the color of the sample was homogenous throughout without a color distinction between seasonal layers.

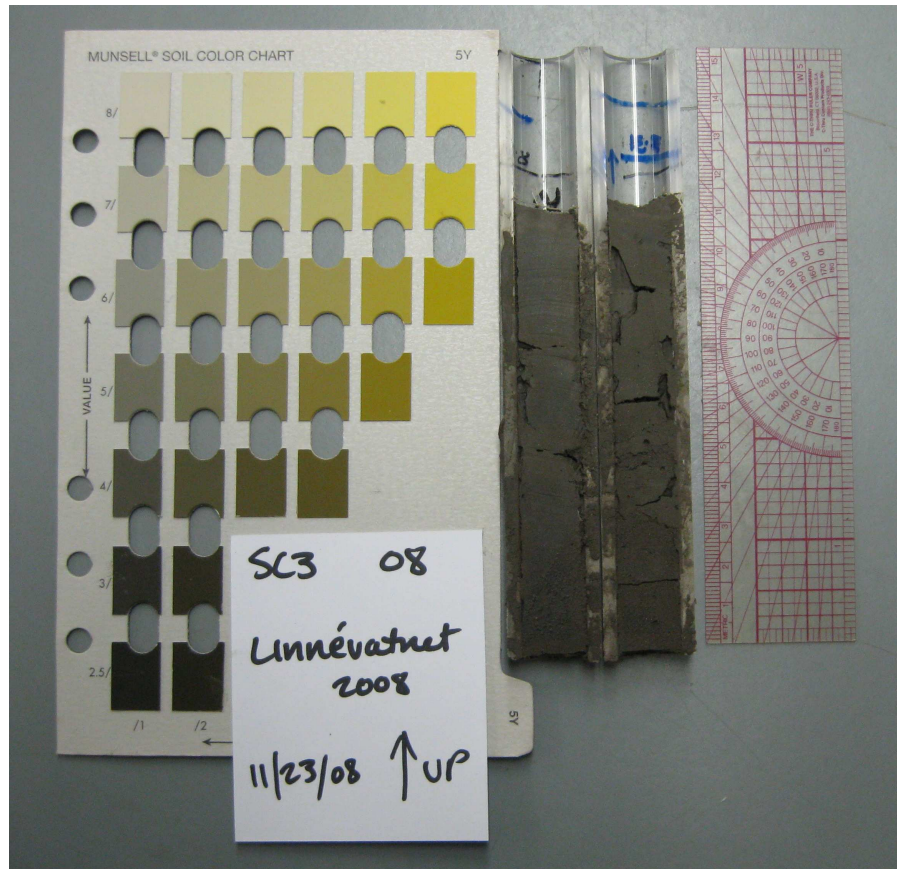


Figure 2.12: An example of the digital photography of the samples. The sample is from the spring trap at Mooring C.

### 2.2.3 – Sediment Flux and Equivalent Thickness

To quantify the sediment accumulation in all of the traps, the raw data had to be corrected for the magnification factor of the funnel size since the year-long traps and the spring traps have different funnel sizes. To compare the two sets of traps, sediment flux was determined from the following equation,

$$\text{Sediment flux} = (\text{mass of sediment in trap}) / (\text{area of funnel opening})$$

$$f = m_t / a$$

in which  $f$  is the sediment flux,  $m_t$  is the mass of the sediment in the trap, and  $a$  is the area of the funnel opening (year-long traps have 115 cm<sup>2</sup> and spring traps have 238 cm<sup>2</sup> openings). The mass of the sediment in each trap was determined by calculating the density from the mass of 0.5 cm<sup>3</sup> samples of dry sediment. These density values were then used with the volume of the sediment (used the lab thicknesses of the samples) to calculate the mass of the sediment in the trap:

$$m_t = (\text{Dry Density}) * (\text{Sediment Volume})$$

The sediment flux from the bottom traps may also indicate the amount of sediment deposition on the lake floor. This vertical thickness ( $t$ ) of mm/year can be calculated using the mean bulk density of 1.8 g/cm<sup>3</sup> calculated from Linnévatnet sediment cores (McKay, 2004). The thickness is calculated with the sediment flux, bulk density, and a factor of 10 to convert from cm to mm:

$$t = (f / 1.8 \text{ g/cm}^3) * 10$$

#### *2.2.4 – Grain Size Analysis*

The grain size analysis was completed using a Beckman Coulter LS 13 320 Particle Size Analyzer at Bates College. To obtain the optimum concentration of sediment for analysis, a volume of 0.125 cm<sup>3</sup> was used. The best halves of the split sediment traps were used for sub-sampling and were sliced from the bottom to top at 0.25 cm. The dimensions of the slices were 1 cm x 0.25 cm x 0.5 cm (Figure 2.13). Each sub-sample was placed in a 47 mL Oak Ridge centrifuge tube and covered with 1 mL of hydrogen peroxide to disintegrate organic matter. The samples were capped and sat overnight.

The following day a mixture of 20 mL dionized water and 17 mL of a dispersant solution (0.7 g/L sodium metaphosphate) was added to each sample. A Fisher Scientific 60 Sonic Dismembrator was then used to deflocculate any fine particles that remained aggregated; each sample was sonicated for two minutes.

The Coulter LS 320 measures particle size using a single wavelength laser diffraction analysis (Figure 2.14). A laser beam shot through a chamber with the particle solution and light was scattered by the particles at known patterns; grain size was inferred from these patterns. The Coulter LS 13 320 measured a range of grain size from 0.4 to 2000 microns.

For particle size analysis, each sample was completely washed out of the centrifuge tube with dispersant into the Coulter sample well and was sonicated during the loading. The Coulter sonicated the sample as it ran through a series of laser diodes and photodetectors. Three runs were completed for each sample but the last run data were used to complete this study since the samples were most disaggregated at that point.



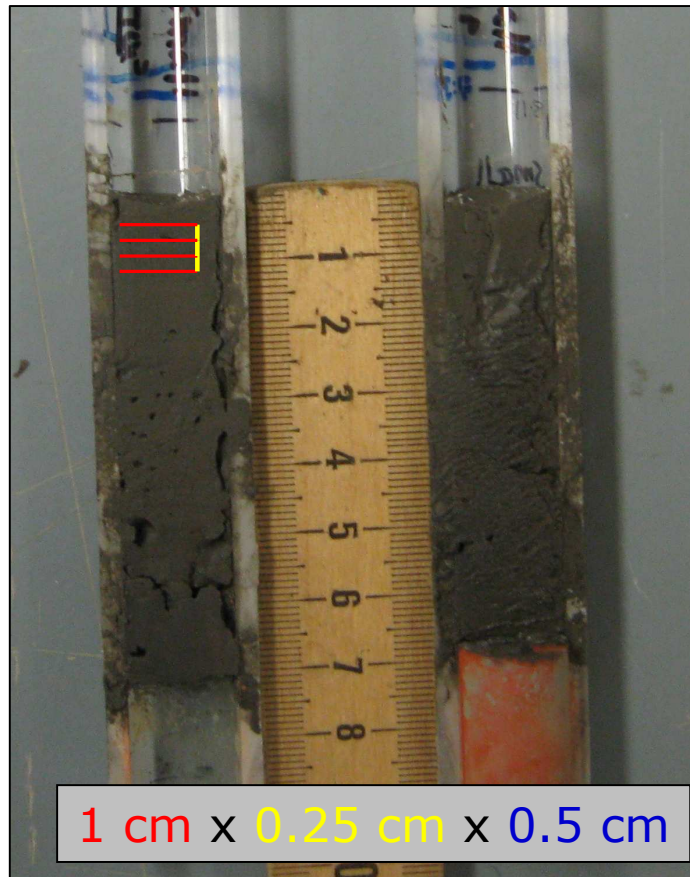


Figure 2.13: The dimensions of the sediment slices. The 0.5 cm is the vertical depth of the sediment.

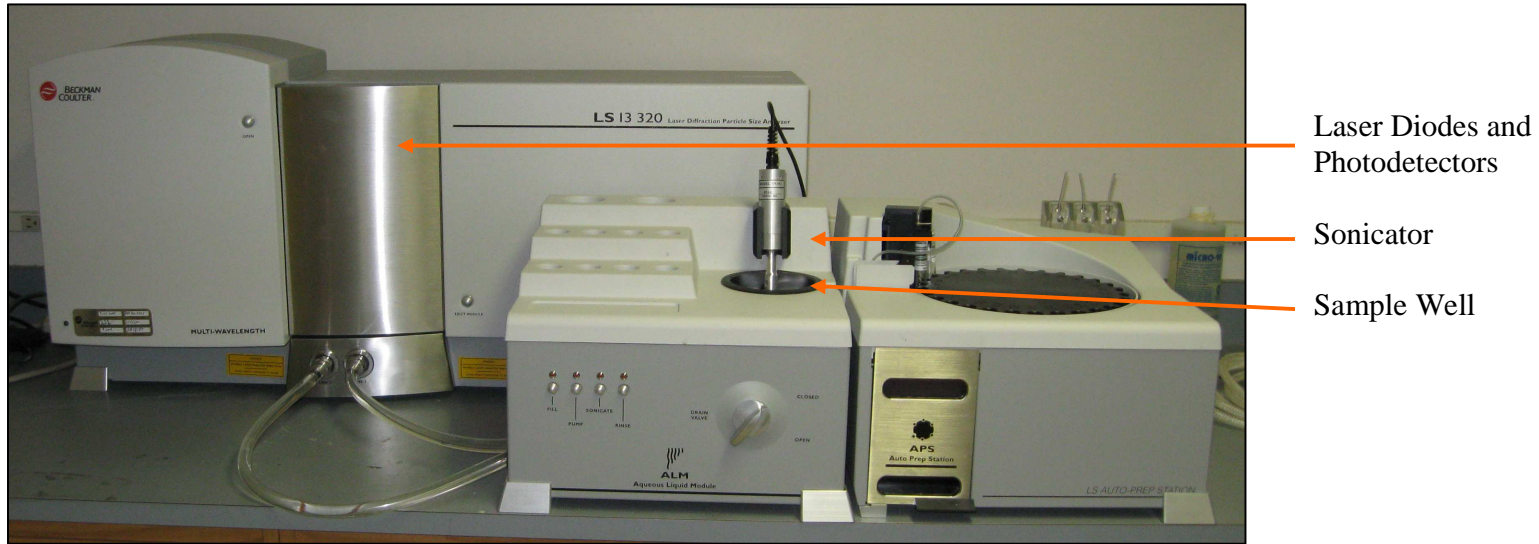


Figure 2.14: A diagram of the Beckman Coulter LS 13 320 at Bates College. The samples were washed into the sample well, sonicated, and analyzed in the laser compartment.



### *2.2.5 – Thin Section Preparation*

For the sediment core analysis, a core from Mooring C and a core from Mooring D were prepared for thin sections. The thin sections provide the optimal visualization for analyzing sediment stratigraphy. The desired samples were removed with aluminum trays which had 1/8 inch holes drilled into all sides. The trays were made from aluminum cutouts of 7 x 2 x 1 cm dimensions. Labels were scratched into the aluminum. The trays were pushed open-side down into the sediment with the top of the core just inside the container. The samples were cut out with an X-Acto knife and fishing line.

A freeze-drying method was used to remove the interstitial pore water from the samples (Leon, 2006). First, the samples were frozen with liquid nitrogen (Figure 2.15). A container of liquid nitrogen was set at an angle and the samples were placed at the highest position of the container. In order to prevent cracks in the sediment, the samples were slowly (5 minutes) pushed down the incline from the shallow end to deep end until submerged. After a minute of submersion, the samples were transferred to another box with sufficient liquid nitrogen for another submersion of 10 minutes.

While the samples were freezing, the Labconco freeze drier was prepared by cooling the collector coil to approximately -43 °C. The samples were placed in the vacuum chamber with enough space between to permit substantial air flow. The vacuum was then slowly applied to prevent the sediments from exploding. The samples were left in the freeze drier for 3 days and were removed by slowly releasing the vacuum to prevent damage to the samples.

A solution of low viscosity epoxy resin was prepared to embed the samples (Clark, 1995; Lamoureux, 1994). The mixture included Vinylcyclohexene dioxide

(VCD), Diglycidyl ether of polypropyleneglycol (DER 36), Nonenyl succinic anhydride (NSA), and Dimethylaminoethanol (DMAE). The chemicals were mixed in a plastic deli cup by weight to a total of 300 g and stirred for a full minute. The components of the epoxy mixture were mixed by a ratio of mass.

$$\text{VCD} : \text{DER} : \text{NSA} : \text{DMAE} :: 10 : 4 : 26 : 0.4$$

<b>Component</b>	<b>Mass (g)</b>	<b>Cumulative Mass (g)</b>
VCD	74.20	74.20
DER	28.8	103.00
NSA	194.00	297.00
DMAE	3.20	300.2

Table 2.2 describes the mass and cumulative mass of the epoxy components which were mixed on the balance.

When the epoxy was thoroughly mixed, the samples were placed in a plastic dish with the orientation and labels written on the outside of the container. The epoxy was then gradually poured along the side of the dish until it reached a third of the samples' height (Figure 2.16). To assist the impregnation, the samples were placed in a vacuum chamber. The vacuum was created by a hose attached to a valve on a faucet. The vacuum was slowly increased to 25 – 30 inHg. The samples were left in the chamber for several hours until they had absorbed the epoxy. Once the surface of the samples appeared wet, they were removed, placed in a smaller dish, and epoxy was added until the samples were completely submerged. The dish was placed in an oven at a temperature of 50° C for 48 hours to allow the epoxy to cure. When the epoxy could not be scratched by a fingernail, the samples were removed.

A band saw was used to trim the sides of the samples to cut away the aluminum cradle with minimal disturbance to the sediment. Labels were scratched into the top of the bricks. The samples were then packed and shipped to Mt. Holyoke College Earth and Environment Department for mounting on slides, grinding, and polishing.



Figure 2.15: The slanted box was used for the liquid nitrogen slow submersion while the standing box was used for complete submersion (From Leon, 2006).



Figure 2.16: This image illustrates the epoxy impregnation. The box on the right has epoxy half-way up the side of the freeze-dried blocks. The box on the left shows the samples fully submerged (From Leon, 2006).

## CHAPTER THREE

### RESULTS



### **3.1 Visual Stratigraphy**

#### *3.1.1 – Trap Description*

In the field, immediately after collection, all of the sediment traps showed distinct light and dark layers. Although the stratigraphy was recorded in the field, the sediment thickness changed greatly as the samples dried. Unfortunately after the traps were split the color homogenized throughout all of the traps, losing the color stratigraphy. All of the traps showed a uniform color of 5Y 3/1 according to the Munsell Soil Color chart throughout the sediment.

#### *3.1.2 – Digital & X-ray Images*

Several photographs were captured of each trap in the field and in the lab. These images are on the attached CD. The traps were shown with a scale and a Munsell Soil Color chart. X-ray images were collected for traps C3, C4, D3, and D4. These images were captured in attempt to show the density change between winter and summer sediment. Figure 3.1 shows the sediment traps C4 and D4 X-rays. The density changes are slight but visible.

#### *3.1.3 – Core & Thin Section Description*

The C1 core was not used for this study since there was a significant amount of suspended sediment above the sediment-water interface when it was collected. The sediment core C2 was used in this study for thin section analysis (Figure 3.2). Textural and color variation of individual laminae were visible in the 16.5 cm long core. The laminae alternated in light and dark brown color.

The thin section was 7 cm long and showed good sediment stratigraphy for the upper laminae (Figure 3.3). However, the thin section is damaged in the middle.



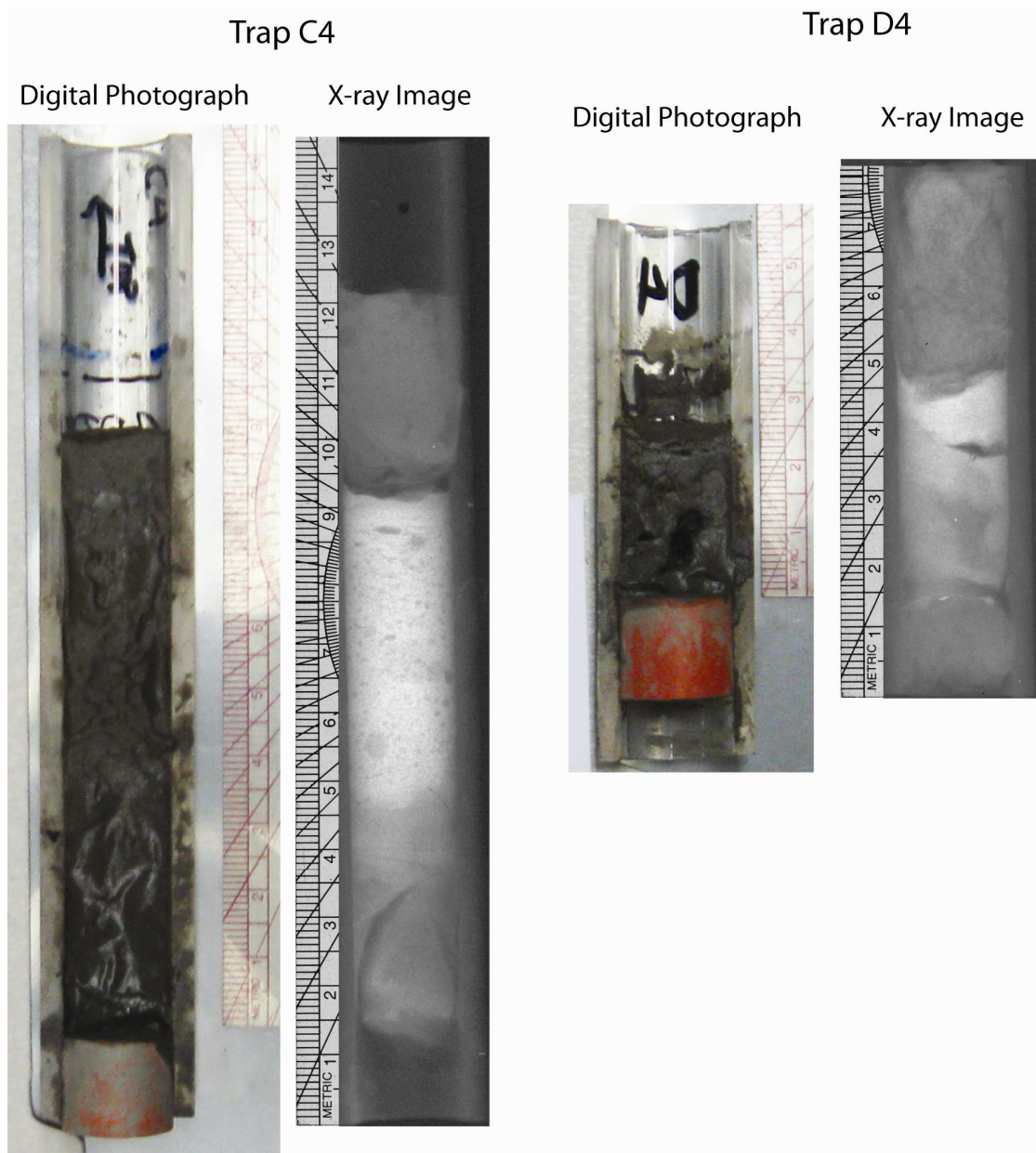


Figure 3.1: The digital photographs and the X-rays for traps C4 and D4. Both sets of images are in the same scale. The changes from light to dark in the X-rays are visible indicating the boundary between fine winter sediment and coarse summer sediment. The tops of the traps are aligned with the top of the page.

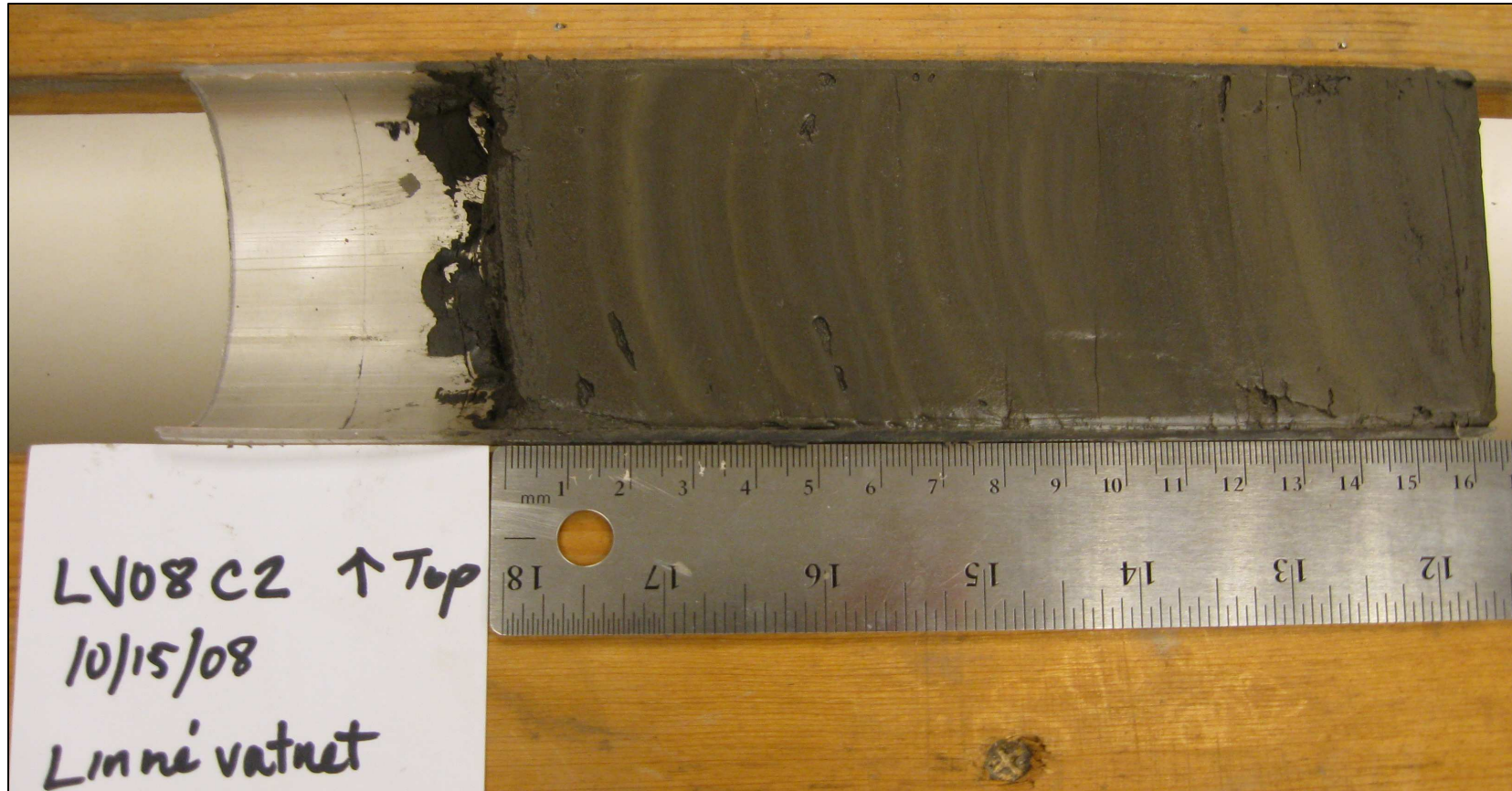


Figure 3.2: Image of the C2 core that was used for the thin section analysis. The laminae are visible by color and texture.



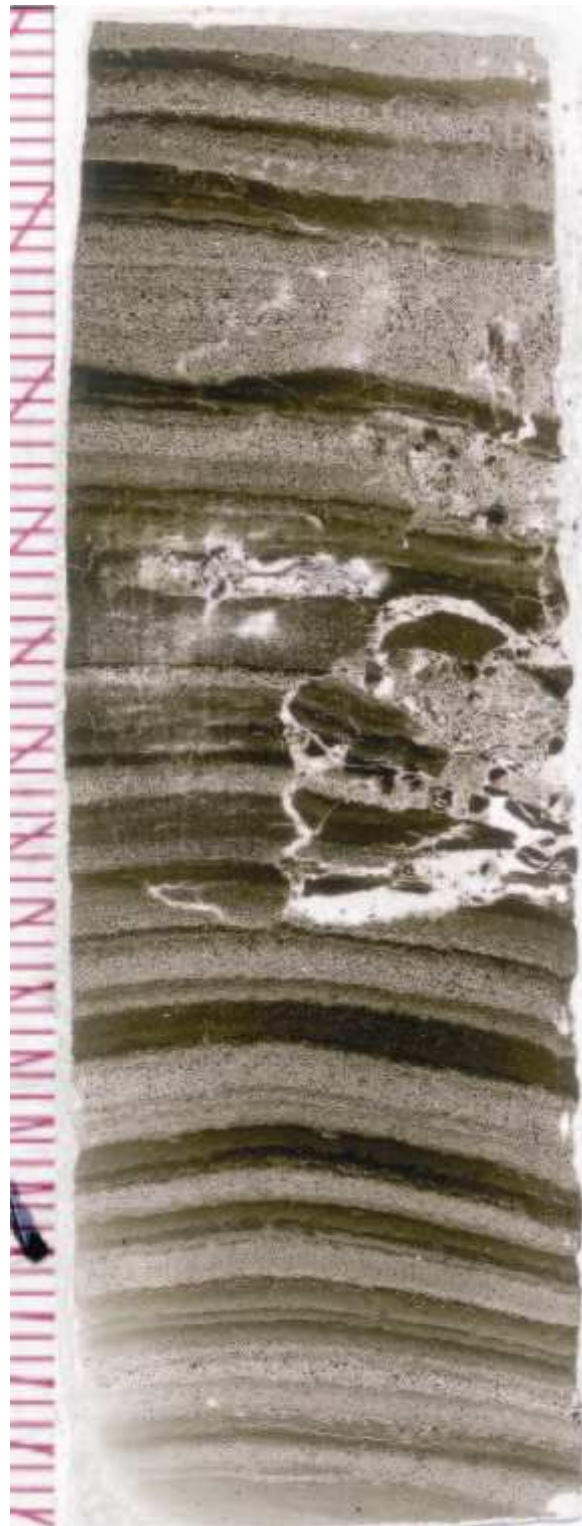


Figure 3.3: Thin section of core C2. The scale to the left is in mm. This thin section has sediments from the uppermost layers of the core. Top of the thin section is aligned with the top of the page.

### 3.2 – Sediment Flux and Equivalent Thickness

Table 3.1 and Figure 3.4 describe the total sediment flux of each trap. The sediment flux account corrects for differing funnel size, thus allowing the spring traps compare with year-long traps. The sediment flux from the bottom traps reflect mass of sediment per unit area deposited on the lake floor. The lake bottom accumulation is calculated from the sediment flux and the mean bulk density from Linnévatnet sediment cores to show the vertical thickness of the depositional laminae.

<u>Year-Long Trap</u>	<u>Sediment Flux</u>	<u>Lake Bottom Accumulation</u>	<u>Spring Trap</u>	<u>Sediment Flux</u>	<u>Lake Bottom Accumulation</u>
	<i>g/cm<sup>2</sup></i>	<i>mm/yr</i>		<i>g/cm<sup>2</sup></i>	<i>mm/yr</i>
C2	0.117		SC1	0.045	
C3	0.075		SC2	0.072	
<b>C4</b>	<b>0.164</b>	<b>0.9</b>	<b>SC3</b>	<b>0.089</b>	<b>0.5</b>
D1	0.050				
D2	0.029				
D3	0.030				
<b>D4</b>	<b>0.044</b>	<b>0.3</b>			
E1	0.080				
<b>E2</b>	<b>0.076</b>	<b>0.4</b>			
F1	0.024				
F2	0.034				
<b>F3</b>	<b>0.046</b>	<b>0.3</b>			
G1	0.016				
G2	0.036				
G3	0.040				
G4	0.032				
<b>G5</b>	<b>0.092</b>	<b>0.5</b>			

Table 3.1: The sediment fluxes for each trap give corrections for funnel size. Equivalent thicknesses for the bottom traps are given for lake bottom accumulation.

The sediment fluxes at Mooring C for the year-long trap are 0.117, 0.075, and 0.164 g/cm<sup>2</sup> for C2, C3, and C4 respectively. It was expected for C4 to accumulate the most sediment throughout the year and thus have the greatest sediment flux. The spring-

moorings were corrected for funnel size with the sediment flux equations. The fluxes for spring Mooring C were 0.045, 0.072, and 0.089 g/cm<sup>2</sup> for SC1, SC2, and SC3 respectively. Trap SC3 was expected to accumulate the most sediment in the spring since it is located at the bottom of the lake. The sediment flux for SC3 is 54% of the year-long C4 sediment flux, thus the spring and summer sedimentation consists of 54% of yearly accumulation.

Trap C4 indicates that the expected lake bottom deposition is 0.9 mm/year and SC3 indicates that 0.5 mm/yr is expected deposition. Thus, 56% of lake deposition at Mooring C is expected to be spring / summer sediment. The spring flux and deposition percentage of the year's sedimentation correspond well.

Mooring D and E show sediment fluxes which are not the greatest on the bottom, but rather the top traps. Trap D1 has 0.050 g/cm<sup>2</sup> and trap D4 has a flux of 0.044 g/cm<sup>2</sup>. On Mooring E, E1 has a flux of 0.080 g/cm<sup>2</sup> while E2 has 0.076 g/cm<sup>2</sup>. Moorings F and G describe fluxes which have a general increasing trend with depth. Trap F3 has a flux of 0.046 g/cm<sup>2</sup> and trap G5 shows a flux of 0.092 g/cm<sup>2</sup>.

The basin sites Moorings D and F show equivalent thicknesses which decrease with distance from the inlet. Mooring C has a thickness of 0.9 mm/yr; Mooring D and F show a thickness of 0.3 mm/yr. However, the deep-basin Mooring G does not express a decrease of lake bottom deposition with distance. Trap G5 expresses an equivalent thickness of 0.5 mm/yr, which is twice the thickness at Moorings D and F. Mooring E is on a bathymetric rise, thus is not comparable to the basin accumulation.

### Sediment Flux for 2007 - 2008

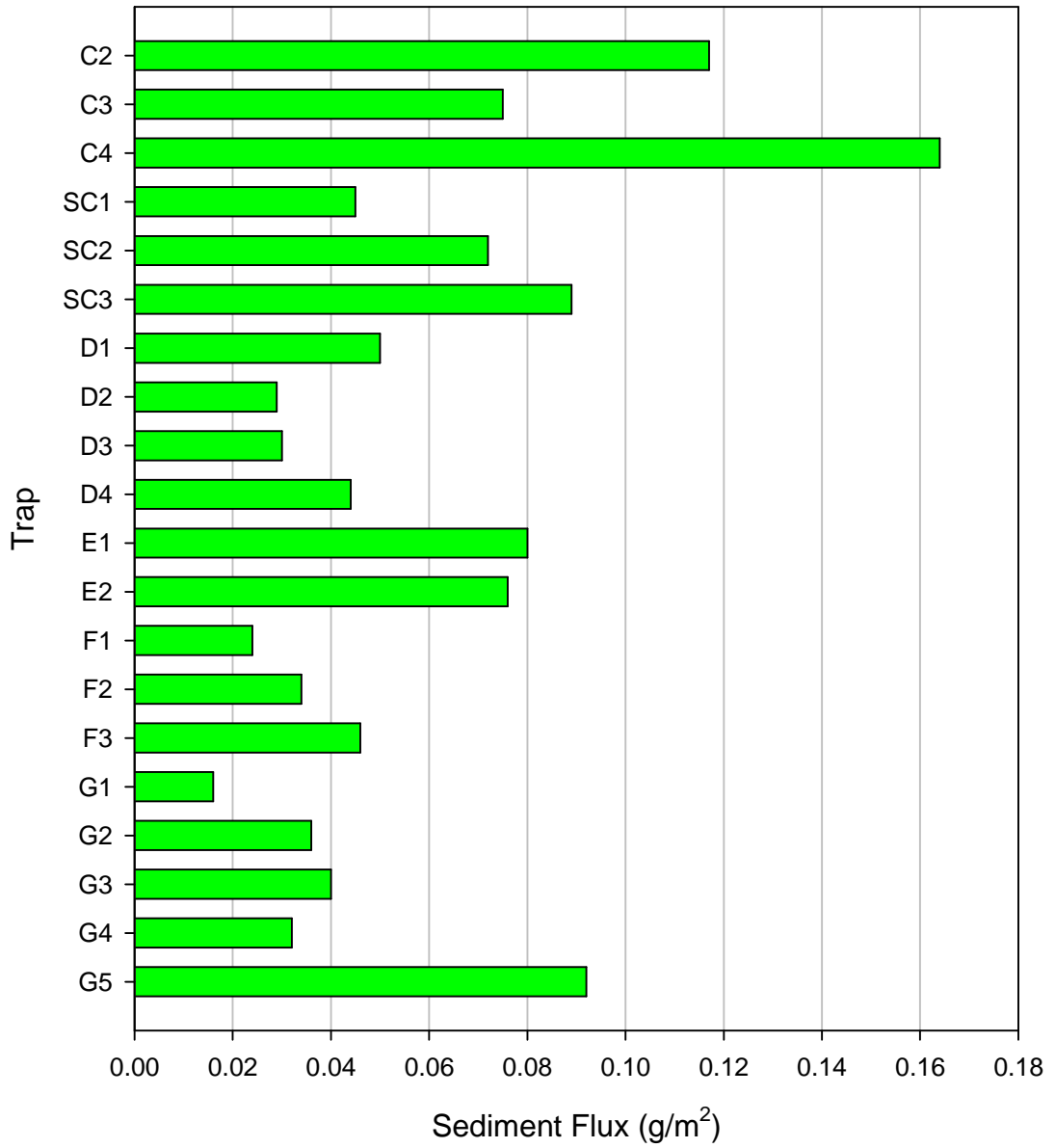


Figure 3.4: A graphical representation of sediment flux in all of the sediment traps.

### **3.3 – Grain Size Analysis**

#### *Mooring C: Year-Long Traps (Figure 3.5)*

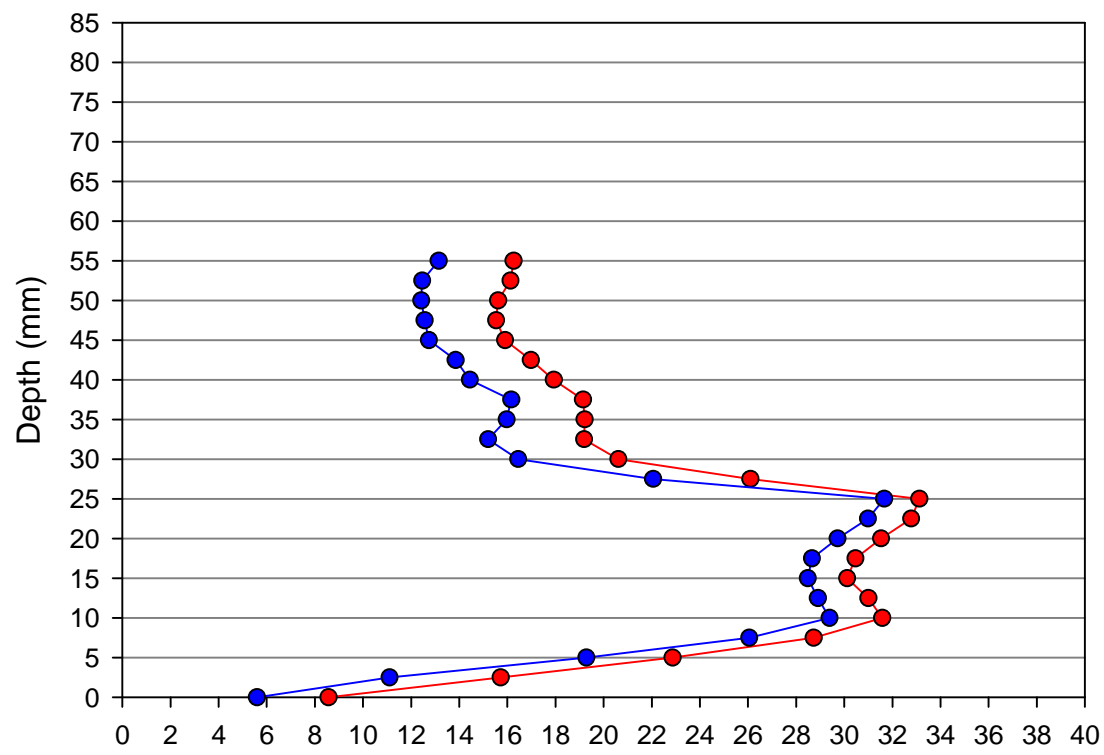
Trap C1, situated at three meters depth, was lost during the retrieval of the mooring line and thus will not be discussed.

Trap C2 was located at six meters depth. The first sediment in the trap at 0 mm has a mean grain size of 8.6 microns. The grain size increases to 31.6 microns at 10 cm. From 10 mm to 25 mm the grain size ranges from 31.6 to 33.1 microns. At 30 mm the mean particle size is 20.6 microns and continues to fine to 16.3 microns at 55 mm.

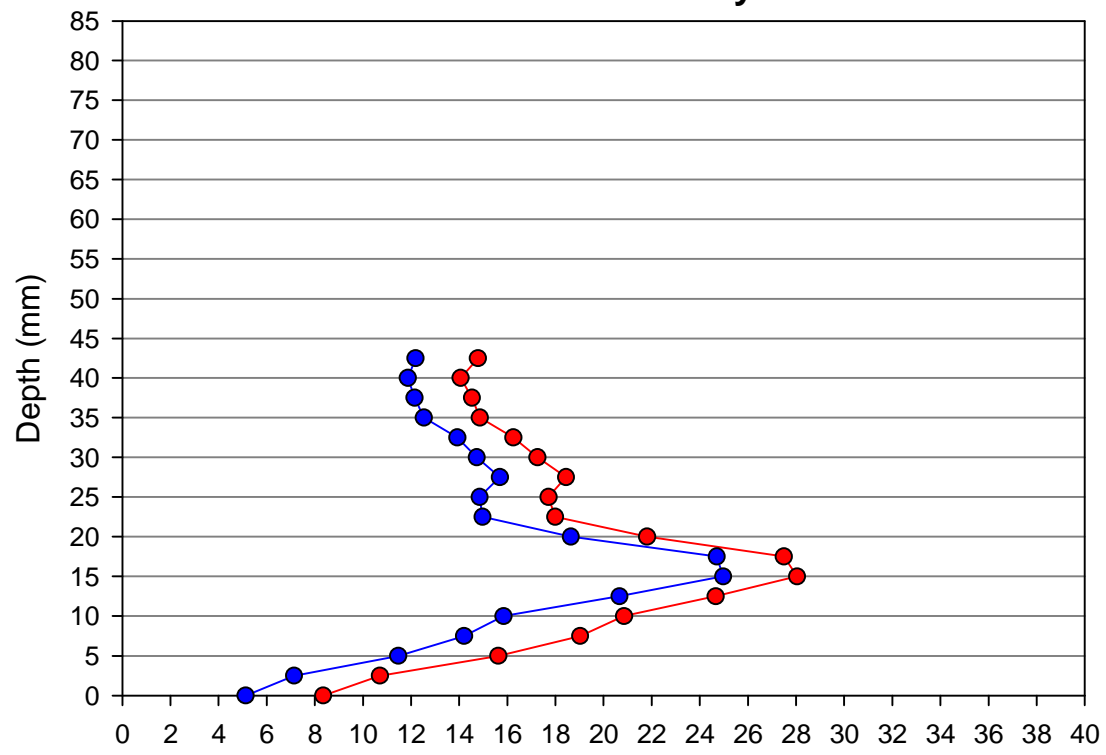
Trap C3 is situated at ten meters depth. The initial sedimentation at 0 mm is 8.3 microns which increases to a sharp peak at 15 mm with 28.0 microns. The particle size then decreases to 18.0 microns at 22.50 mm. From 22.50 mm to 42.50 mm the grain size gradually decreases to 14.8 microns.

The trap at the greatest depth of fourteen meters is C4. At 0 mm the grain size is 7.4 microns. The sediment slightly coarsens to 11.0 microns at 20 mm. At 27.5 mm there is a sharp coarse peak of 16.6 microns. The particle size then decreases to 13.1 microns at 32.5 mm. The second coarse peak occurs rapidly at 42.5 mm with 26.9 microns. The sediment then quickly fines to 17.3 microns at 55 mm. From 55 mm to 82.5 mm the grain size gradually decreases from 17.3 to 14.7 microns.

### C2 Grain Size Analysis



### C3 Grain Size Analysis



### C4 Grain Size Analysis

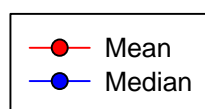
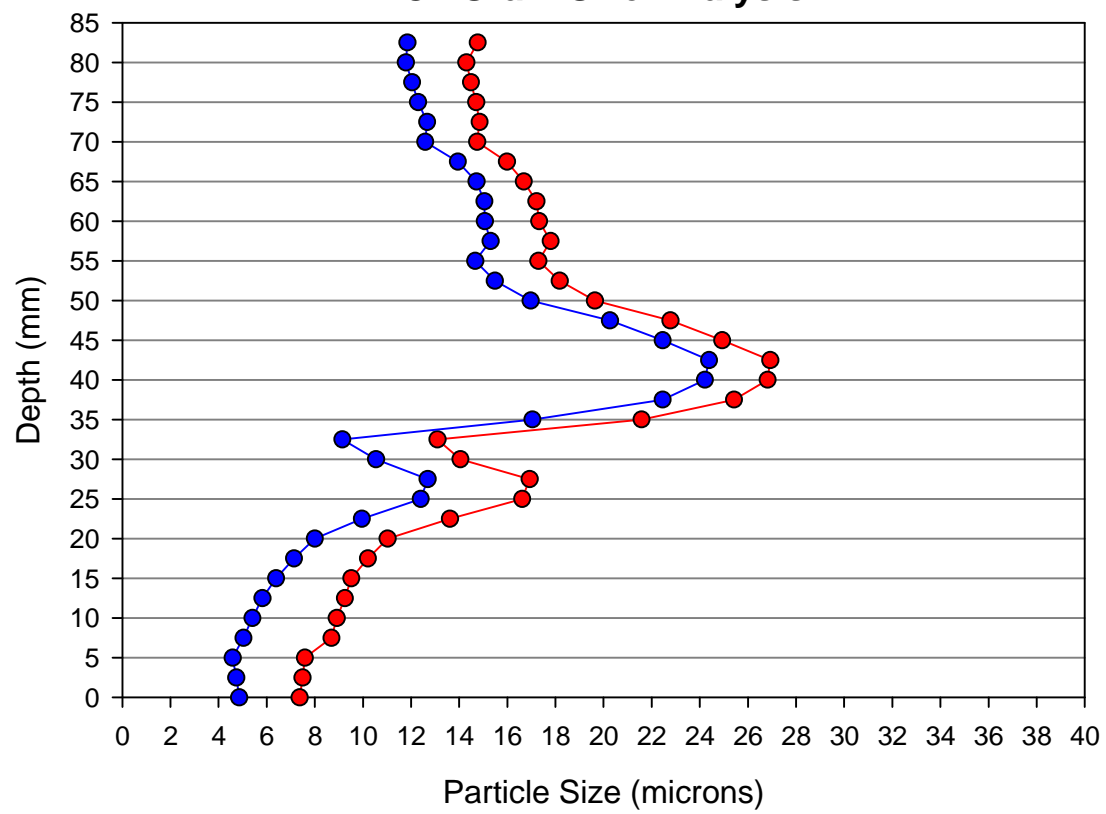


Figure 3.5: Mooring C, year-long trap grain size analysis. Note that 0 cm marks the bottom of the trap.

*Mooring C: Spring Traps (Figure 3.6)*

Trap SC1 is located at three meters depth. This trap expresses grain size of 18.4 and 18.7 microns at 0 and 2.5 mm respectively. The particle size then quickly decreases to 15.8 at 5 mm. From 5 mm to 60 mm the sediment ranges consistently from 15.8 to 14.2 microns without coarse peaks.

The next trap, SC2, is situated at eight meters depth. The initial grain size is 24.0 microns. From 0 to 25 mm the grain size increases with slight variation from 24.0 to 30.6 microns. The particle size then quickly decreases to 16.7 microns at 32.5 mm. From 32.5 to 80 mm the grain size trends finer from 16.7 to 13.8 microns with a slight coarse peak of 18.0 microns at 45 mm.

The bottom-most spring trap is SC3 at 14 meters depth. The initial sedimentation jumps from 22.8 to 26.1 microns then down to 24.5 microns at 0, 2.5, and 5 mm respectively. Particle size then gradually decreases to 22.3 microns at 27.5 mm which is followed with a quick decrease to 14.3 microns at 42.5 mm. The particle size then varies from 14.3 to 17.4 microns with several small coarse peaks as the grain size decreases gradually to 13.8 microns.

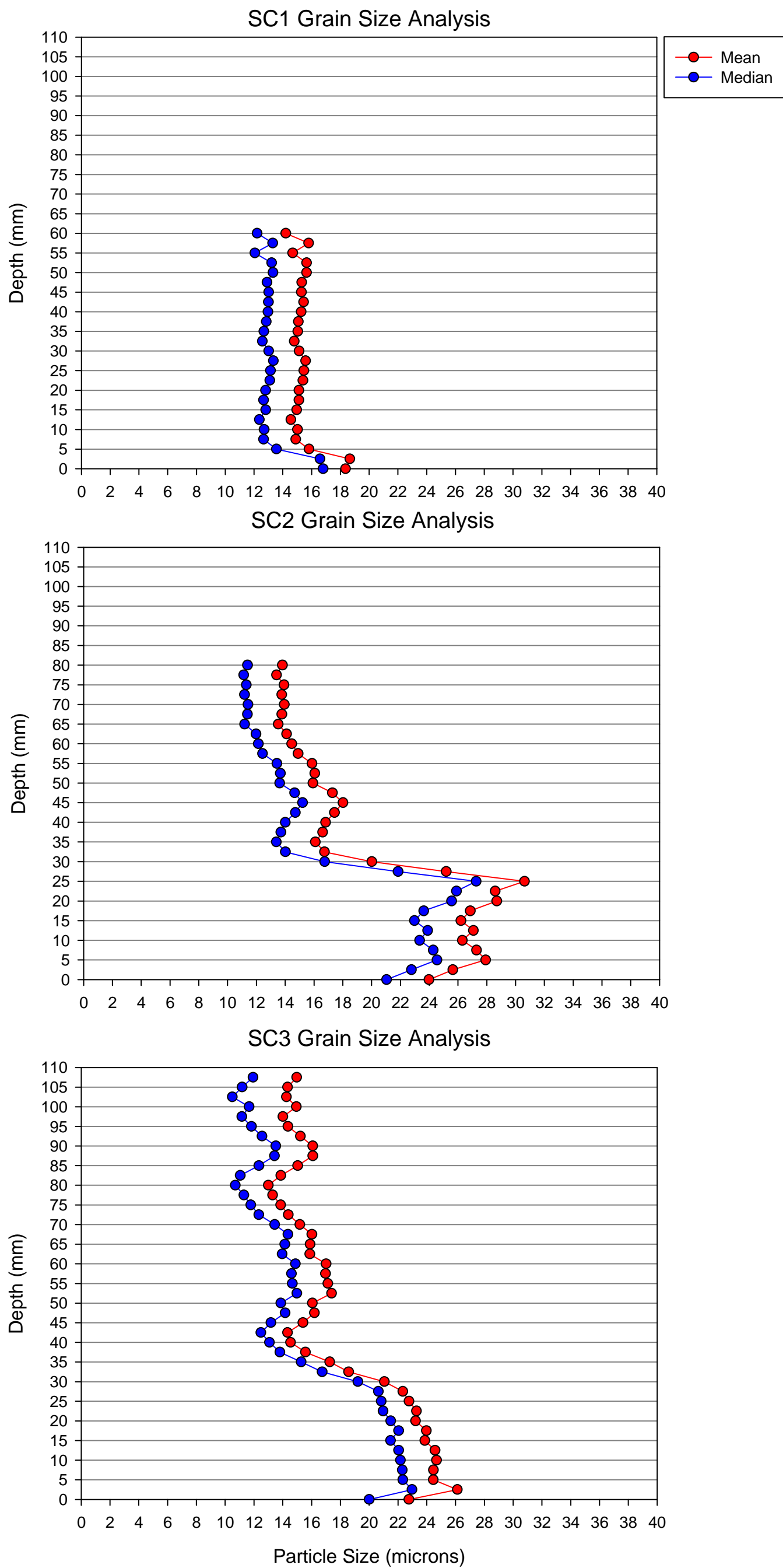


Figure 3.6: Mooring C, spring trap grain size data. Note that 0 cm marks the bottom of the trap.



*Mooring D: Year-Long Traps (Figure 3.7)*

The upper-most trap at Mooring D is D1, which is located at four meters depth. The grain size varies slightly throughout the whole trap with an initial sedimentation of 8.0 microns 0 mm. The only coarse peak in the trap occurs at 5 mm with 13.4 microns. The following sediment ranges from 10.3 to 12.3 to 11.3 microns at 7.5, 15, and 20 mm respectively.

The next trap, D2, is situated at seven meters depth. The trap expresses initial sedimentation of 8.3 at 0 mm with one coarse peak of 12 microns at 5 mm. The subsequent sediment decreases to 10.9 microns at 12.5 mm.

Trap D3 is at eleven meters depth and illustrates a well defined coarse sediment peak. The initial sedimentation is 8.6 microns and increases to 16.3 microns at 5 mm. The particle size then slowly decreases from 12.7 to 12.4 microns from 7.50 to 15 mm.

The bottom trap D4, is situated at fourteen meters depth. The sediment coarsens gradually from 0 mm to 12.5 mm with 7.9 to 10.6 microns respectively. A peak occurs at 15 mm with 16.1 microns. Particle size then gradually decreases to 11.7 microns at 27.5 mm.

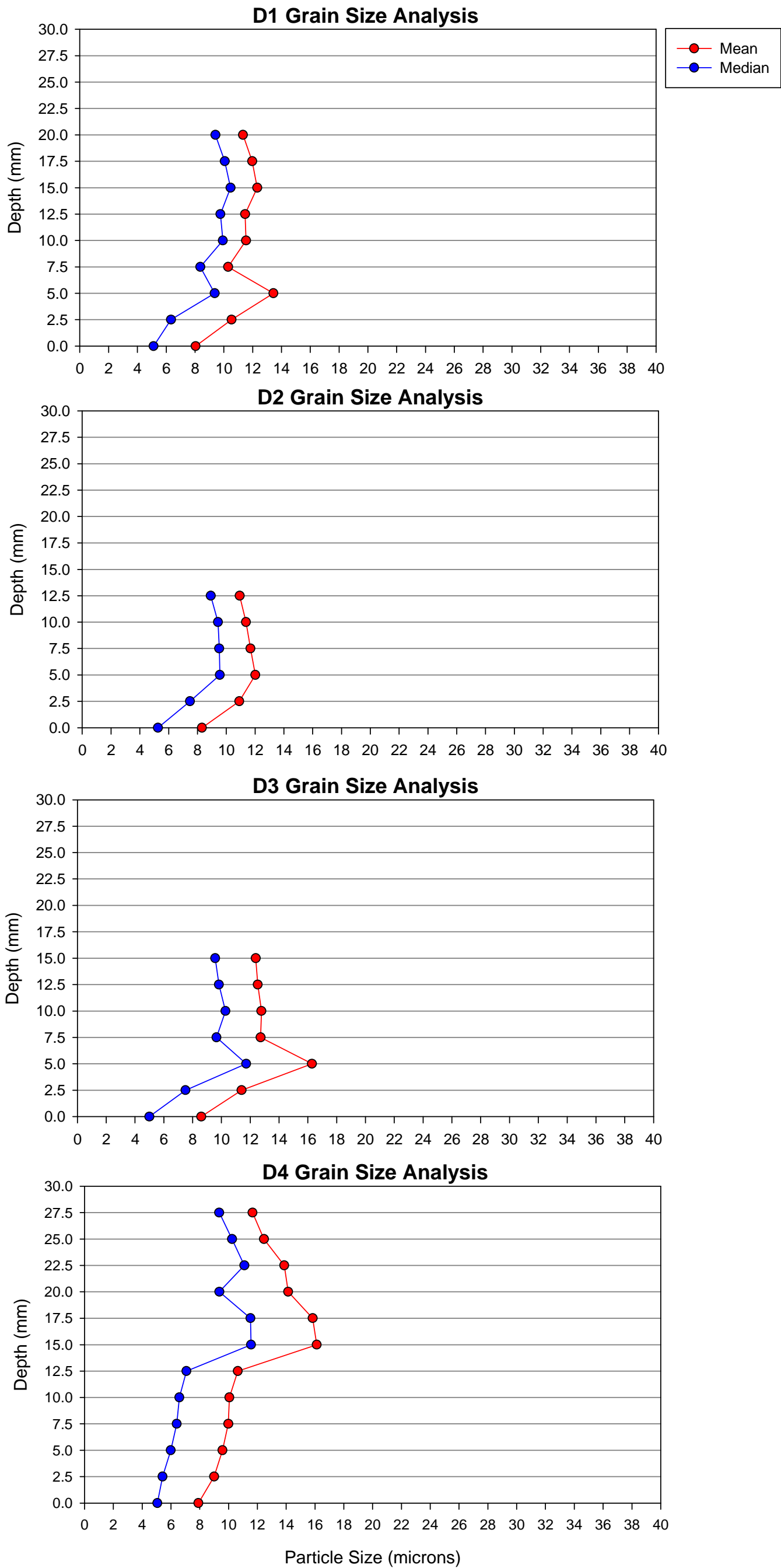


Figure 3.7: Mooring D year-long grain size data. Note that 0 cm marks the bottom of the trap.

*Mooring E: Year-Long Traps (Figure 3.8)*

Trap E1 is located at three meters depth on the bathymetric rise separating the East and West Basins. The basal sediment is 7.5 microns. Grain size steadily increases to 16.3 microns at 10 mm. The subsequent sediment decreases gradually from 16.4 microns at 12.5 mm to 13.2 microns at 30 mm.

The bottom trap E2 is situated at five meters depth. The grain size analysis expresses an increase of particle size from 9.4 to 18.8 microns from 0 to 12.50 mm. The particle size then gradually decreases to 13.3 microns at 37.5 microns.

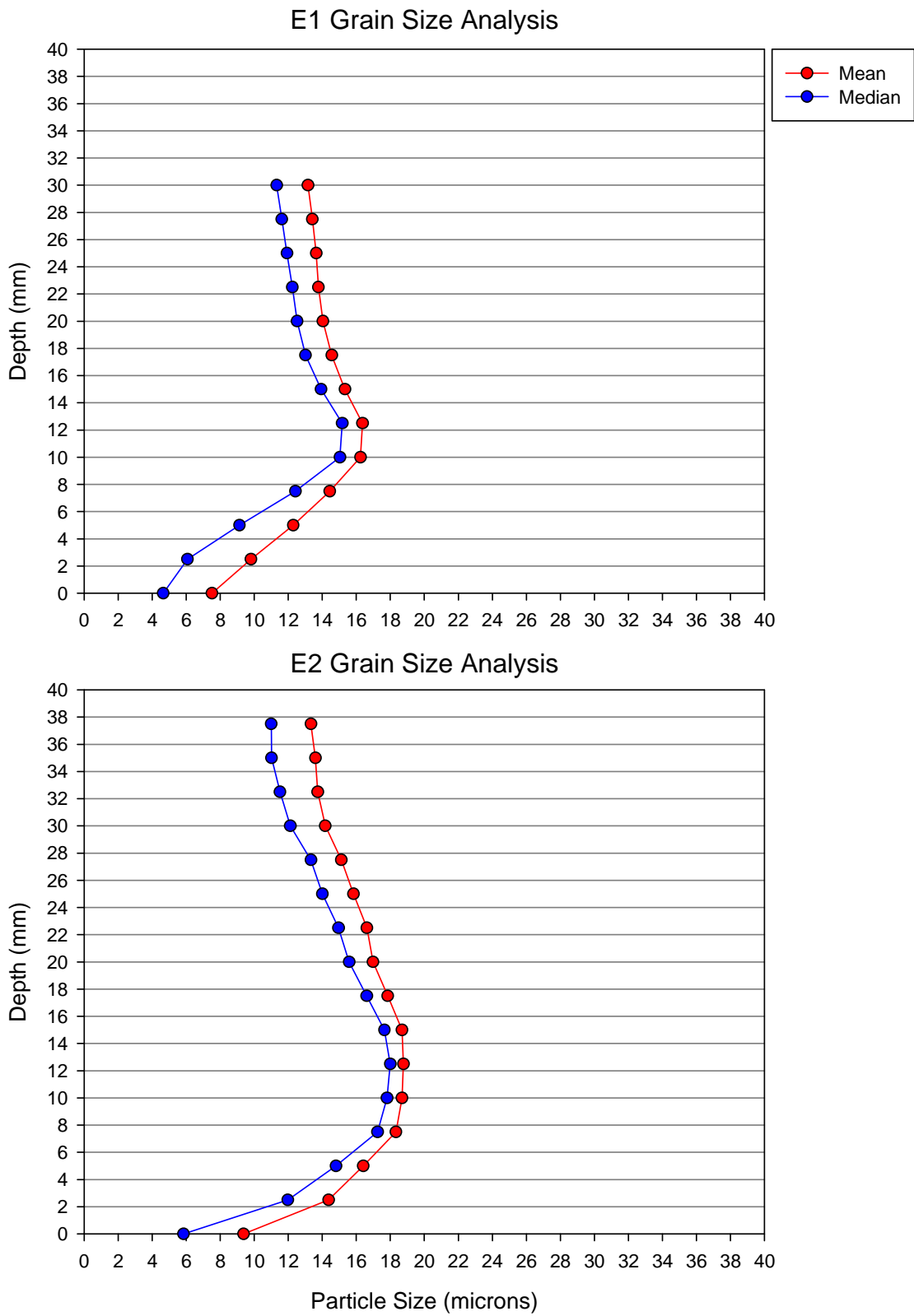


Figure 3.8: Mooring E year-long grain size data. Note, 0 cm is the bottom of the trap.

*Mooring F: Year-Long Traps (Figure 3.9)*

The upper-most trap, F1 is at three meters depth. The sediment has an initial particle size of 6.7 microns at 0 mm. The grain size then coarsens to 12.0 microns at 7.50 mm and decreases to 11.3 microns at 10 mm.

The middle-depth trap at six meters is F2. The basal sediment is 6.7 microns and gradually increases to 12.8 microns at 10 mm. The grain size then decreases to 11.8 microns at 15 mm.

The bottom-most trap, F3, is located at nine meters depth. At 0 – 2.5 mm grain size is 8.0 to 8.7 microns. The particle size decreases to 8.1 microns at 5 mm and subsequently increases to 14.0 microns at 10 mm. The grain size then gradually decreases to 12.8 microns at 22.5 mm.

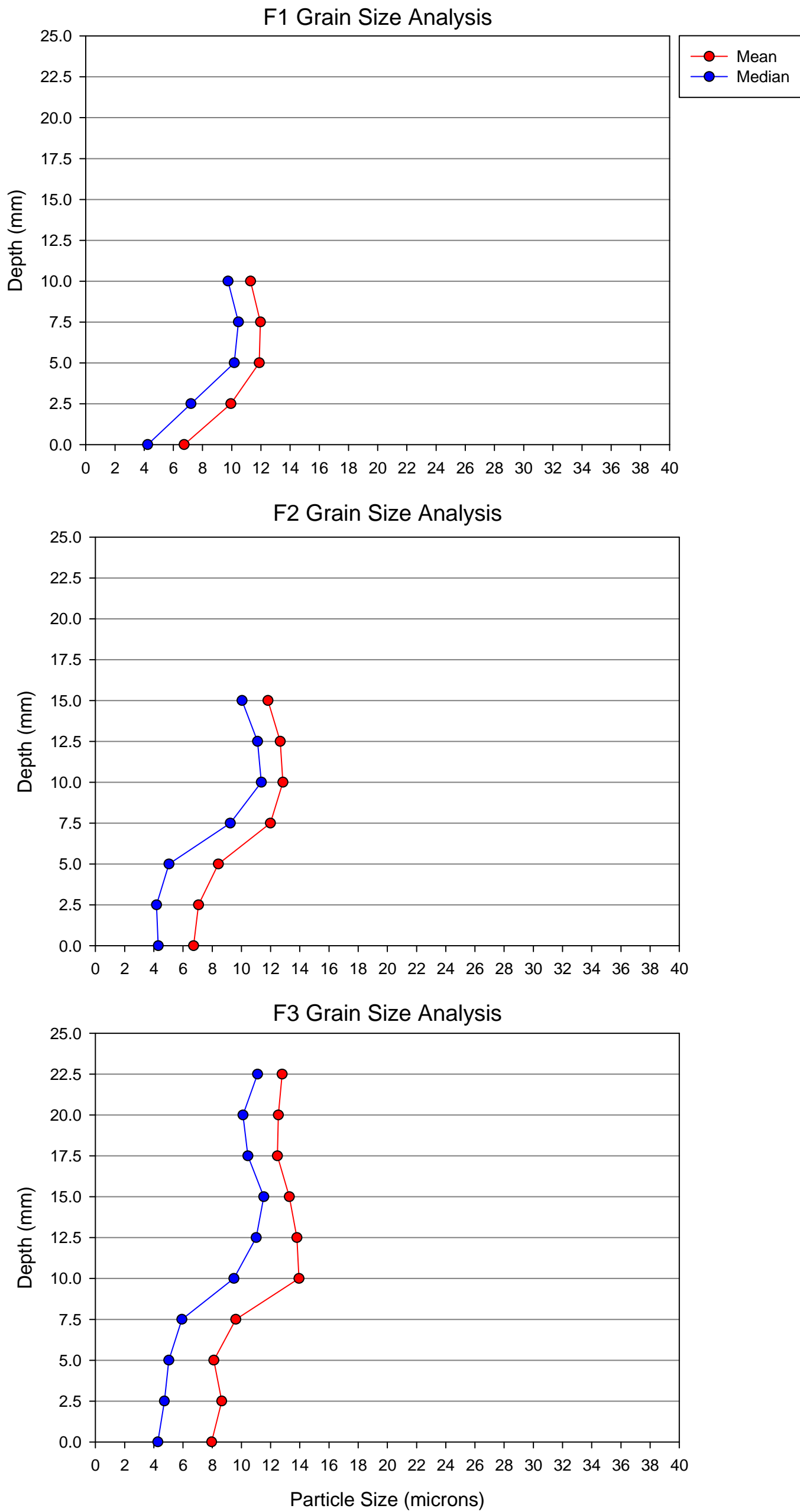


Figure 3.9: Mooring F year-long grain size data. Note that 0 cm marks the bottom of the trap.

*Mooring G: Year-Long Traps (Figure 3.10)*

Trap G1 is located at three meters depth and shows a steady increase of grain size from 5.9 microns to 9.1 microns from 0 to 5.0 mm.

The second trap, G2, is situated at nine meters depth. The first three sub-samples (0 mm, 2.5 mm, and 5 mm) exhibit grain sizes of 6.2, 6.6, and 5.3 microns. The particle size then increases to 11.7 microns at 10 mm as a coarse peak. The subsequent sediment steadily decreases to 8.0 at 17.5 microns.

The middle trap at twenty meters depth is G3. This particle size is gradually increasing from 6.0 to 9.5 microns from 0 to 12.5 mm. A defined coarse peak ranging from 15 mm to 17.5 mm with the maximum coarse particles as 14.3 microns at 17.5 mm. The subsequent particles grade to 9.0 microns at 25 mm.

Trap G4 is situated at twenty nine meters depth. The grain size gradually increases from 5.9 to 8.6 microns at 0 to 10 mm respectively. The coarse peak occurs at 12.5 to 15 mm with grain size of 13.9 and 14.3 microns. The following particle size steadily decreases to 8.8 microns at 22.5 mm.

The bottom-most trap is G5 at thirty four meters depth. The grain size gradually increases from 5.5 microns at 0 mm to 9.0 microns at 22.5 mm. The major coarse peak occurs at 32.5 mm with a mean size of 13.3 microns. Particle size then gradually and step-wise decreases to 9.1 microns at 45 mm.



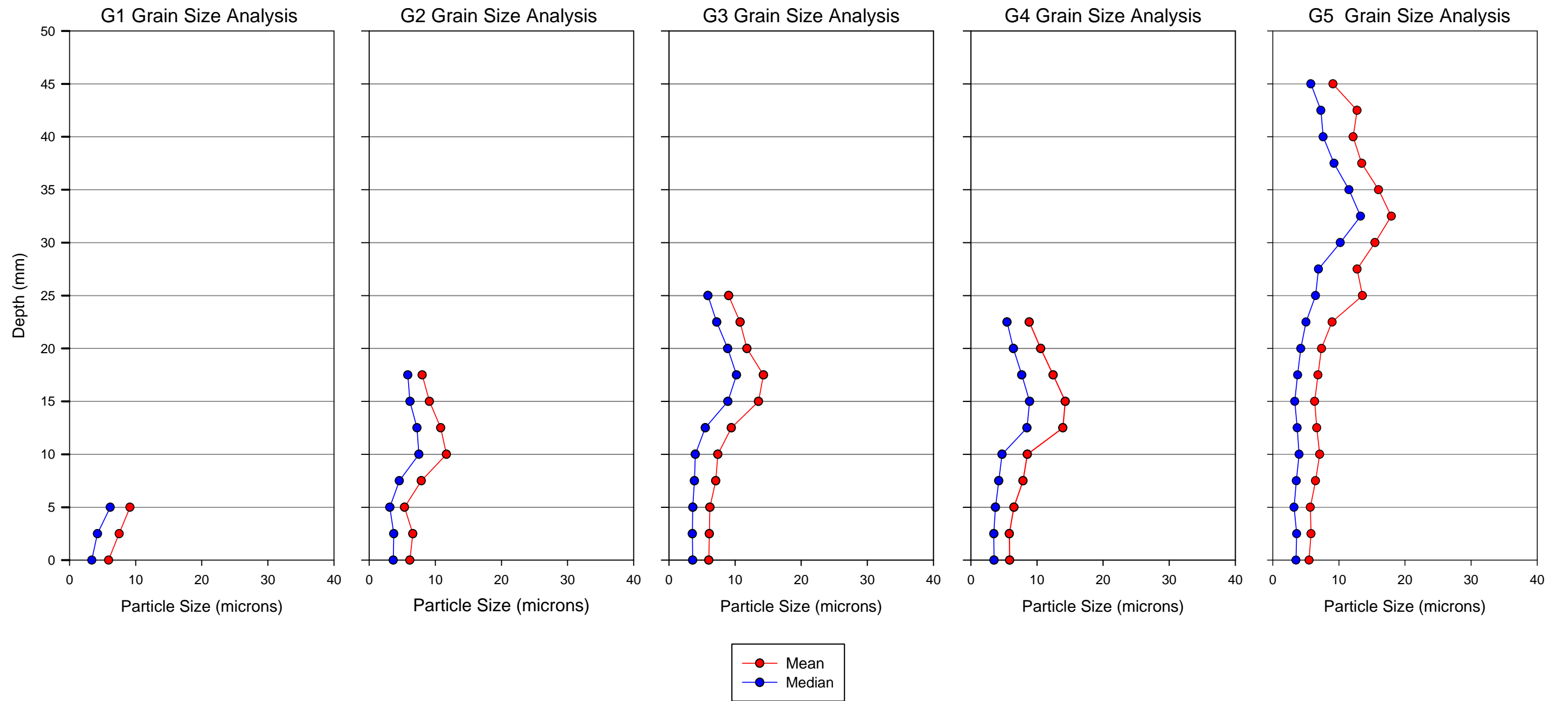


Figure 3.10: Mooring G year-long grain size data. Note that 0 cm marks the bottom of the trap.

### **3.4 – Weather & Environmental Data in Linnédalen**

#### *3.4.1 – Air Temperature (Figure 3.11)*

The air temperature follows a general trend of low variability in the spring and summer months and high variability in the winter months. The late July and early August temperature ranged from 6 – 14 °C and gradually decreased to 0 – 6 °C by late August. The temperature began to fluctuate greatly in October with a range from -13 – 5 °C. The temperature continued to be highly variable with highs of 3°C in December and January to lows of -20 to -25 °C in February and March. The temperature began to reach consistent values in late May with lows of -1 °C to highs of 12 °C in July. The maximum temperature for 2007 – 2008 was August 2, 2007 with 14.09 °C and the minimum was March 2, 2008 with -25.18 °C.

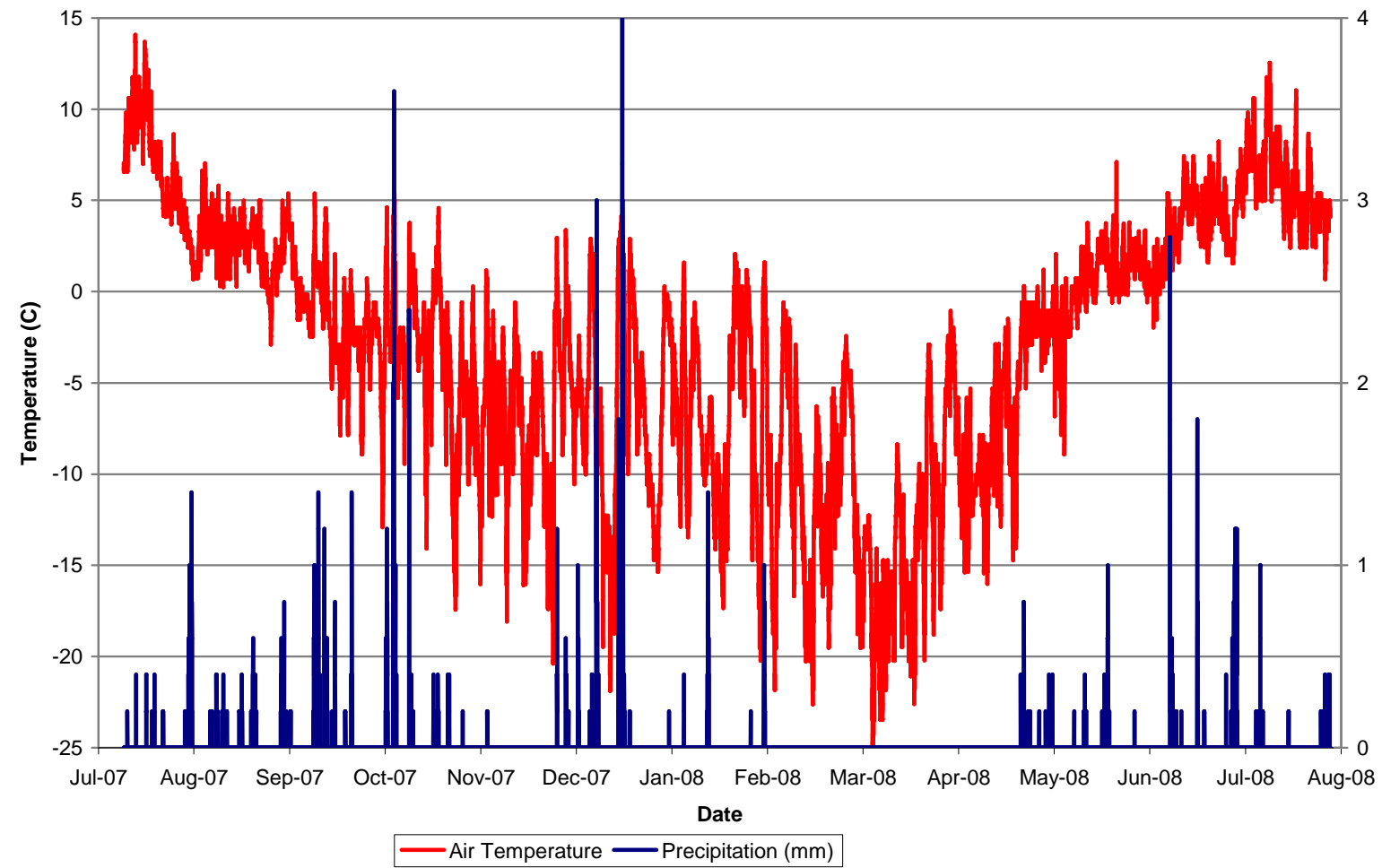
#### *3.4.2 – Precipitation (Figure 3.11)*

The precipitation throughout 2007 and 2008 was the greatest in the fall and spring months (May – October). The two largest rain events in the fall and summer months occurred on October 22, 2007 and June 22, 2008. The winter was dry the most part except for two large events on December 25, 2007 and January 1 – 2, 2008 both of which accumulated 3 mm or more precipitation. The greatest precipitation event for 2007 – 2008 was on January 1-2, 2008 with 4 mm.

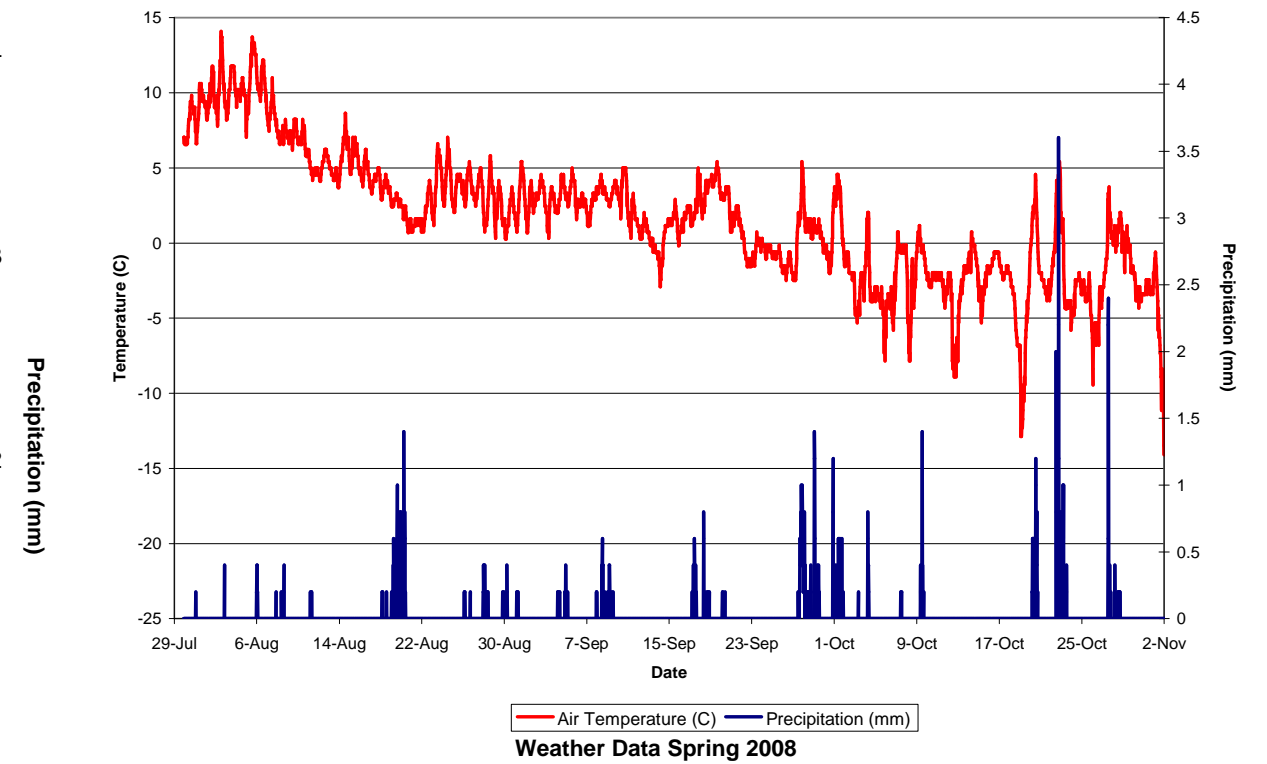
There were six major fall 2007 precipitation events. August 18<sup>th</sup> – 20<sup>th</sup>, September 27<sup>th</sup> – October 1<sup>st</sup>, and October 9<sup>th</sup> all had a maximum accumulation of 1.4 mm. October 20<sup>th</sup> had a maximum of 1.2 mm. The most significant precipitation event was October 22<sup>nd</sup> – 23<sup>rd</sup> with a maximum of 3.6 mm accumulation. The last major event of October was the 27<sup>th</sup> – 28<sup>th</sup> with a maximum accumulation of 2.4 mm.

The spring precipitation events decreased in magnitude of accumulation as the season progressed. The first major event was June 22 – 25<sup>th</sup> with a maximum accumulation of 2.8 mm. The next major event was June 30<sup>th</sup> – July 1<sup>st</sup> with 1.8 mm of precipitation. July 11<sup>th</sup> – 13<sup>th</sup> was the next occurrence of high precipitation with 1.2 mm. The last event before the sediment traps are recovered was July 19<sup>th</sup> – 21<sup>st</sup> with 1.0 mm accumulation.

Weather Data 2007-2008



Weather Data Fall 2007



Weather Data Spring 2008

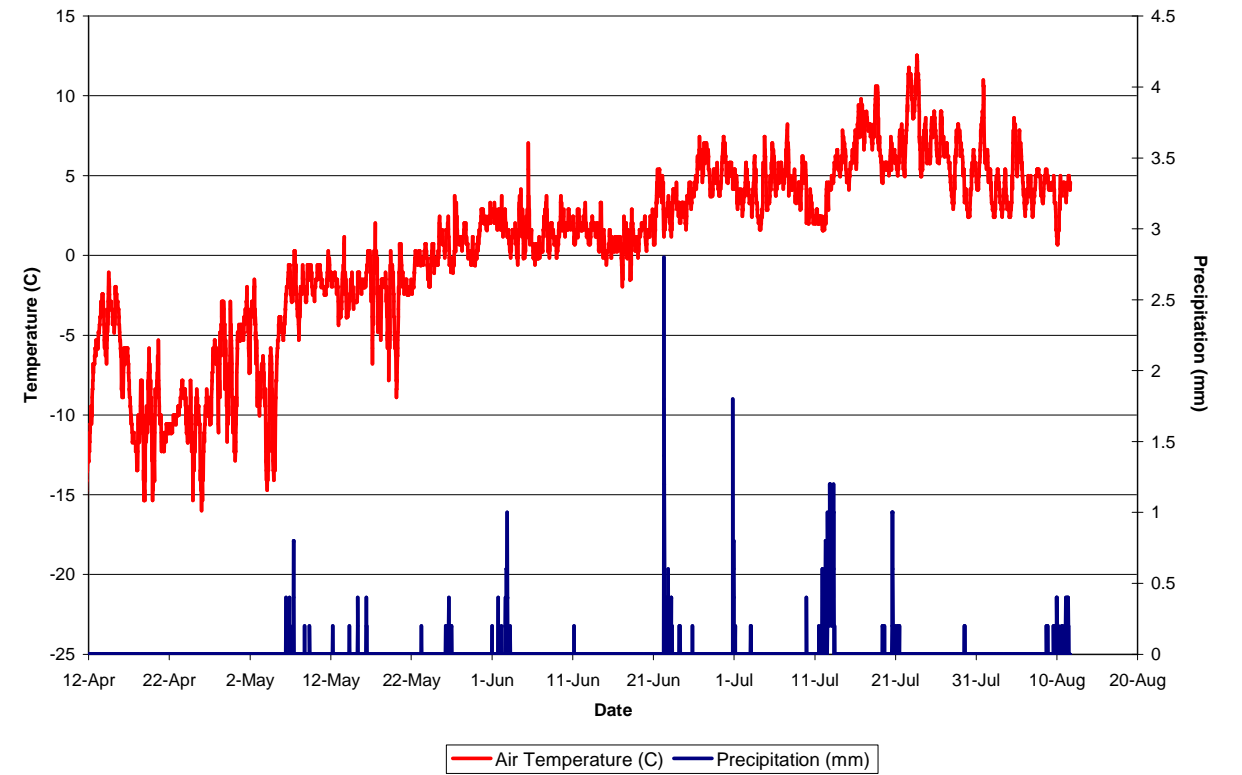


Figure 3.11: Air temperature and precipitation data for 2007 – 2008. The two graphs on the right highlight the fall and spring data. The fall data is presented July 29 to November 2, 2007. The spring data is presented from April 12 to August 15, 2008.

### *3.4.3 – Solar Radiation (Figure 3.12)*

The solar radiation in July 2007 began to decrease as the summer months passed. By the end of October, 2007 there was minimal solar radiation as the region was covered by 24 hour darkness. In mid-February, 2008 the light returned and increased to a maximum in the June and July 2008 months when the region was sunlit 24 hours. The maximum solar radiation was July 14, 2008 with  $813.1 \text{ W/m}^2$  at 3:00 in the afternoon.

Figure 3.13 and Table 3.2 describe the maximum values for solar radiation, temperature, and precipitation events for June 22 – July 22, 2008. There were days when the solar radiation maximum was directly related to the temperature maximum, but some days were delayed. On this scale, the solar radiation magnitude exceeded temperature until July 15<sup>th</sup>.

### Solar Radiation 2007 - 2008

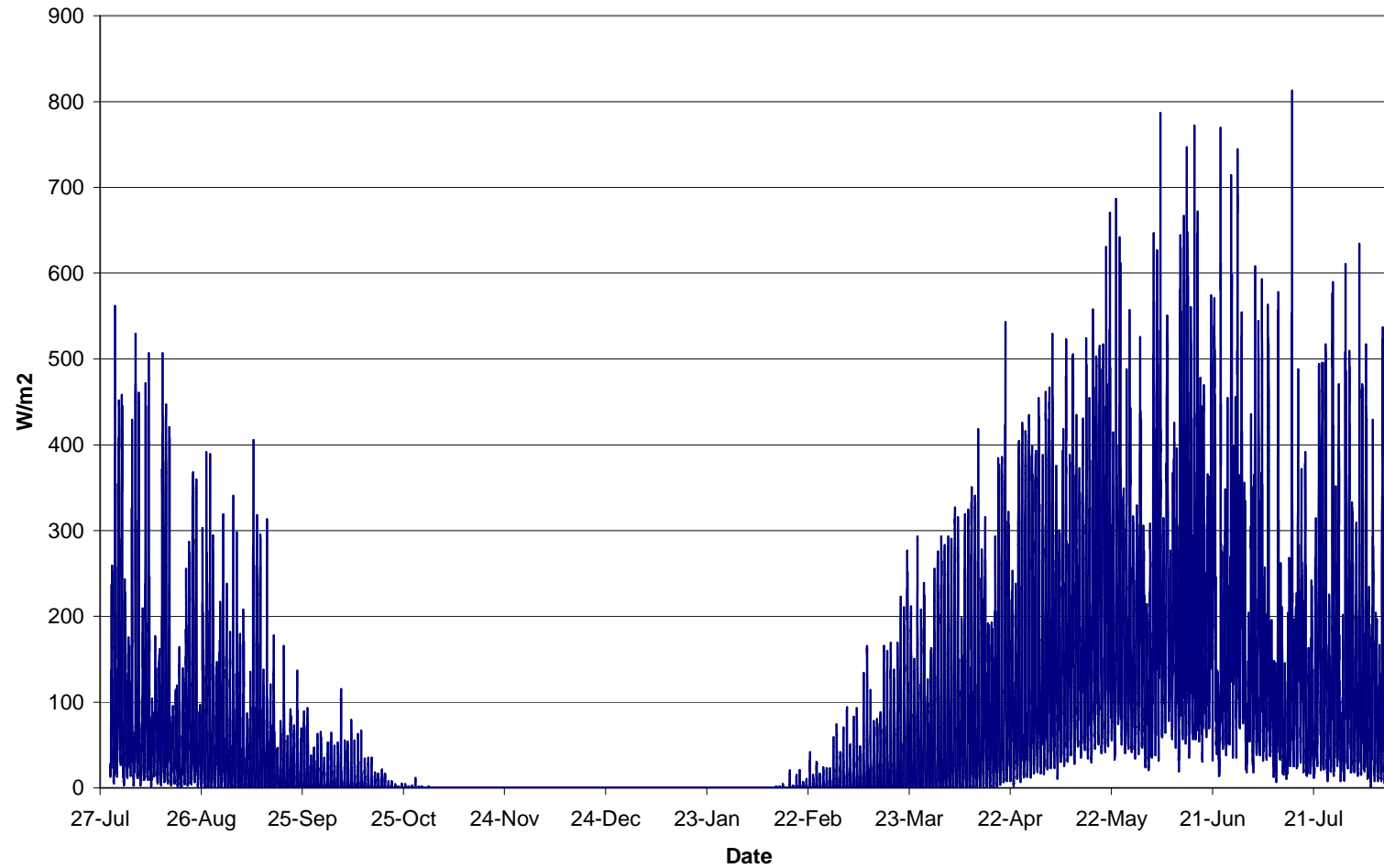


Figure 3.12: The solar radiation data for the 2007 – 2008 year. The hiatus of data from October 25, 2007 to February 15, 2008 was due to polar night. Solar radiation was highest in June and July due to 24 hour sunlight.

### Maximum Daily Weather Values

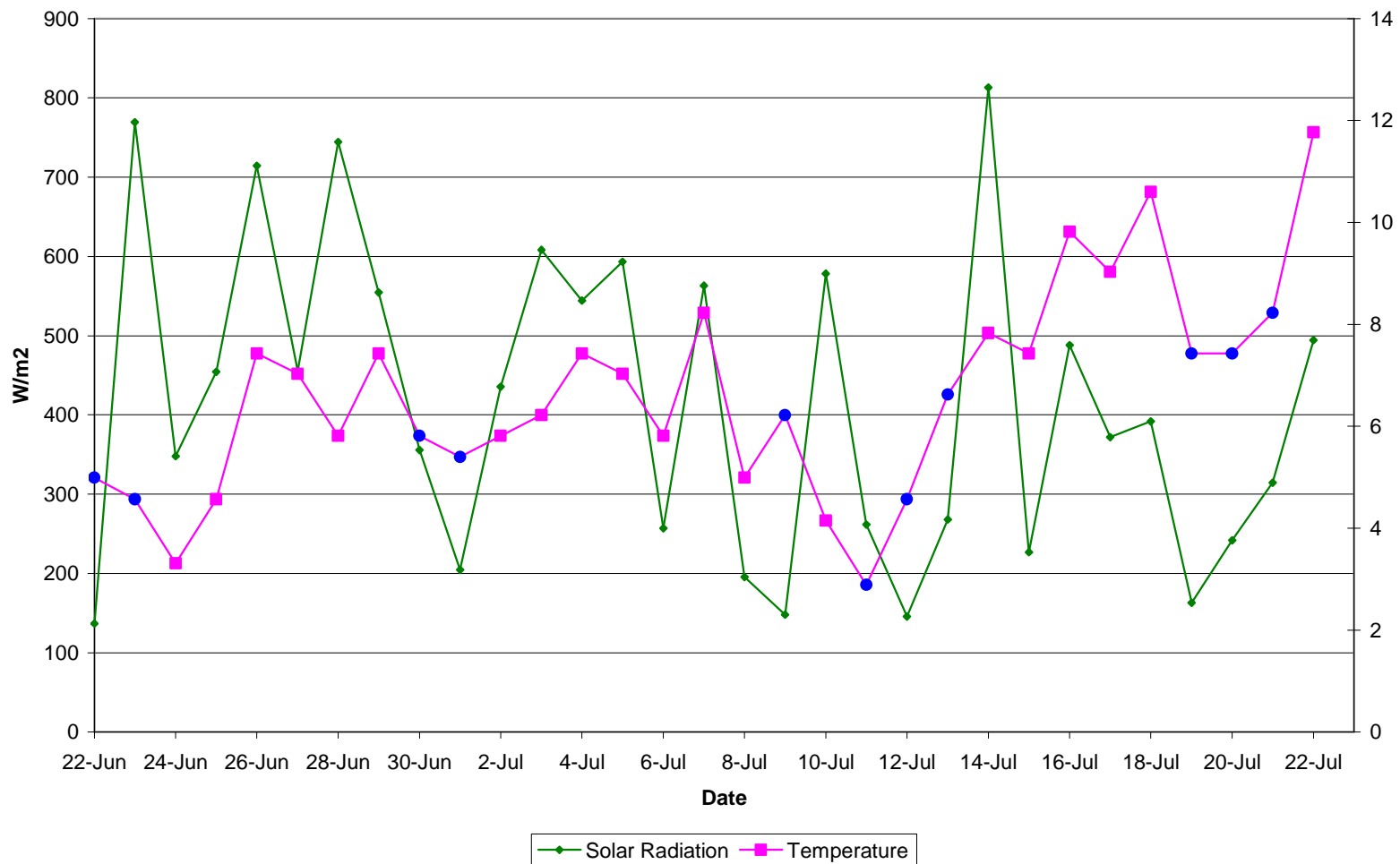


Figure 3.13: This graph describes the maximum values for solar radiation, temperature, and the blue dots represent days with precipitation. Table 3.2 corresponds to these dates.



<b>Table 3.2: Spring 2008 Weather Data</b>			
<b>Date</b>	<b>Max Precip.</b>	<b>Max Solar Radiation</b>	<b>Max Temp</b>
	<i>mm</i>	<i>W/m2</i>	<i>C</i>
22-Jun	2.80	136.9	4.99
23-Jun	0.40	769.4	4.57
24-Jun	0.20	348.1	3.31
25-Jun	0.00	454.4	4.57
26-Jun	0.00	714.4	7.43
27-Jun	0.00	455.6	7.03
28-Jun	0.00	744.4	5.81
29-Jun	0.00	554.4	7.43
30-Jun	1.80	355.6	5.81
1-Jul	0.20	204.4	5.4
2-Jul	0.00	435.6	5.81
3-Jul	0.20	608.1	6.22
4-Jul	0.00	544.4	7.43
5-Jul	0.00	593.1	7.03
6-Jul	0.00	256.9	5.81
7-Jul	0.00	563.1	8.23
8-Jul	0.00	195.6	4.99
9-Jul	0.40	148.1	6.22
10-Jul	0.00	578.1	4.15
11-Jul	0.20	261.9	2.89
12-Jul	1.20	145.6	4.57
13-Jul	1.20	268.1	6.62
14-Jul	0.00	813.1	7.83
15-Jul	0.00	226.9	7.43
16-Jul	0.00	488.1	9.82
17-Jul	0.00	371.9	9.03
18-Jul	0.00	391.9	10.6
19-Jul	0.20	163.1	7.43
20-Jul	0.60	241.9	7.43
21-Jul	0.20	314.4	8.23
22-Jul	0.00	494.4	11.77

Table 3.2: This table describes the maximum values of precipitation, solar radiation, and air temperature for June 22 – July 22, 2008.

#### *3.4.4 –Snow Tree (Figure 3.14)*

The snow tree collected the daily light intensity values from July 2007 until the snow fell in October. The two bottom loggers (7 cm and 15 cm) were covered on October 2, 2007. The uppermost logger at 45 cm was covered on October 7, 2007. The rungs were not exposed until July 11, 2008 when the two uppermost (45cm and 30 cm) loggers collected light intensity. They were likely not fully exposed until July 13, 2008 when the light intensity increases dramatically. The third logger at 15 cm followed with an exposure on July 14<sup>th</sup> and the bottom rung at 7 cm was the last on July 17<sup>th</sup>.

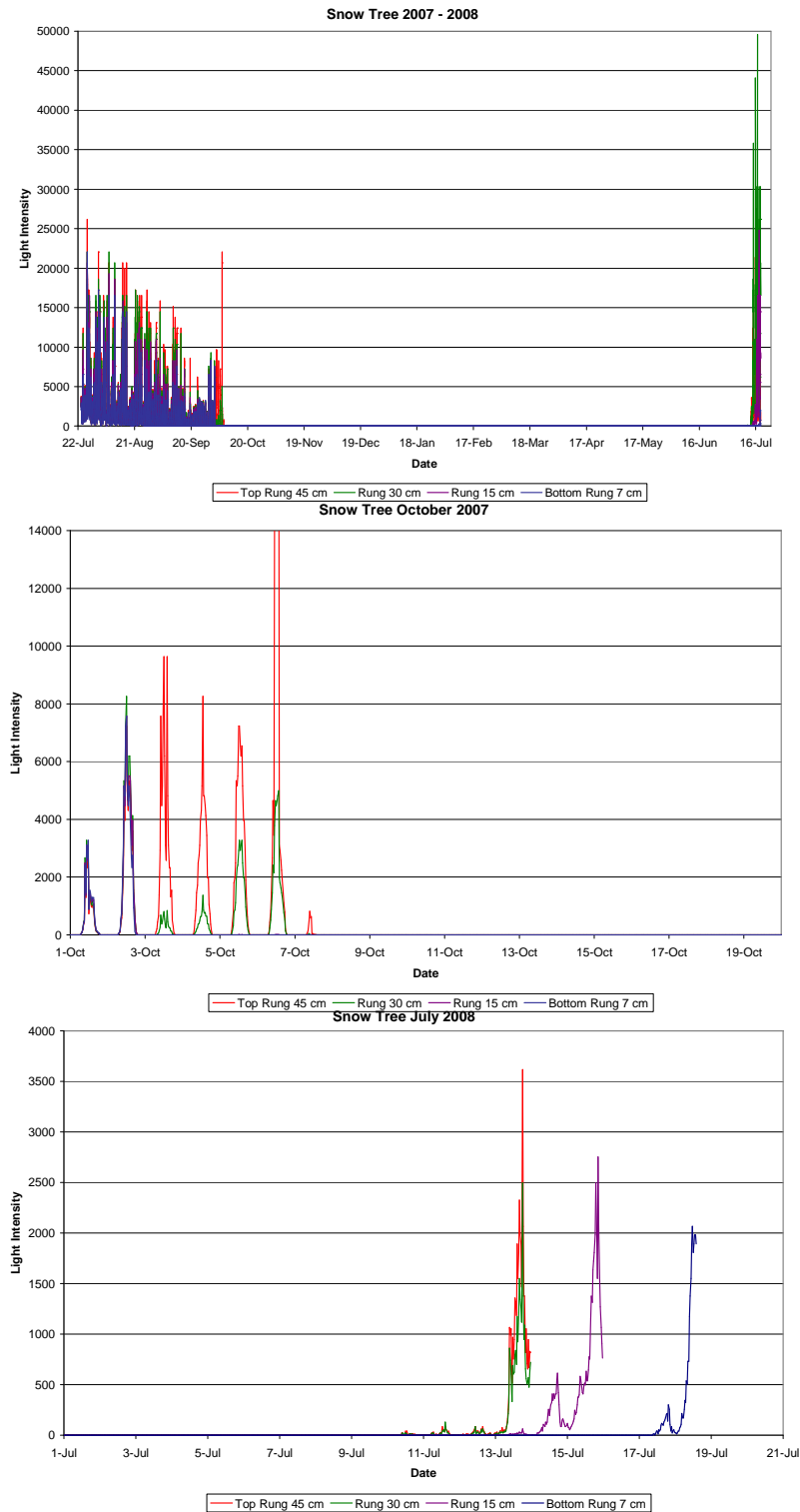


Figure 3.14: These three graphs describe the snow tree data. The uppermost is the yearly data, the middle is the October 2007, and the bottom is July 2008. The October data shows when the loggers were covered with snow and the July data shows when the loggers were exposed to the light again.

### *3.4.5 – Stream Temperature (Figure 3.15)*

The stream temperature was high (5 – 12 °C) throughout late July and into August, 2007. The diurnal pattern ranged 4 – 6 °C between afternoon and night temperatures. On August 21<sup>st</sup> temperature dropped dramatically near 0 °C. The diurnal pattern continued with a high of 6.8 °C on August 24<sup>th</sup> until the temperature reached 0 °C on September 10<sup>th</sup>. An anomalous spike in temperature occurred on September 18<sup>th</sup> – 20<sup>th</sup> when the temperature reached 2.8 °C. September 22<sup>nd</sup> was when the temperature reached 0 °C and remained throughout the winter.

On June 26, 2008 the stream temperature reached + 0.5 °C for the first time since September 2007. The stream quickly warmed in a diurnal pattern to 1 °C on June 29<sup>th</sup>, then 2 °C on July 3<sup>rd</sup>, 3 °C on July 4<sup>th</sup>, and past 4 °C on July 5<sup>th</sup>. The stream reached a maximum temperature of 12.4 °C on July 23, 2008.

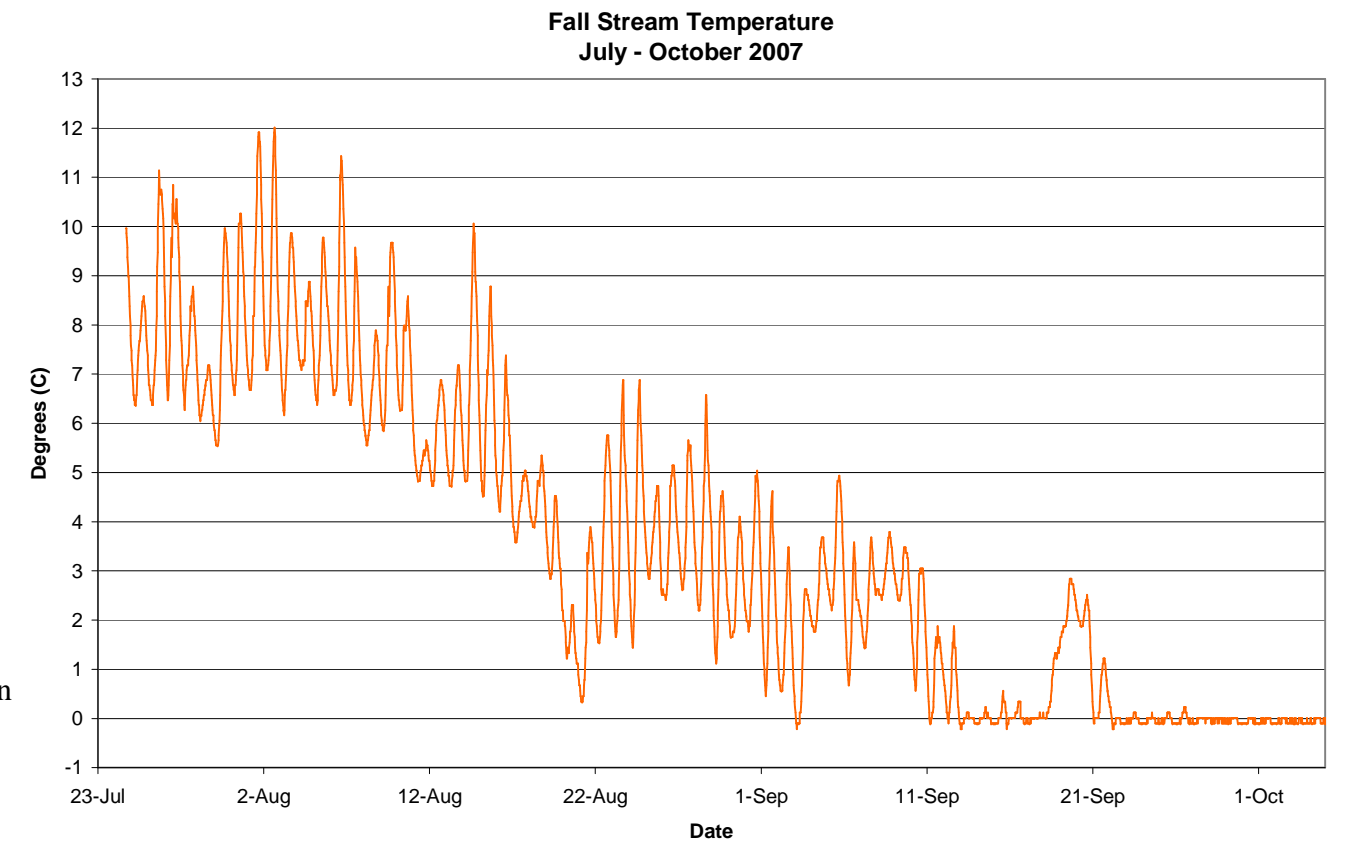
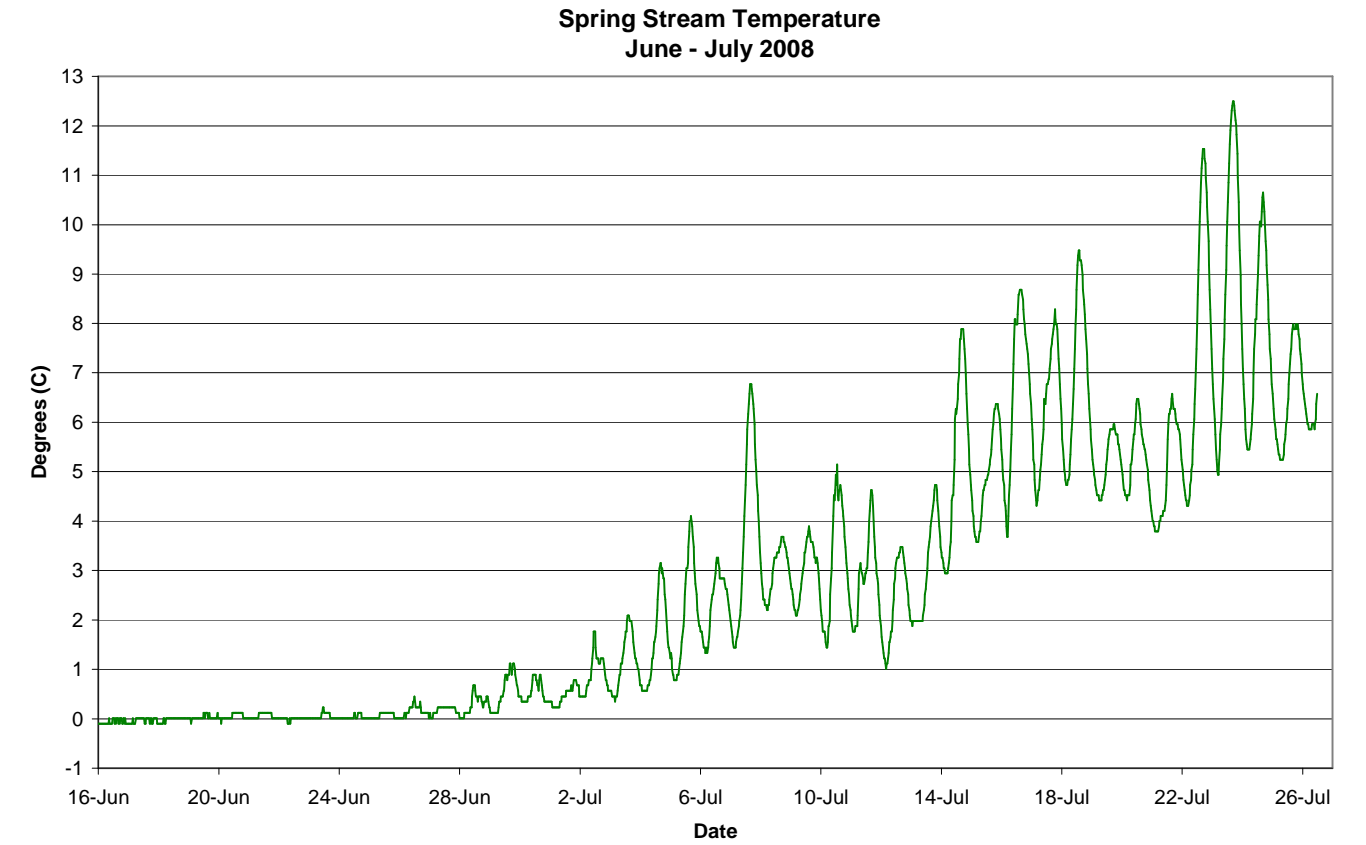
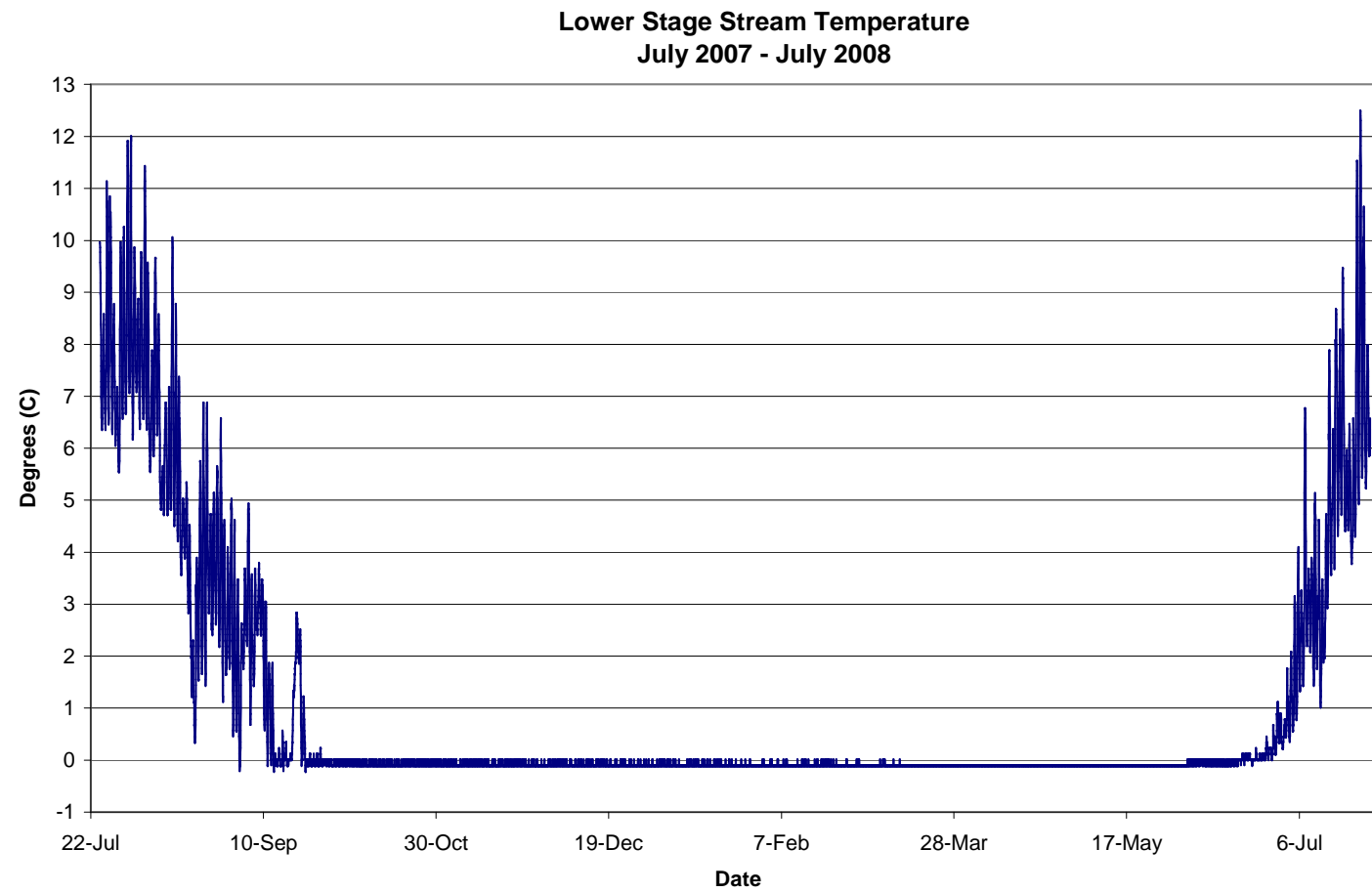


Figure 3.15: These graphs illustrate the stream temperature at the Lower Stage. The upper graph is July 2007 – July 2008, the long straight line during the winter months is when the stream is completely frozen. The graphs on the right illustrate the fall and spring stream temperature and the diurnal pattern.

#### *3.4.6 – The Intervalometer (Figure 3.16)*

The intervalometer showed sediment accumulation beginning on August 12, 2007. The first major sedimentation event began on September 2<sup>nd</sup> and continued until September 7<sup>th</sup>. After a brief calm, the second fall event occurred on October 2<sup>nd</sup>. Minor events occurred throughout the winter. The first sediment event of spring 2008 occurred on June 27<sup>th</sup> which was followed by a significant event on July 3<sup>rd</sup> – 6<sup>th</sup>. The next major event was on July 14<sup>th</sup> – 15<sup>th</sup>. A minor event occurred on July 21<sup>st</sup>.

**Intervalometer Data  
July 2007 - July 2008**

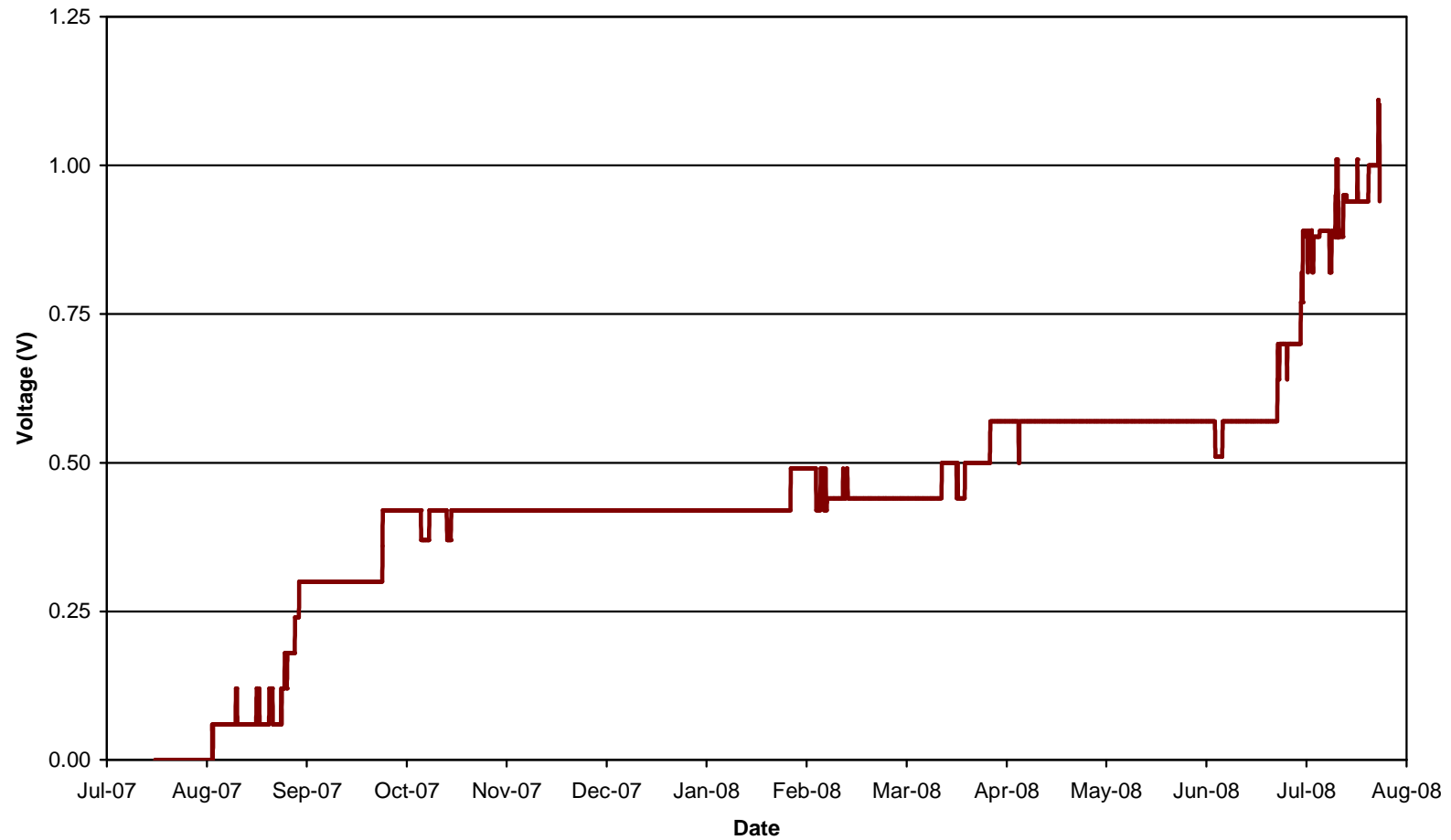


Figure 3.16: The intervalometer illustrates the dates of sediment accumulation at Mooring C. Note that the sediment continually increased with time with major events in August – September 2007 and June – July 2008.



### *3.4.7 – Mooring C Temperature Loggers (Figure 3.17)*

The year-long temperature loggers at Mooring C collected measurements at 30 minutes intervals. The lake temperature in the fall of 2007 reached a high of 6.6 °C on August 15<sup>th</sup> as measured in the loggers at 3 meters and 6 m depth. The loggers at all depths reflect diurnal temperature changes as the lake water gradually decreased in temperature until October 3<sup>rd</sup>. On October 3<sup>rd</sup> the bottom water (14 m) began to show temperature warmer than the upper water (3 m and 6 m) as the whole water column dropped below 3 °C. Lake water continued to decrease in temperature until October 14<sup>th</sup> when the whole column warmed to near 1 °C. The temperature continued to drop until October 26<sup>th</sup> – 27<sup>th</sup> when the whole column reached 0 °C. As the winter months progressed the bottom water (14 m) warmed to approximately 0.7 – 0.9 °C while the upper water (0-10 m) ranged from 0 – 0.1 °C.

On June 4, 2008 the 3 – 10 m water began to slightly warm above 0 °C. The top water gradually warmed until June 30<sup>th</sup> when the temperature exceeded 1°C. The water at 6 m depth warmed past 1 °C on July 3<sup>rd</sup>. The following day, July 4<sup>th</sup>, marked the first significant temperature increase from 3 – 10 meters depth. The next warm water event at depth 3 – 10 m occurred on July 7 – 9<sup>th</sup>. However, the 14 m water did not change until July 13<sup>th</sup> when temperature increased from 1 °C to 2 °C on July 15<sup>th</sup>. The water column continued to warm through July with a maximum temperature at 3 m of 3.1 °C.

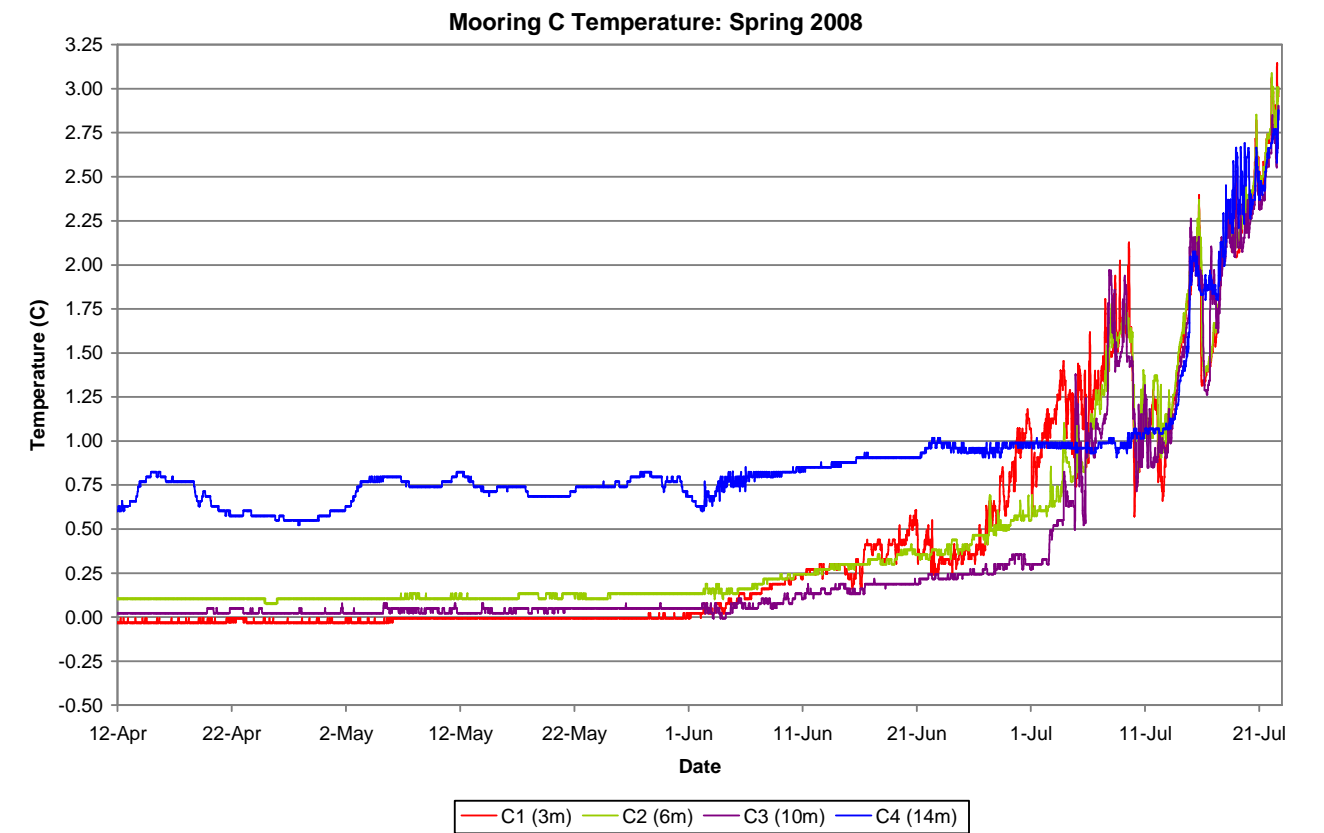
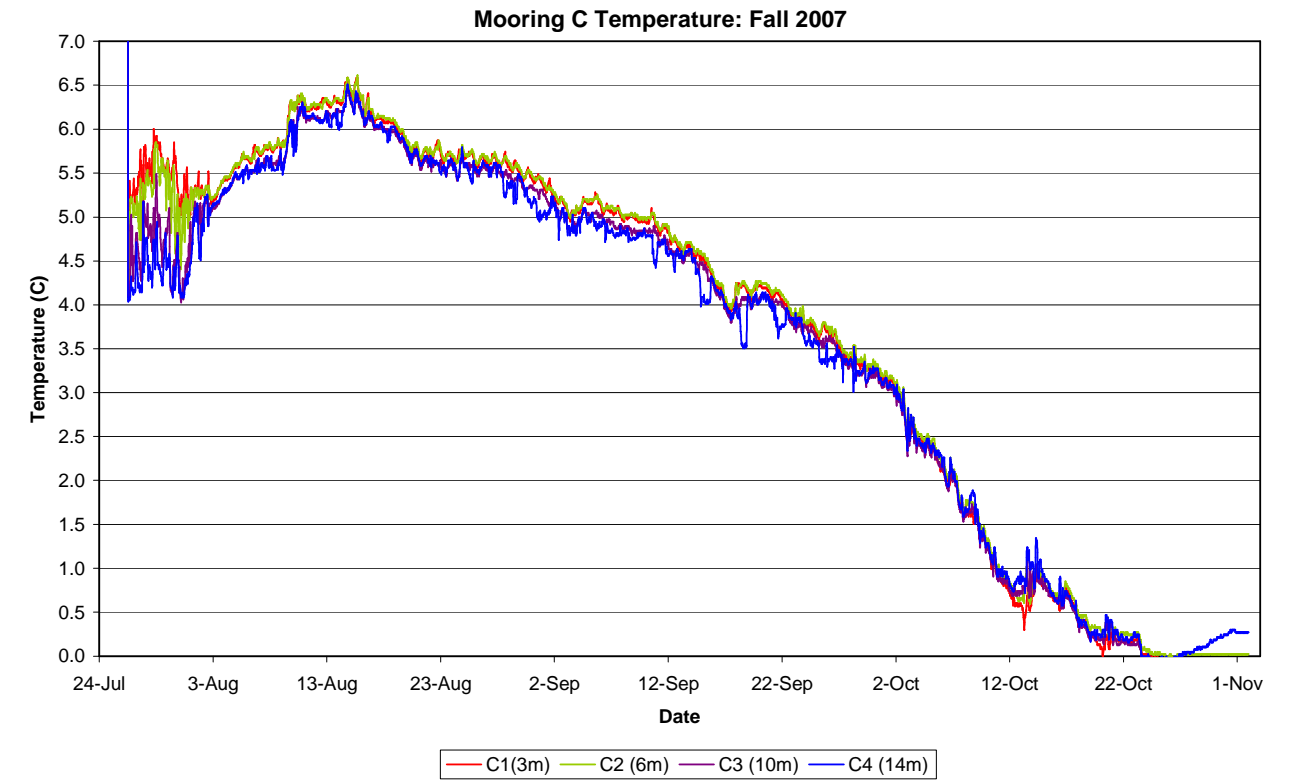
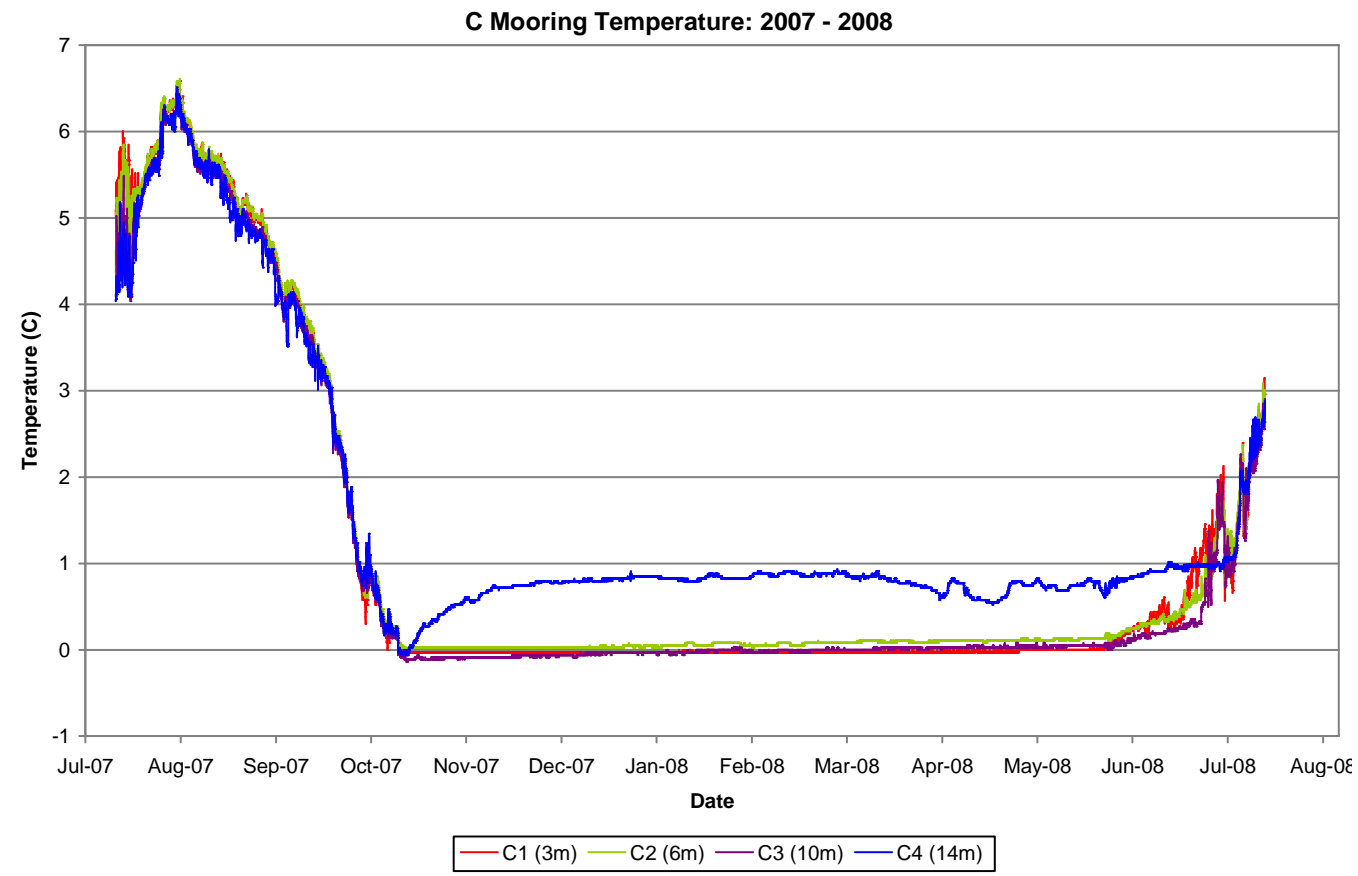


Figure 3.17: The Mooring C temperature logger data are presented in these three graphs with the upper image of the July 2007 – July 2008, the upper right image fall 2007 and the lower right image spring 2008.

### *3.4.8 – Spring Turbidity and Temperature at Mooring C (Figure 3.18)*

The In-Situ Troll was deployed at 14 meters at Mooring C on April 13, 2008 and collected measurements of turbidity and temperature at 2 minute intervals. Turbidity from April 13<sup>th</sup> to June 22<sup>nd</sup> remained consistently between 0.05 – 0.1 FNU. June 22<sup>nd</sup> to July 3<sup>rd</sup> marked a rapid increase in turbidity from 0.1 to 0.5 FNU. The first major turbidity event occurred on July 4 - 5 when the values increased from 0.5 to 27.5 FNU.

Several subsequent turbidity events occurred but with lower magnitude. July 7<sup>th</sup> shows turbidity of 15.2 FNU and July 13<sup>th</sup> shows 21.7 FNU. These turbidity events, except for July 13<sup>th</sup>, match with temperature spikes. July 5<sup>th</sup> the temperature reached 2.6 °C, July 7<sup>th</sup> temperature is 2.8°C, and July 14<sup>th</sup> (slightly delayed from July 13<sup>th</sup>) had a temperature of 3.3 °C.

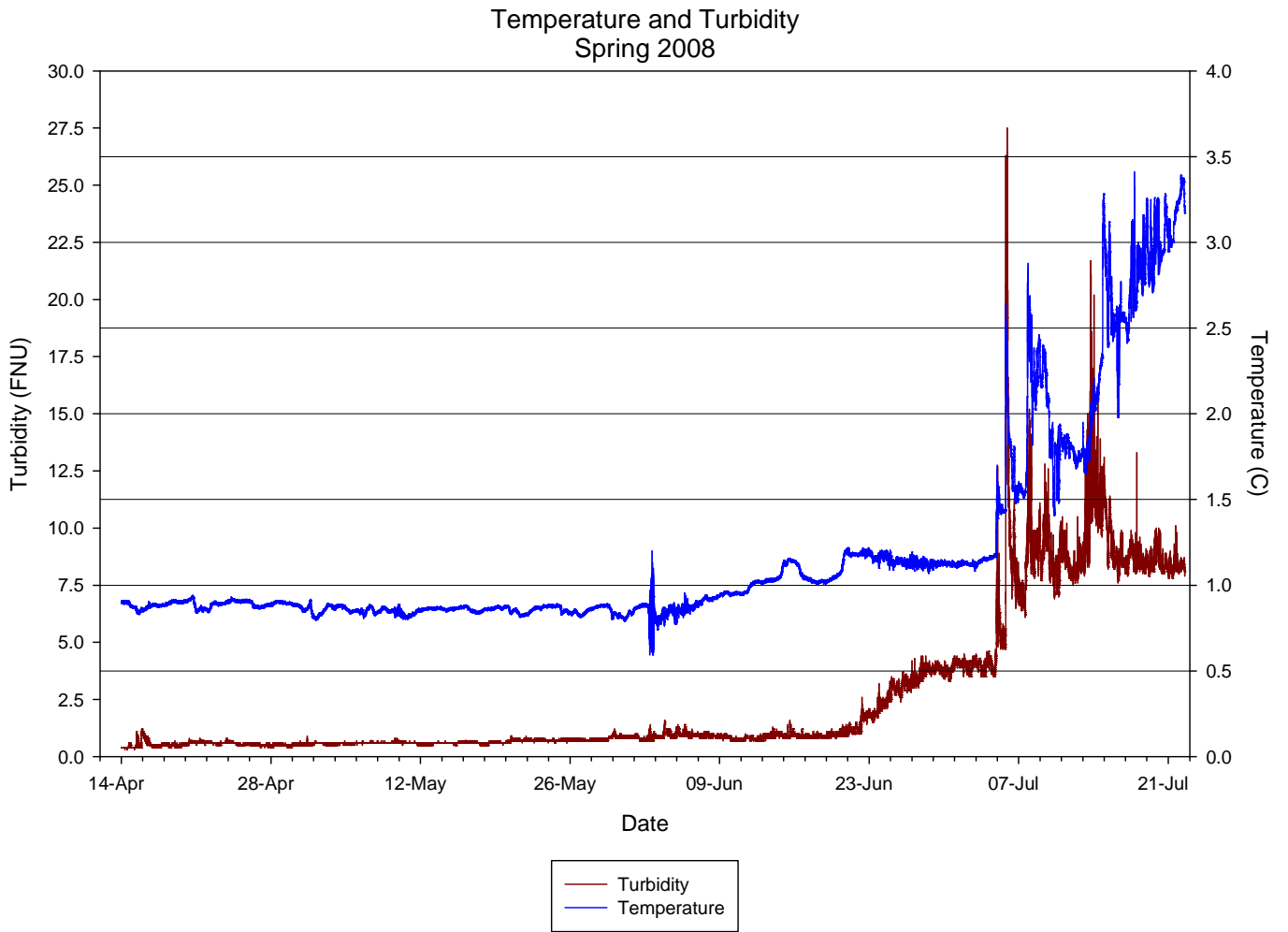


Figure 3.18: The Troll turbidity and temperature data are presented in this image. The red line is the turbidity. Note the turbidity spikes generally match with the temperature spikes.

# CHAPTER FOUR

## DISCUSSION



The stratigraphic and textural changes seen in the sediment traps are interpreted as the components which form varves. A varve is defined by a couplet representing a year of deposition. The couplet is classified as coarser summer silt layer overlain by a finer clay layer (Smith and Ashley, 1985; Sturm, 1979). The sharp change in grain size, from fine silt to coarse silt, seen in all of the sediment traps each year, reflects the boundary of two different varves. A classic varve couplet in a depositional year is defined as coarse “summer” sediment grading into a fine “winter” layer. However, because of the time of deployment and retrieval, a sediment trap year begins with fine winter layers overlain by coarse summer sediment. Thus each trap contains parts of two varves. For the purpose of comparing this study with the previous four, the following discussion refers to sediment trap years unless otherwise specified.

#### **4.1 – Interpretations of Grain Size Analysis**

The grain size results from Mooring C year-long and spring traps are interpreted with the weather data results in this section. Each sediment event seen in year-long trap C4 and spring trap SC3 are described in detail with weather and temperature logger data to determine the driving force of each event. The weather data figures refer to those shown in Chapter 3, Results.

##### *4.1.1 – Fall Event: Weather & Watershed Data*

Through comparisons of stratigraphy of the year-long and spring bottom traps at Mooring C, a coarse layer in shown in C4 was found not to be in SC3 (Figure 4.1). The first coarse spike is determined to have occurred prior to April 13, 2008. This event was not present in the Mooring D traps, thus likely a weak event. This coarse event followed

fine silty sediment ranging from 7 – 10 microns with 16 micron sediment. The intervalometer data shows evidence of a significant sediment pulse event at Mooring C on September 2 – 7, 2007 (Figure 3.16). The air and stream temperature had started to show a decreasing temperature trend with greater diurnal variability (3 to 5 °C for air temperature, 5 to 7 °C for stream temperature) from August 22; however, air temperature and stream temperature had a prolonged high September 3 – 5 (Figures 3.11 & 3.15). The temperature increased stepwise with up to 1 °C diurnal variability from September 3 – 5. The combination of the consistent warmer temperatures and a precipitation event on September 4<sup>th</sup> created enough energy in Linnéelva to flow more coarse sediment. Following this spike, the grain size decreased and represented the completion of summer sedimentation in Linnévatnet for 2007.

#### *4.1.2 – First Spring Sediment Event: Weather & Watershed Data*

The first sedimentation of the 2008 melt season increased from 11 microns to 27 microns in trap C4 and ranged from 22 to 26 microns in SC3 (Figure 4.2). This first sediment event was shown in the intervalometer and turbidity data on July 4 – 6, 2008 (Figures 3.16 & 3.18) and the influences include temperature, solar radiation, and stream temperature. May 22<sup>nd</sup> marked the conclusion of high winter diurnal air temperature variability of 5 – 8 °C (Figure 3.11). The subsequent air temperature followed an increasing trend with low diurnal variability (3 – 7 °C). July 2 – 5 held a prolonged increasing temperature trend. Solar radiation had also been increasing since May with high diurnal values (Figures 3.12 & 3.13). Throughout June the solar radiation greatly varied day to day ranging from highs greater than 500 W/m<sup>2</sup> to lows of 120 W/m<sup>2</sup>. However, from July 3 – 5, the solar radiation maximum values remained consistently



above  $500 \text{ W/m}^2$ . Stream temperature behaved similarly with the diurnal temperature changes beginning June 20 (Figure 3.15). The daily maximum increased to  $1^\circ\text{C}$  by June 29. On July 3<sup>rd</sup> the temperature reached  $2^\circ\text{C}$ , July 4<sup>th</sup> it was  $3^\circ\text{C}$ , and on July 5<sup>th</sup> the temperature reached  $4^\circ\text{C}$ . The lack of precipitation suggests that this inflow sedimentation event was caused by nival melt when the snowpack eventually becomes isothermal with increasing radiation and temperatures (Woo, 1993). The plume camera images also suggest nival melt (Figure 4.3).

The temperature, solar radiation, and stream temperatures were consistently high from July 2 – 4. The catchment responded to the consistent warming with the spring freshet on July 4<sup>th</sup>. The stream maximum temperature of July 4 was  $3^\circ\text{C}$  at 5:30 pm. On the night of July 4<sup>th</sup> at 11:00 pm, the lake temperature loggers showed the warm inflowing stream water at 10 meters with cooler water above and below (Figure 3.17). The temperature offset was due to the distance of the stream gage from the mooring. July 5<sup>th</sup> showed similar behavior; with water at the 3 m and 10 m levels water increasing in temperature. The water at depth, 14 m, remained unchanged throughout the event, thus indicating that the event was determined to be an interflow.

Because the temperature of the water at 14 m depth remained consistent throughout the first sedimentation pulse, the bottom water was still in “winter stratification.” However, this first showed an increase in temperature at 10 m indicating that the lake stratification was changing synchronously. While the bottom water remained cold, the inflowing current flowed at the 10 m level, thus behaving as an interflow (Figure 4.4). In this situation stream flow lagged air temperature and ripening of the snowpack as it likely retained meltwater for several days (Figure 4.5) (Woo, 1993).

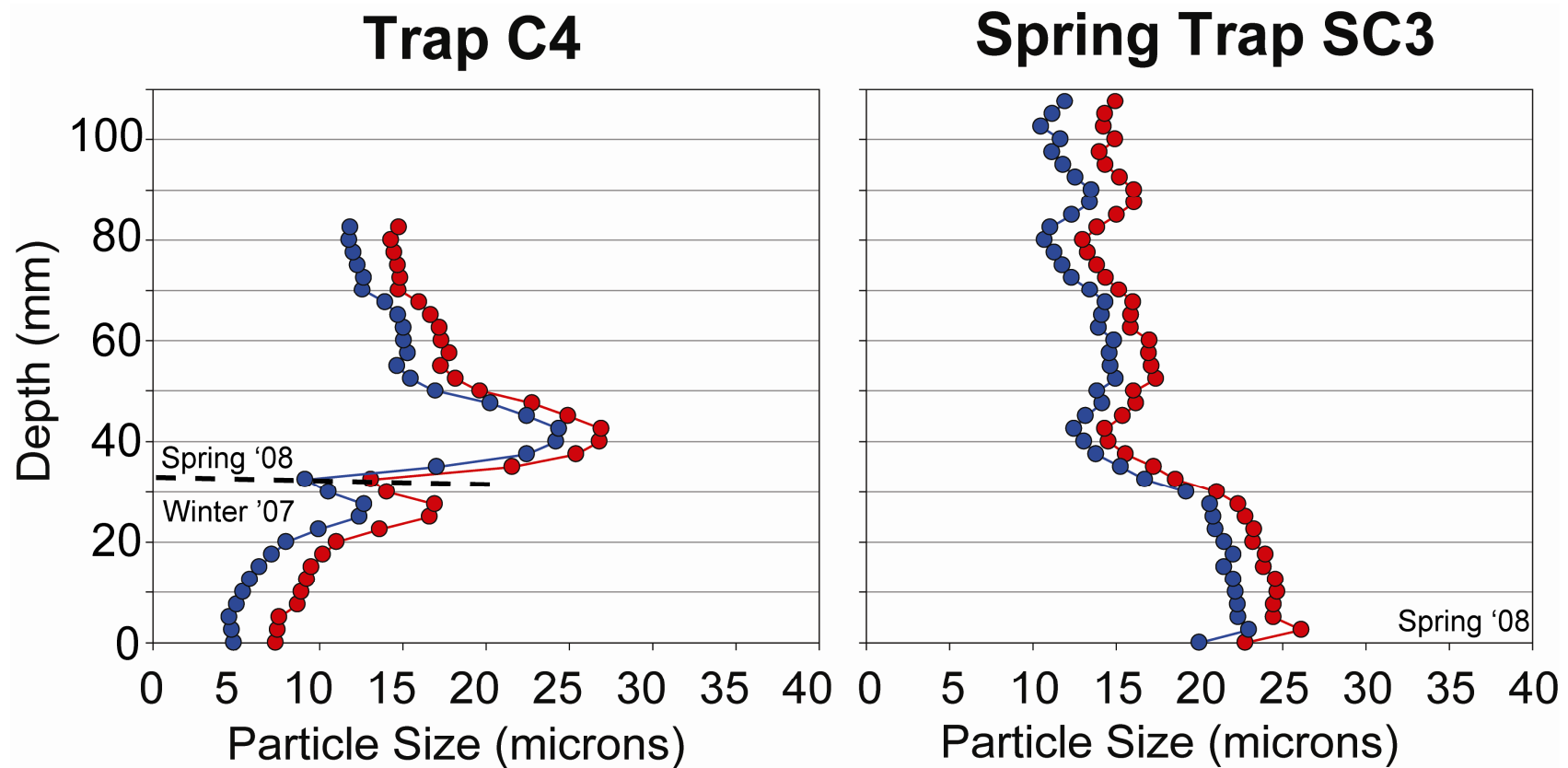


Figure 4.1: The dotted dashed line represents the conclusion of winter sedimentation and the beginning of spring sedimentation. The coarse peak seen below the dotted dashed line in C4 is not seen in SC3, thus occurred prior to the deployment of SC3. The dotted line represents the conclusion of winter sedimentation and the beginning of spring sedimentation.

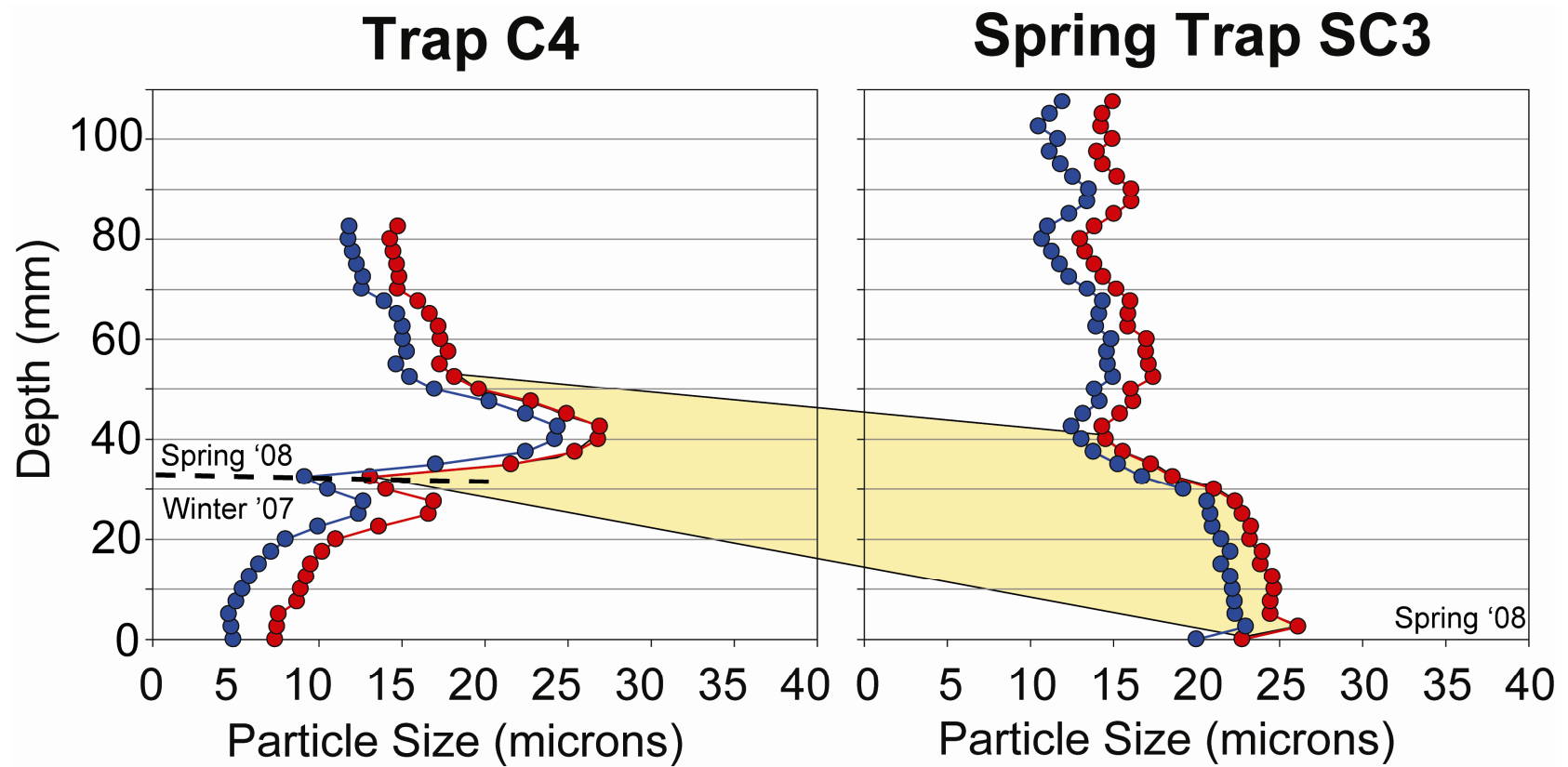


Figure 4.2: The first sedimentation event on July 3 – 5, 2008. The event was determined to be an interflow.



*June 24, 2008 at 4:10 pm*



*July 4, 2008 at 4:10 pm*

Figure 4.3: These two plume pictures depict the great amount of snow melt that occurred in Linnédalen from June 24 to July 4, 2008. The pictures indicate that the July 4-5, 2008 sediment event must have occurred as a nival melt flow.

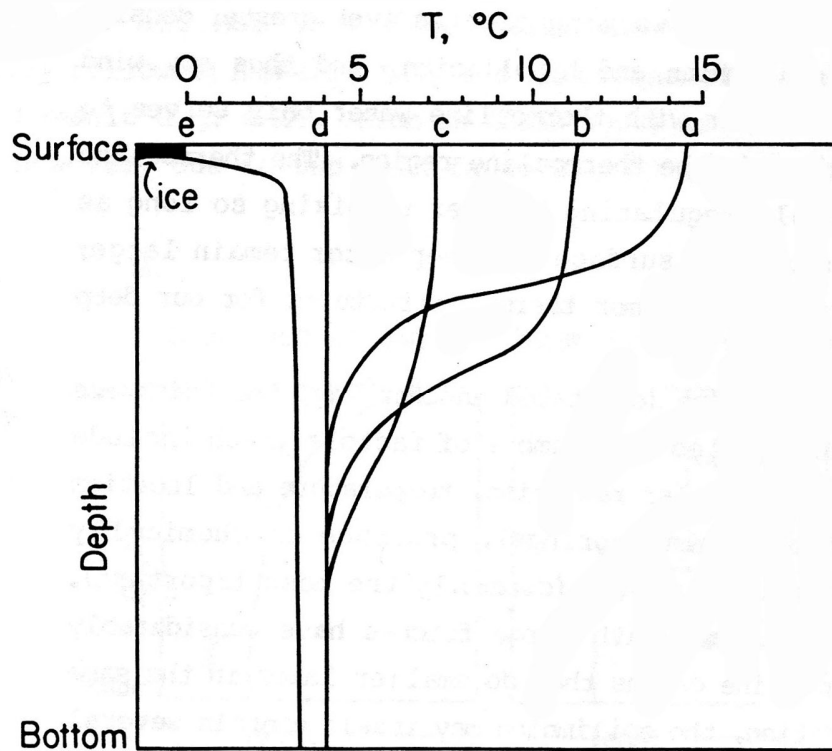


Figure 4.4: Lake stratification from mid-summer “a” to winter “e”. Note that in the winter, the bottom water is warmer and in the summer, the bottom water is colder. From Smith and Ashley, 1985.

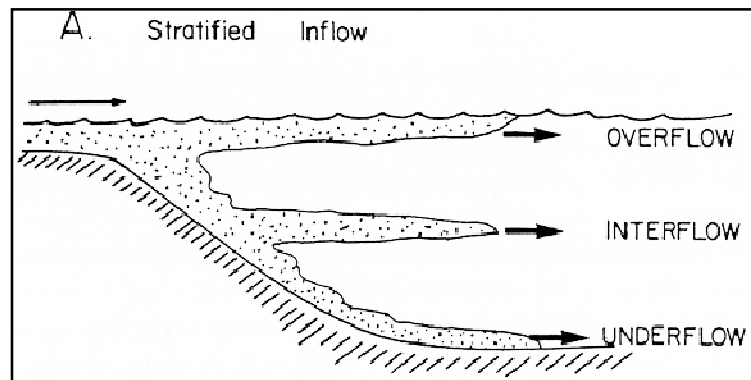


Figure 4.5: Stratified inflows of turbid water. For the first sedimentation event in Linnévatnet, an interflow was determined. From Smith and Ashley, 1985.

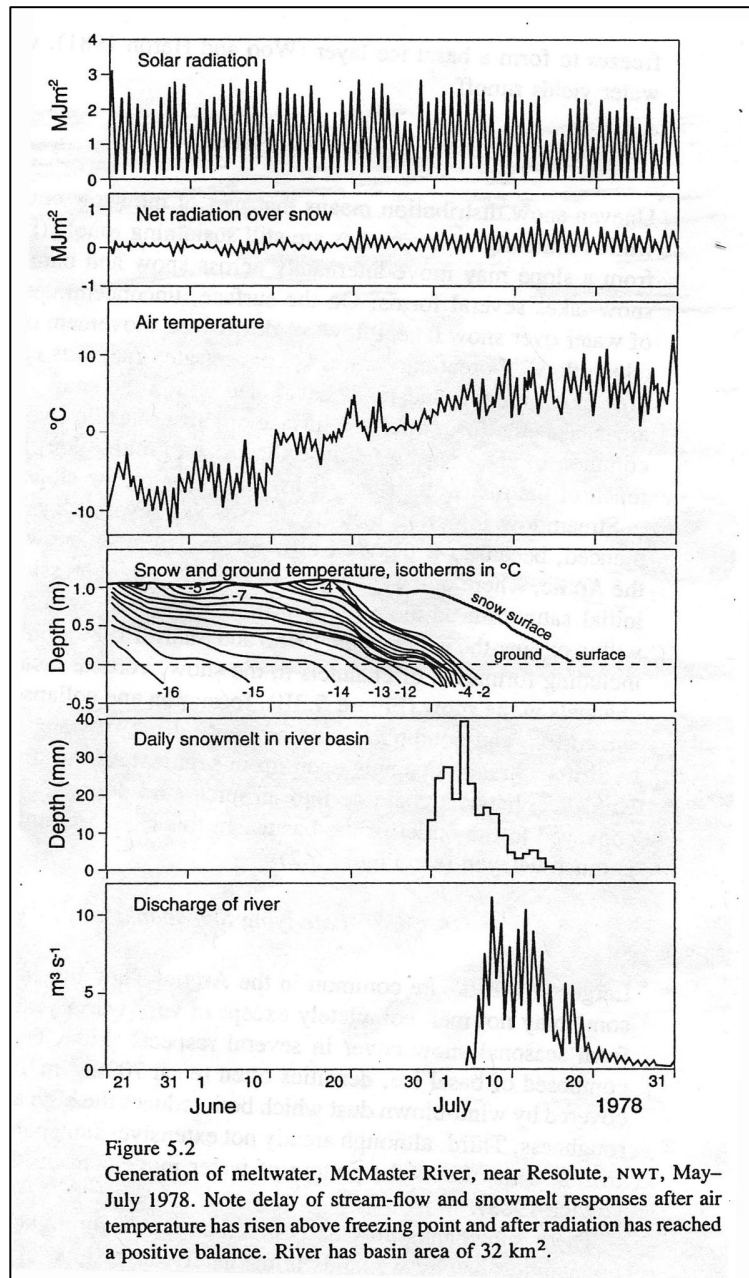


Figure 4.6: Diagram by Woo, 1993, describing the delay in discharge of an Arctic river. Note the increasing temperature trend lasting a couple of weeks and snow melt several days prior to river discharge. The peak discharge in the river is slightly offset from the peak snowmelt.

#### *4.1.2 – Minor Events: Weather & Watershed Data*

The intervalometer and turbidity data show minor sediment events occurred on July 6-8 between the first and second major events (Figures 3.16 & 3.18). On July 7 the stream temperature reached a maximum of 6.7 °C (Figure 3.15) and the air temperature reached 8.3 °C (Figure 3.11). The mooring temperature loggers showed that on July 7 – 9 there was activity at 10 meters with spikes nearing 2 °C (Figure 3.17). At 3 m and 6 m, there were temperature spikes asynchronous with the temperature at 10 m. These spikes were likely associated with overflows. Meanwhile, water at 14 m water remained undisturbed.

#### *4.1.3 – The Second Major 2008 Event: Weather & Watershed Data*

The second major sedimentation at Mooring C had particle size range of 16 – 20 microns in trap C4 while trap SC3 ranged from 14 – 17 microns (Figure 4.7). This second major sedimentation as seen in the intervalometer and turbidity data occurred on July 13 – 15 (Figures 3.16 & 3.18). Unlike the earlier spring freshet pulse, this event followed a precipitation event that occurred on July 12 and July 13 (Figure 3.11). Also, between July 12 and July 14, the diurnal low air temperature increased from 1.6 °C to 5 °C while the diurnal highs increased from 4.6 °C to 7.8 °C. Solar radiation was low, below 300 W/m<sup>2</sup>, on July 12 and 13; On July 14<sup>th</sup> the radiation jumped to a maximum of 813 W/m<sup>2</sup> (Figures 3.12 & 3.13). Stream temperature greatly increased within this time frame as well; July 12 was 3.4 °C, July 13 was 4.6 °C, and July 14 was 7.9 °C (Figure 3.15).

The second sediment pulse strongly affected the lake stratification since 14 m water had finally warmed from 1.3 °C on July 13 to 2 °C on July 14. The whole water column increased in temperature on the morning of July 13 to the evening of July 14, thus this event behaved as a homopycnal flow (Figure 4.9). The traps SC1, SC2, and



SC3 all reflect homopycnal activity. Loggers from the night of July 14 showed that an underflow occurred that night and then an overflow occurred in the afternoon of July 15.

This event was apparently primarily influenced by precipitation. Plume camera images illustrate the lack of snow in the valley at this time (Figure 4.10). Although the snow tree indicates that significant melting occurred on July 13, the tree was located in a depression where snow was able to linger longer than in the exposed areas. Therefore, this second sedimentation event was produced by a significant precipitation event.

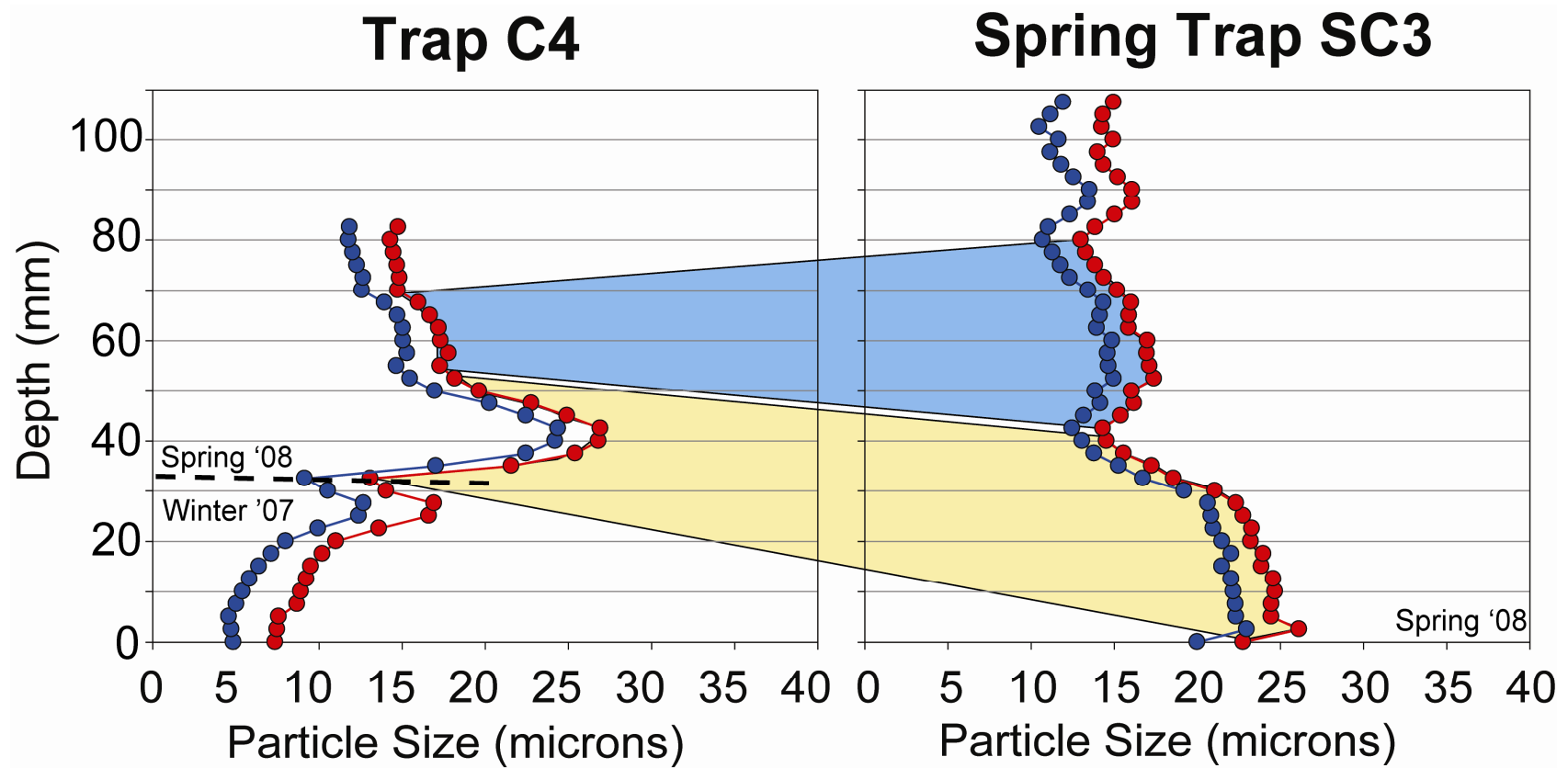


Figure 4.7: The second sedimentation event on July 13 – 15, 2008. This event was determined to be a homopycnal flow followed by smaller interflows and overflows.

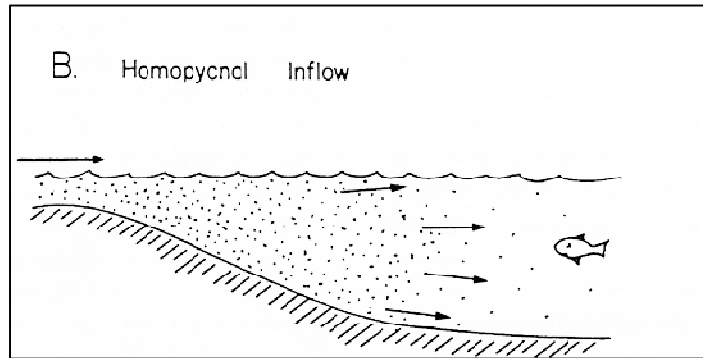


Figure 4.8: A diagram of a homopycnal flow by Smith and Ashley, 1985. The homopycnal flow is a homogenous dispersion of the inflowing turbid water throughout the whole water column.



*July 9, 2008 at 4:10 pm*



*July 13, 2008 at 4:10 pm*

Figure 4.9: Plume camera images show snow melt progression in Linnédalen while the lake ice melts and blows away from the south end of the lake. The second sedimentation event occurred while the lake was ice free.

#### **4.2 – Sediment Flux, 2007 – 2008**

The sediment flux at Mooring C did not exhibit the expected trend of increasing with depth. The flux was  $0.117 \text{ g/cm}^2$  at 6 m,  $0.075 \text{ g/cm}^2$  at 10 m, and  $0.164 \text{ g/cm}^2$  at 14 m. This discrepancy is evidence for a dominance of overflows and interflows over underflows. Overflows would result with more sediment accumulation and coarse grain size at shallow depths; interflows would result in the same at intermediate depths, and underflows at the bottom.

For 2007 – 2008, the interflow dominance was seen in the grain size of SC2 and SC3 (Figure 4.10). Trap SC2 contained coarser grains from the first sedimentation event (24 to 31 microns at 0 – 25 mm) than the deeper SC3 trap (23 to 26 microns 0 – 27.5 mm).

Trap SC1 showed mean grain size with a maximum 18 microns at 0 – 2.5 mm and subsequently 14 – 16 microns to 60 mm. Trap SC1, the upper 40 mm of SC2, and the upper 30 mm of SC3 reflected homopycnal flow since similar 14 – 16 micron grain size existed throughout all three traps.

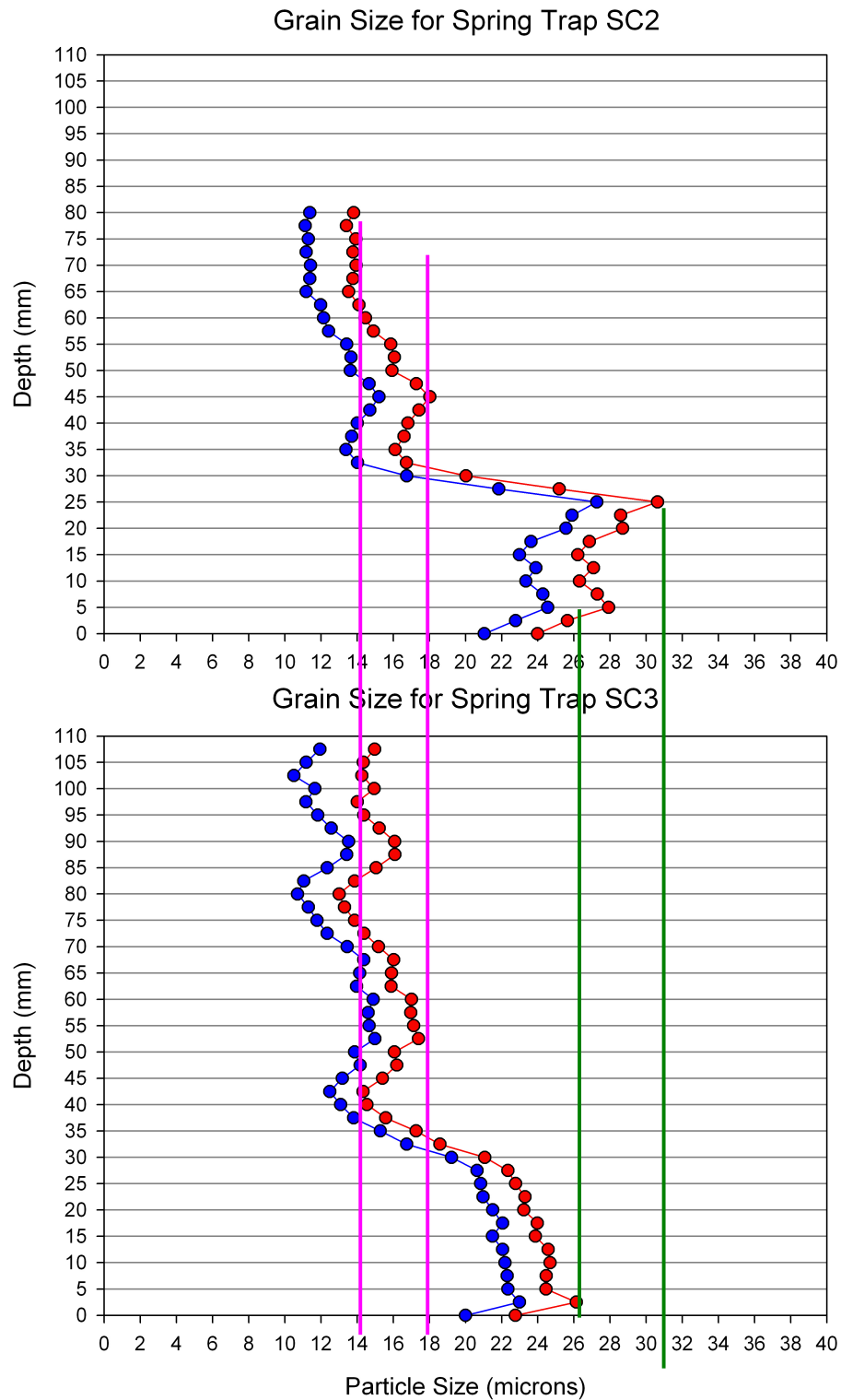


Figure 4.10: Comparison of grain size between SC2 at 10 m and SC3 at 14 m. The green lines are for the 1<sup>st</sup> event and the pink for the subsequent events.

### 4.3 – Comparison of Sediment from Previous Years

The sediment flux is given for each year of Mooring C sediment analysis from 2004 – 2008 in Table 4.1. In 2003 – 2004, the receiving tubes were too short for the accumulation, thus the stratigraphy could not be corrected determined. Due to this lack of data, 2003 – 2004 has been removed from the composite analysis.

<b>Table 4.1: Sediment Flux (g/m<sup>2</sup>) at Mooring C</b>					
<b>Trap</b>	<b>Depth</b>	<b>2004 - 2005</b>	<b>2005 - 2006</b>	<b>2006 – 2007</b>	<b>2007 - 2008</b>
C1	3 meters	0.027	0.240	0.106	LOST
C2	6 meters	0.128	0.310	0.257	0.117
C3	10 meters	0.159	0.320	0.329	0.075
C4	14 meters	0.251	0.299	0.463	0.164

Table 4.1: The data from previous years presented in the table were collected from Motley, 2006; Roop, 2007; and Cobin, 2008. The funnel size values to determine sediment flux were different for each dataset. For 2007 – 2008 an average of the 4 funnel size was used.

From 2004 – 2007 the sediment flux was increasing at Mooring C while in the 2007 – 2008, it decreased dramatically. The 2007 – 2008 flux was only 35% of the previous flux. The first and third sets of data show the expected trend of flux increasing with depth. The second and fourth show variability at the mooring; 2005 – 2006 increased in flux from C1 to C3 but decreased at C4 while 2007 – 2008 show a higher C2 and a maximum C4. Both years had to have been dominated by interflows and/or overflows for this variability to occur.

A composite of grain size analysis of the lowermost trap at Mooring C for all four years is presented in Figure 4.11. The summer of 2005 sediment showed four distinct coarse peaks decreasing from the 23 micron freshet in mean grain size as the season progressed (Motley, 2005). The summer 2005 layer ranged from 5 cm to 13 cm in the composite sequence. The winter 2005 layer was approximately 5 cm thick and contained

a minimum grain size of 6 microns (Roop, 2006). The grain size subsequently increased to two peaks of 38 microns in the summer 2006. The summer of 2006 was 19 cm to 26 cm. The winter 2006 accumulated approximately 10 cm of sediment ranging from 5.5 – 12.5 microns (Cobin, 2008).

The summer of 2007 accumulated the most sediment out of the four years (33 cm to 49 cm). There were six distinct coarse sediment events. The first was 25 microns and the fourth was 33 microns. As the sediment grain size decreased to winter characteristics there were two small peaks. The winter of 2007 was 5 cm thick and finished with a coarse peak of 17 microns. The summer of 2008 is characterized by one major event of 27 microns and a minor event of 18 microns. The total accumulation of the four years culminated in the summer 2008 with 61 cm.

The grain size from the tops of the 2005 – 2006 and the 2006 – 2007 plots do not match with the basal grain size of the subsequent trap. This is possibly due to sloughing of coarser grain particles during trap retrieval, differences in statistical analysis of the grain size, or missing sedimentation between retrieval and re-deployment of the next set of traps.



Four Years of C4 Trap Analyses  
Winter 2004 - Summer 2008

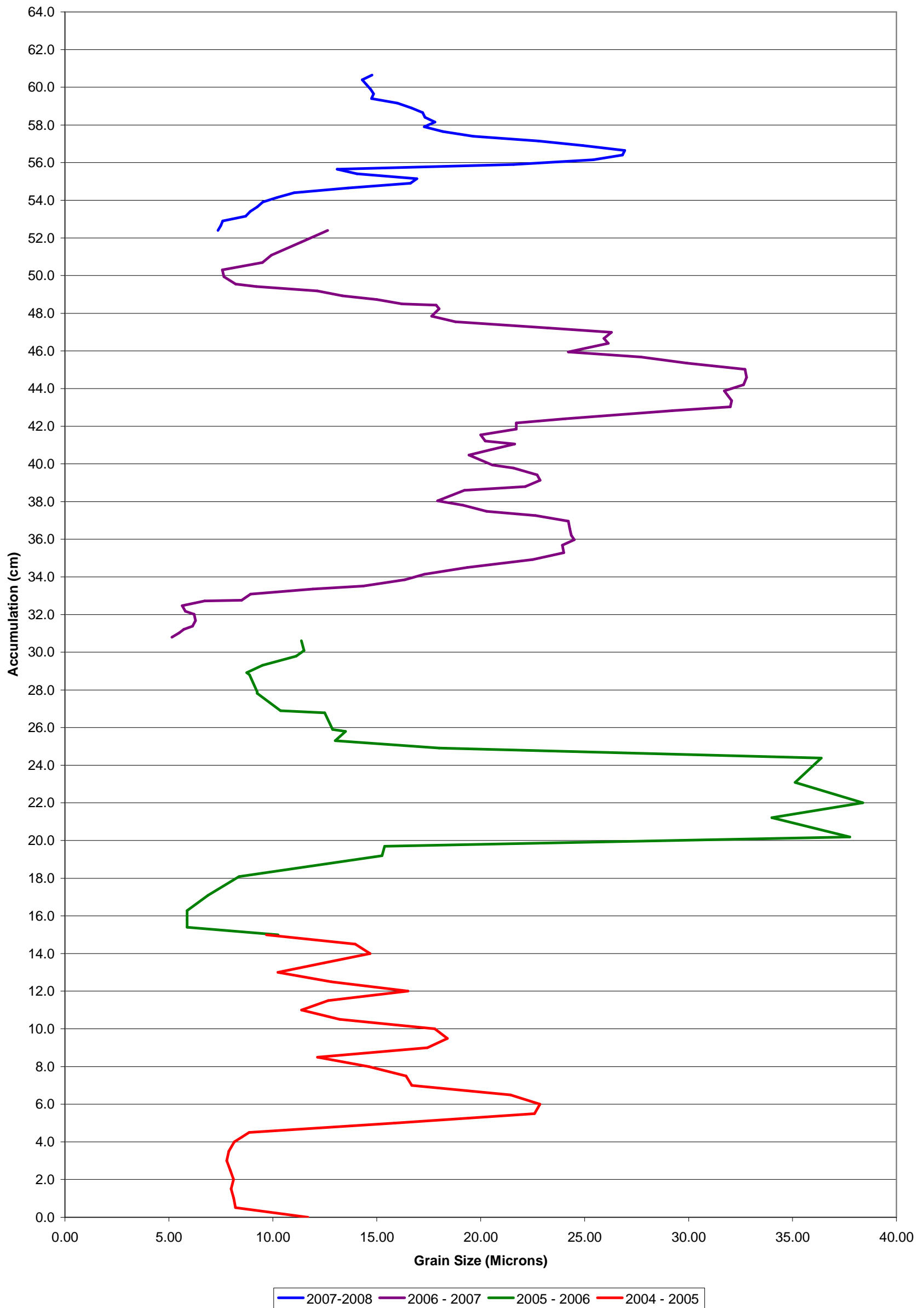


Figure 4.11: This is a compilation of the previous three years of C4 grain size data. Each color represents a different trap year with the blue as the data from the analysis of year 2008.

#### **4.4 – Comparison of Weather from 2004 - 2008**

Weather data had been continuously collected from the fall of 2004 to the summer of 2008 at the weather station near the south end of Linnévatnet. The composite weather data are presented in depositional years.

The average monthly air temperature data showed that May temperatures were typically approximately  $-2\text{ }^{\circ}\text{C}$  for three of the years. A temperature of  $0\text{ }^{\circ}\text{C}$  in 2006 was an exception (Table 4.2, modified from Cousot, 2008). The June and July temperatures decreased by  $0.9 - 1.4$  degrees from 2006 to 2008. The August temperatures decreased from between 2005 and 2008, whereas the September temperatures increased over the same period. The winters had variable temperatures with March typically the coldest month.

The solar radiation data showed that annual radiation increased from 2005 – 2008 to from  $736\text{ W/m}^2$  to  $816\text{ W/m}^2$  (Table 4.3, modified from Cousot, 2008). From 2005 – 2007 the maximum solar radiation occurred in May while in 2008 the maximum occurred in June.

Precipitation showed a decreasing trend between 2004 and 2008 from 977 mm to 269 mm annually (Table 4.4, modified from Cousot, 2008). The July and August precipitation decreased over time as well. Each year showed significant precipitation in the fall and winter months.

<b>Table 4.2</b>	<b>2004 – 2005 Summer - Winter</b>	<b>2005 – 2006 Summer - Winter</b>	<b>2006 – 2007 Summer - Winter</b>	<b>2007 – 2008 Summer - Winter</b>	<b>2008 – 2009 Summer - Winter</b>
<b>MAY</b>		<b>-2.02</b>	<b>-0.02</b>	<b>-2.18</b>	<b>-2.05</b>
<b>JUNE</b>		<b>3.16</b>	<b>3.75</b>	<b>3.45</b>	<b>2.31</b>
<b>JULY</b>		<b>5.99</b>	<b>6.56</b>	<b>6.50</b>	<b>5.66</b>
<b>AUGUST</b>	<b>5.91</b>	<b>6.40</b>	<b>5.68</b>	<b>5.49</b>	
<b>SEPTEMBER</b>	<b>1.44</b>	<b>0.05</b>	<b>1.03</b>	<b>1.65</b>	
<b>OCTOBER</b>	<b>-3.10</b>	<b>-5.33</b>	<b>-5.72</b>	<b>-2.29</b>	
<b>NOVEMBER</b>	<b>-10.91</b>	<b>-3.66</b>	<b>-4.42</b>	<b>-5.54</b>	
<b>DECEMBER</b>	<b>-6.49</b>	<b>-3.37</b>	<b>-6.51</b>	<b>-7.39</b>	
<b>JANUARY</b>	<b>-7.17</b>	<b>-2.70</b>	<b>-9.01</b>	<b>-5.88</b>	
<b>FEBRUARY</b>	<b>-6.54</b>	<b>-9.03</b>	<b>-8.64</b>	<b>-8.07</b>	
<b>MARCH</b>	<b>-14.30</b>	<b>-12.71</b>	<b>-6.46</b>	<b>-13.31</b>	
<b>APRIL</b>	<b>-8.65</b>	<b>-0.51</b>	<b>-9.60</b>	<b>-10.02</b>	

Table 4.2: Average monthly air temperature in °C from the Linnédalen weather station. Modified from Cousot, 2008 to represent depositional years.

<b>Table 4.3</b>	<b>2004 – 2005 Summer - Winter</b>	<b>2005 – 2006 Summer - Winter</b>	<b>2006 – 2007 Summer - Winter</b>	<b>2007 – 2008 Summer - Winter</b>	<b>2008 – 2009 Summer - Winter</b>
<b>MAY</b>		<b>204.53</b>	<b>171.67</b>	<b>199.72</b>	<b>193.29</b>
<b>JUNE</b>		<b>174.99</b>	<b>154.47</b>	<b>187.17</b>	<b>213.16</b>
<b>JULY</b>		<b>136.68</b>	<b>123.91</b>	<b>150.06</b>	<b>146.15</b>
<b>AUGUST</b>	<b>81.00</b>	<b>63.05</b>	<b>74.37</b>	<b>87.96</b>	
<b>SEPTEMBER</b>	<b>35.51</b>	<b>31.29</b>	<b>34.47</b>	<b>35.57</b>	
<b>OCTOBER</b>	<b>4.63</b>	<b>5.17</b>	<b>5.92</b>	<b>4.92</b>	
<b>NOVEMBER</b>	<b>0.60</b>	<b>0.60</b>	<b>0.60</b>	<b>0.60</b>	
<b>DECEMBER</b>	<b>0.60</b>	<b>0.60</b>	<b>0.60</b>	<b>0.60</b>	
<b>JANUARY</b>	<b>0.60</b>	<b>0.60</b>	<b>0.60</b>	<b>0.60</b>	
<b>FEBRUARY</b>	<b>1.56</b>	<b>1.87</b>	<b>1.66</b>	<b>1.93</b>	
<b>MARCH</b>	<b>27.19</b>	<b>30.26</b>	<b>26.62</b>	<b>33.11</b>	
<b>APRIL</b>	<b>102.63</b>	<b>86.26</b>	<b>101.26</b>	<b>112.95</b>	
<b>Annual solar radiation</b>	<b>254.32</b>	<b>735.9</b>	<b>696.15</b>	<b>815.19</b>	

Table 4.3: The average monthly solar radiation in  $W/m^2$  for each varve year. The annual solar total solar radiation is summed in the bottom row. Modified from Cousot, 2008 to represent depositional years.

<b>Table 4.4</b>	<b>2004 – 2005 Summer - Winter</b>	<b>2005 – 2006 Summer - Winter</b>	<b>2006 – 2007 Summer - Winter</b>	<b>2007 – 2008 Summer - Winter</b>	<b>2008 – 2009 Summer - Winter</b>
<b>MAY</b>		<b>9.40</b>	<b>12.40</b>	<b>2.20</b>	<b>8.00</b>
<b>JUNE</b>		<b>8.40</b>	<b>30.00</b>	<b>40.40</b>	<b>28.20</b>
<b>JULY</b>		<b>73.60</b>	<b>40.00</b>	<b>32.60</b>	<b>0.03</b>
<b>AUGUST</b>	<b>56.00</b>	<b>54.80</b>	<b>46.60</b>	<b>31.60</b>	
<b>SEPTEMBER</b>	<b>19.40</b>	<b>44.80</b>	<b>26.00</b>	<b>43.40</b>	
<b>OCTOBER</b>	<b>32.20</b>	<b>22.00</b>	<b>4.60</b>	<b>0.04</b>	
<b>NOVEMBER</b>	<b>180.24</b>	<b>10.80</b>	<b>17.80</b>	<b>4.80</b>	
<b>DECEMBER</b>	<b>279.05</b>	<b>48.60</b>	<b>22.00</b>	<b>28.80</b>	
<b>JANUARY</b>	<b>122.41</b>	<b>126.00</b>	<b>4.20</b>	<b>73.20</b>	
<b>FEBRUARY</b>	<b>155.02</b>	<b>15.80</b>	<b>0.40</b>	<b>11.80</b>	
<b>MARCH</b>	<b>132.82</b>	<b>3.40</b>	<b>57.80</b>	<b>0.00</b>	
<b>APRIL</b>	<b>3.00</b>	<b>8.40</b>	<b>3.20</b>	<b>0.00</b>	
<b>TOTAL ANNUAL</b>	<b>977.14</b>	<b>426.00</b>	<b>265.00</b>	<b>268.84</b>	

Table 4.4: The total monthly precipitation accumulation in mm. The total annual precipitation is summed in the bottom row. Modified from Cousot, 2008 to represent depositional years.

The weather data show that there was an annual decreasing trend in temperature, an increasing trend in solar radiation, and a decreasing trend in precipitation from year to year. However, the sediment flux evidence is not consistent with these trends. The sediment flux increased from 2004 to 2007 and decreased in 2008. The highest annual solar radiation and the least sediment flux for 2007 – 2008 is incongruous. The 2006 – 2007 year is the intermediate of the decreasing precipitation and temperature trends yet yields the greatest sediment flux. Thus, looking at weather trends alone over the four

years does not provide conclusive evidence as to what drives sedimentation in Linnévatnet. Each year is unique in temperature, solar radiation, precipitation, snow accumulation, etc. which all influence sedimentation to varying degrees. Therefore each sediment event in Linnévatnet may be unique in the driving force.

#### 4.5 – Comparison of Lake Bottom Deposition from 2004 – 2008

The equivalent thicknesses for lake bottom deposition from the previous studies are presented as “trap years” which start with winter layers and progress to summer layers. However, the conventional varves start with summer lamina then to winter lamina. Thus, the equivalent thicknesses calculated in the previous theses are not applicable to varved deposition on the lake bottom (Table 4.5).

<b>Table 4.5: Lake Bottom Deposition at Mooring C – Equivalent Thickness</b>					
<b>Trap</b>	<b>Depth</b>	<b>2004 - 2005</b>	<b>2005 - 2006</b>	<b>2006 – 2007</b>	<b>2007 - 2008</b>
C4	14 meters	1.4	1.7	2.6	0.9

Table 4.5: The equivalent thicknesses for lake bottom deposition as calculated by previous studies. These values are presented as trap years and cannot be applied to varve chronology.

The thin section from the top of the core collected at Mooring C shows recent laminae of varying thicknesses. The light layers are interpreted to be coarse summer layers while the dark are finer winter layers. It must be noted that the core was not collected at the exact location of Mooring C, although it was collected in the general vicinity.

Figure 4.7 shows the sediment core with the interpreted trap years – starting with 2008 as the first summer layer at the top, assuming that the top of the core represents the

newest sediment. Table 4.6 describes the thickness of each single lamina and the total thickness of the couplet.

<b>Table 4.6: Thickness of Lamina from C Core</b>		
<b>Lamina</b>	<b>Average mm</b>	<b>Year</b>
Summer 1	1.7	2008
Winter 1	1.5	2007 - 2008
Summer 2	1.9	2007
<b>Total</b>	<b>3.4</b>	
Winter 2	0.6	2006 - 2007
Summer 3	1.7	2006
<b>Total</b>	<b>2.3</b>	
Winter 3	2.9	2005 - 2006
Summer 4	7.3	2005
<b>Total</b>	<b>10.1</b>	
Winter 4	2.3	2004 - 2005
Summer 5	3.7	2004
<b>Total</b>	<b>6.0</b>	

Table 4.6: The average mm is the average of the thickness of each lamina from the right and left sides of the thin section. The first layer is assumed to be summer 2008.

The couplets vary in size from 2.3 mm to 10.1 mm. The largest couplet is summer 2005 to winter 2006. The smallest complete couplet is summer 2006 to winter 2007 with 2.3 mm.

The interpretations of the trap stratigraphy and the thin section laminae are shown in Figure 4.12. The first layer is assumed to be 2008 and the ages are counted back subsequently by lamina.

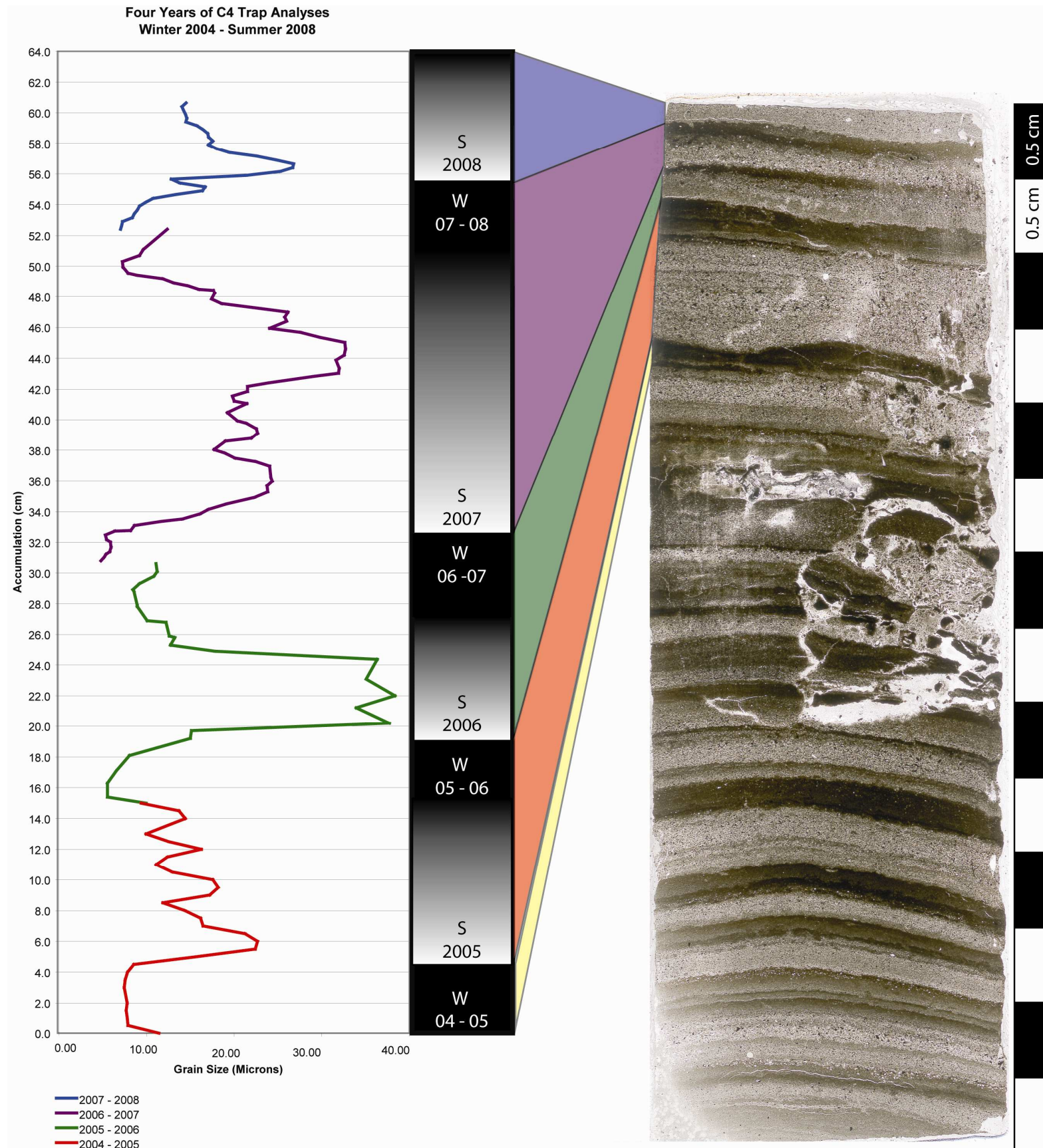


Figure 4.12: Comparison of the thin section with the four years of collected grain size data. The gradients express the graded beds of individual varves. The top summer layer is assumed to be summer 2008.



Table 4.7 describes the composite sediment accumulation thickness in the traps as depositional varves.

<b>Table 4.7: Composite Trap Accumulation</b>			
<b>Trap</b>	<b>cm</b>	<b>mm</b>	<b>Year</b>
Summer	5	50	2008
Winter	5	50	2007 - 2008
Summer	18	180	2007
Total	23	230	
Winter	9	90	2006 - 2007
Summer	6	60	2006
Total	15	150	
Winter	10.8	108	2005 - 2006
Summer	3.0	30	2005
Total	13.8	138	
Winter	4.3	43	2004 - 2005
Summer	NA	NA	2004
Total	NA	NA	

Table 4.7: The values of layer thickness from the composite graph of 4 years of sediment trap accumulation. Summer 2004 is unavailable.

The greatest sediment accumulation in sediment traps at Mooring C was the 2007 – 2008 depositional year with 230 mm. However, this layer on the thin section does not relate to sediment trap correlation if the top layer is assumed to be summer 2008. The thickest varve on the thin section is designated 2005 which accumulated 138 mm. Relatively, the thickest layer in the thin section should correspond to the thickest sediment accumulation in the trap. However, the thickest layer in the thin section cannot apply to the summer of 2007 because there are varves on top. Thus, it is likely that the top of the core must have lost sediment during retrieval or transportation. The 71 – 90% efficiency of the sediment trap (Gardener, 1980) may have also participated in the discrepancy.

**CHAPTER FIVE**

**CONCLUSIONS**



Sediment trap stratigraphy is greatly controlled by seasonal sedimentation. The winter sedimentation is fine-grained silt and generally a thinner unit than the summer layer. The winter layers occur after the summer peaks of air temperature, stream temperature, and solar radiation. The summer sedimentation is silt, 14 – 27 microns, and strongly influenced by air temperature, solar radiation, and/or precipitation. Multiple fining upward sublayers within the summer sediment reflect multiple inlet stream discharge events. The events may have occurred by different influences such as snowmelt peak and summer precipitation.

Traps C4 and SC3 describe the sedimentation for the 2007 – 2008 trap year. The difference between the two traps is the appearance of finer grained basal sediment in C4. The sharp and significant boundary between the fine and coarse sediments indicate that the sediment reflects the characteristics of varves. The finer grained sediment was the conclusion of the 2007 deposition year and the coarse grained sediment was the beginning of the 2008 year.

The grain size characteristics of C4 and SC3 compared with the weather and environmental data indicate that the first sedimentation pulse of the 2008 meltseason occurred on July 4 – 5, 2008 and was an interflow. The plume camera images determined that the pulse was due to a nival flow following several days of high temperature and solar radiation. The nival flow was likely delayed because meltwater retention in the snow. The snowpacks melted steadily from June 24 to July 4, 2008, but did not affect the lake inflow until July 4<sup>th</sup>.

The second sediment event was determined to occur during July 13 – 15<sup>th</sup>. This event was influenced by a significant precipitation event on July 12 – 13, 2008. Since the

majority of the snow had melted during the first sedimentation event, the precipitation strongly affected the stream. The resulting stream flow entered the lake as a homopycnal flow.

The sediment accumulation for 2007 – 2008 deposition year was large with 230 mm as compared with previous years which were 150 mm and 138 mm for 2006 and 2005 respectively. The air temperature and precipitation were lower than the previous year (2006 – 2007) while solar radiation was consistently higher throughout May – September, 2007. Thus the influence, as compared to previous years, for the 2007 – 2008 deposition year was high solar radiation.

Correlation between varve thickness and weather data from the past four years do not reveal significant trends. More complete analysis is needed to determine the influence of weather on annual sediment yields.

Comparison of thin section stratigraphy with the four years of sediment trap accumulation was not conclusive. The laminae in the core did not appear to correspond directly to the composite sediment trap stratigraphy. It is suggested that the lack of correlation may be due to loss of the upper lamination in the core due to problems in core retrieval, handling, or thin section production. Alternatively, it may be possible that due to the positioning of the inflow in the water column, a key layer or part of a sequence is missing from the sediment traps and misaligns the correlation. Better core retrieval and continued modern process work may allow for better correlation in the future.

The ultimate goal of this project was to determine the influences of sediment deposition in Linnévatnet for the purpose of calibrating laminae from greater depths in order to facilitate paleoclimate/paleoenvironmental reconstruction. This study has

determined that the influences are unique to the intraseasonal processes depending on air temperature, solar radiation, precipitation, and snow melt.

To further continue the study and produce more successful results, a series of sediment cores from the Mooring C location would provide more details for deposition. The multiple cores would relate to each other and show how sedimentation changes by slight changes in locality near the inlet. Also, a multi-year sediment trap would provide a continuous sediment trap record that would correlate well to a sediment core since there would be no discontinuities between years. Further analysis of sediment trap data and lake deposition with meteorological data would provide a more detailed record and a more accurate calibration tool.

## REFERENCES

- Arctic Report Card: J. Overland, J. Walsh, M. Wang, 2008, Arctic Report Card 2008, <http://www.arctic.noaa.gov/reportcard>.
- Bennett, M.R., and Glasser, N.F., 1996, *Glacial Geology, Ice Sheets and Landforms: England*, John Wiley and Sons Ltd.
- Bøyum, A. and Kjensmo, J. 1978, Physiography of Lake Linnevatnet, Western Spitsbergen. *Verein Limnology*. v. 20, p. 639-614.
- Clark, J.S., Royall, P.D., 1995, Particle-size evidence for source areas of charcoal accumulation in Late Holocene Sediments of eastern North American lakes: *Quaternary Research*, v. 23, p. 80-89.
- Cobin, P., 2008, Evaluation of modern sedimentation process in a proglacial lake: Linnévatnet, Spitsbergen, Svalbard. Unpublished Mount Holyoke College Thesis.
- Cousot, A., 2008, Short-term meteorological influence on High Arctic Glacier, Linnédalen, Svalbard, Norway. Unpublished independent study at UNIS.
- Hjelle, A., Lauritzen, Ø., Salvigsen, O., and Wisnes, T.S., 1986, Geological map. Svalbard 1:100,000. Sheet B10G Van Mijenfjorden. Nor. Polarinst. Temakart No. 2.
- Ingólfsson, Ó., 2006, Outline of the geography and geology of Svalbard. [http://www.hi.is/~oi/svalbard\\_geology.htm](http://www.hi.is/~oi/svalbard_geology.htm).
- IPCC 2006 Report: [http://www.ipcc.ch/pdf/assessment-report/ar4/syr/ar4\\_syr\\_spm.pdf](http://www.ipcc.ch/pdf/assessment-report/ar4/syr/ar4_syr_spm.pdf)
- Gardner, W.D., 1980, Sediment trap dynamics and calibration; a laboratory evaluation: *Journal of Marine Research*, v. 38, p. 17-39.
- Kane, D.L., Hinzman, L.D., Woo, M.K., and Everett, K.R., 1992, Arctic Hydrology and Climate Change, in Chapin III, F., Jefferies, R., Reynolds, J., Shaver, G., Svoboda, J., and Chu, E., eds., *Arctic Ecosystems in a Changing Climate: San Diego*, Academic Press, Inc., p. 35-55.
- Lamoureux, S.F., 1994, Embedding unfrozen lake sediments for thin section preparation: *Journal of Paleolimnology*, v. 10, p 141-146.
- Leemann, A. & Niessen, F, 1994, Varve formation and the climate record in an alpine proglacial lake; calibrating annually-laminated sediments against hydrological and meteorological data: *The Holocene*, v. 4, p. 1-8.

- Leo, B., 2007, Recent sedimentation chronology of Linnévatnet, a High Arctic proglacial lake, Svalbard, Norway. Unpublished Bates College B.S. thesis.
- Mangerud, J., and Svendsen, J.I., 1990, Deglaciation chronology inferred from marine sediments in a proglacial lake basin, western Spitsbergen, Svalbard: *Boreas*, v. 19, p. 249-272.
- McKay, N., 2004, Characterization of Climatic Influences on Modern Sedimentation in an Arctic Lake, Svalbard, Norway. Unpublished independent study.
- Motley, B., 2006, Sedimentation in Linnévatnet, Svalbard during 2004-2005: a modern process study using sediment traps. Unpublished Bates College B.S. Thesis.
- NSIDC Arctic Climatology and Meteorology Primer (<http://nsidc.org/arcticmet/>)
- Overpeck, J., Hughen, D., Bradley, R., Case, R., Douglas, M., Finney, B., Gajewski, K., Jacoby, G., Jennings, A., Lamoureux, S., MacDonald, G., Moore, J., Retelle, M., Smith, S., Wolfe, A., Zielinski, G., 1997, Arctic Environmental Change of the Last Four Centuries: *Science*, v. 278, p. 1251-1256.
- Roop, H., 2007, Sedimentation in a proglacial lake: Interpreting inter and intra-annual sedimentation in Linnévatnet, Spitsbergen, Norway. Unpublished Mount Holyoke College B.A. Thesis.
- Rouse, W.R., 1993, Northern Climates, in French, H.M. and Slaymaker, O., eds, *Canada's Cold Environments: Quebec*, McGill Queen's University Press, p. 117-142.
- Serreze, M.C., Walsh, J.E., Chapin III, F.S., Osterkamp, T., Dyrgerov, M., Romanovsky, V., Oechel, W.C., Morison, J., Zhang, T., and Barry, R.G., 2000, Observational evidence of recent change in the northern high-latitude environment: *Climatic Change*, v. 46, p. 159-207.
- Siegert, M.J., Dowdeswell, J.A., Svendsen, J.I., Elverhøi, A., 2002, Eurasian Arctic During the Last Ice Age: *American Scientist*, v. 90, p. 32-39.
- Smith, N.D., and Ashley, G., 1985, Proglacial lacustrine environments. Ch. 4, in *Glacial Sedimentary Environments*, eds. Ashley, G., Shaw, J., and Smith, N.D.; S.E.P.M. short course no. 16, pgs. 135-215.
- Snyder, J.A., Werner, A., and Miller, G.H., 2000, Holocene cirque glacier activity in western Spitsbergen, Svalbard: Sediment records from proglacial Linnevatnet: *Holocene*, v. 10, p. 555-563.

- Sturm, M.N., 1979, Origin and composition of clastic varves, in Schluster, A. (ed.), Moraines and varves, Rotterdam, A.A. Balkema, p. 281-285.
- Svendsen, J.I., Alexanderson, H., Astakhov, V.I., Demidov, I., Dowdeswell, J.A., Funder, S., Gataullin, B., Henricksen, M., Hjort, C., and Houmark-Nielsen, M., 2004, Late Quaternary ice sheet history of northern Eurasia: Quaternary Science Reviews, v. 23 p. 1229-1271.
- Svendsen, J.I., Landvik, J.Y., Mangerud, J., and Miller, G.H., 1989, Denudation rates in the Arctic estimated from lake sediments on Spitsbergen, Svalbard: Palaeogeography, Palaeoclimatology, Palaeoecology, v. 76, p. 153-168.
- Svendsen, J.I., and Mangerud, J., 1997, Holocene glacial and climatic variations on Spitsbergen, Svalbard: Holocene, v. 7, p. 45-57.
- Werner, Al, 2007, <http://www.mtholyoke.edu/proj/svalbard/welcome.shtml>.
- Woo, M.K., 1993. Northern Hydrology, in French, H.M. and Slaymaker, O., eds, Canada's Cold Environments: Quebec, McGill Queen's University Press, p. 117-142.



**APPENDIX A: SEDIMENT TRAP NOTES**

<b>Table 1: Split Sample Total Thickness</b>			
Trap	Lower (cm)	Higher (cm)	Total (cm)
C2	5.7	6.1	5.90
C3	4.0	4.0	4.00
C4	8.8	8.8	8.80
SC1	6.1	6.1	6.10
SC2	7.8	8.5	8.15
SC3	11.0	11.3	11.15
D1	2.4	2.6	2.50
D2	1.6	1.6	1.60
D3	1.6	1.6	1.60
D4	2.6	2.6	2.60
E1	3.6	3.8	3.70
E2	4.0	4.5	4.25
F1	1.3	1.5	1.40
F2	1.8	2.0	1.90
F3	2.7	3.0	2.85
G1	1.0	1.1	1.05
G2	2.3	2.3	2.30
G3	4.0	4.4	4.20
G4	2.9	3.0	2.95
G5	5.5	5.5	5.50

<b>Table 2: Difference in Sediment Accumulation (cm)</b>				
Trap	Lab Total	Field Total	Difference	Ratio (L/F)
C2	5.9	8.7	2.8	0.68
C3	4.0	6.8	2.8	0.59
C4	8.8	10.6	1.8	0.83
SC1	6.1	7.3	1.2	0.84
SC2	8.2	10.0	1.9	0.82
SC3	11.2	13.3	2.1	0.84
D1	2.5	4.0	1.5	0.63
D2	1.6	3.2	1.6	0.50
D3	1.6	3.1	1.5	0.52
D4	2.6	5.1	2.5	0.51
E1	3.7	7.2	3.5	0.51
E2	4.3	6.0	1.8	0.71
F1	1.4	2.5	1.1	0.56
F2	1.9	4.3	2.4	0.44
F3	2.9	3.8	1.0	0.75
G1	1.1	2.5	1.4	0.43
G2	2.3	4.4	2.1	0.52
G3	4.2	4.9	0.7	0.86
G4	3.0	6.4	3.5	0.46
G5	5.5	7.7	2.2	0.71

Table 3: Linnévatnet 2008 Dry Sample Analysis Sediment Flux ( f ) and Equivalent Thickness ( t )						
Trap	Dry Density	Dry T	Volume Sed.	mass	f = m/a	t=f/(bd)*10
	$g/cm^3$	cm	$cm^3$	g	$g/cm^2$	mm/yr
C2	1.19	5.90	11.56	13.72	0.117	0.65
C3	1.12	4.00	7.84	8.79	0.075	0.42
C4	1.11	8.80	17.25	19.21	0.164	0.91
SC1	1.05	6.10	11.96	12.54	0.045	0.25
SC2	1.26	8.15	15.97	20.06	0.072	0.40
SC3	1.14	11.15	21.85	25.01	0.089	0.50
D1	1.19	2.50	4.90	5.85	0.050	0.28
D2	1.10	1.60	3.14	3.44	0.029	0.16
D3	1.13	1.60	3.14	3.54	0.030	0.17
D4	1.01	2.60	5.10	5.16	0.044	0.25
E1	1.29	3.70	7.25	9.39	0.080	0.45
E2	1.07	4.25	8.33	8.91	0.076	0.42
F1	1.03	1.40	2.74	2.84	0.024	0.13
F2	1.08	1.90	3.72	4.01	0.034	0.19
F3	0.96	2.85	5.59	5.36	0.046	0.25
G1	0.93	1.05	2.06	1.92	0.016	0.09
G2	0.93	2.30	4.51	4.20	0.036	0.20
G3	0.56	4.20	8.23	4.64	0.040	0.22
G4	0.65	2.95	5.78	3.75	0.032	0.18
G5	1.00	5.50	10.78	10.73	0.092	0.51

- To determine the volume of the sediment, the dry thickness (Dry T) of each sample was multiplied by the area of the cross section of the receiving tube. The tubes were 1.58 cm in diameter and the area was  $1.96 \text{ cm}^2$ .
- Five different funnel sizes were used in the previous studies, the funnel sizes used in this equation are averages the funnel sizes. The Year-Long Traps funnel size was  $a = 116.9 \text{ cm}^2$  and the Spring Traps was  $a = 280.2 \text{ cm}^2$ .
- The dry density was determined from the dry mass of  $0.5 \text{ cm}^3$  sub-samples.
- The “bd” value used for the Equivalent Thickness equation was 1.8, which is the average bulk density of Linnévatnet sediment as determined by McKay, 2005.

## APPENDIX B: GRAIN SIZE DATA

The following are the grain size analysis data. The mean and median values for the 3<sup>rd</sup> run of each sample are given in microns. Sample (0 cm or 0 mm) is from the bottom of the trap. Each sample consists of all sediment between its bottom and the bottom of the next sample. All traps were sampled at the same 0.25 cm or 2.5 mm interval.

The raw data in .ls and .xls file formats are on the attached CD.

<b>C2</b>				
Sample #	cm	mm	Mean (µm)	Median (µm)
1	0.00	0.0	8.570	5.595
2	0.25	2.5	15.72	11.11
3	0.50	5.0	22.87	19.28
4	0.75	7.5	28.73	26.05
5	1.00	10.0	31.58	29.39
6	1.25	12.5	31.00	28.91
7	1.50	15.0	30.12	28.48
8	1.75	17.5	30.47	28.66
9	2.00	20.0	31.53	29.72
10	2.25	22.5	32.78	30.99
11	2.50	25.0	33.12	31.66
12	2.75	27.5	26.1	22.06
13	3.00	30.0	20.61	16.45
14	3.25	32.5	19.19	15.2
15	3.50	35.0	19.21	15.97
16	3.75	37.5	19.15	16.16
17	4.00	40.0	17.93	14.44
18	4.25	42.5	16.98	13.85
19	4.50	45.0	15.91	12.74
20	4.75	47.5	15.53	12.56
21	5.00	50.0	15.62	12.42
22	5.25	52.5	16.13	12.46
23	5.50	55.0	16.26	13.15
<b>C3</b>				
Sample #	cm	mm	Mean (µm)	Median (µm)
1	0.00	0.00	8.348	5.125
2	0.25	2.50	10.71	7.143
3	0.50	5.00	15.63	11.47
4	0.75	7.50	19.03	14.2
5	1.00	10.00	20.85	15.84
6	1.25	12.50	24.66	20.66
7	1.50	15.00	28.04	24.97
8	1.75	17.50	27.49	24.71
9	2.00	20.00	21.81	18.64
10	2.25	22.50	17.99	14.97
11	2.50	25.00	17.72	14.85

12	2.75	27.50	18.44	15.69
13	3.00	30.00	17.25	14.73
14	3.25	32.50	16.25	13.92
15	3.50	35.00	14.86	12.53
16	3.75	37.50	14.53	12.15
17	4.00	40.00	14.06	11.87
18	4.25	42.50	14.78	12.19
<b>C4</b>				
Sample #	cm	mm	Mean (µm)	Median (µm)
1	0.00	0.0	7.368	4.863
2	0.25	2.5	7.494	4.739
3	0.50	5.0	7.586	4.586
4	0.75	7.5	8.694	5.033
5	1.00	10.0	8.913	5.409
6	1.25	12.5	9.253	5.829
7	1.50	15.0	9.516	6.398
8	1.75	17.5	10.21	7.137
9	2.00	20.0	11.03	8.006
10	2.25	22.5	13.62	9.953
11	2.50	25.0	16.62	12.40
12	2.75	27.5	16.93	12.69
13	3.00	30.0	14.05	10.55
14	3.25	32.5	13.10	9.149
15	3.50	35.0	21.58	17.04
16	3.75	37.5	25.42	22.46
17	4.00	40.0	26.82	24.21
18	4.25	42.5	26.93	24.39
19	4.50	45.0	24.93	22.46
20	4.75	47.5	22.78	20.27
21	5.00	50.0	19.64	16.97
22	5.25	52.5	18.18	15.48
23	5.50	55.0	17.29	14.67
24	5.75	57.5	17.80	15.31
25	6.00	60.0	17.32	15.07
26	6.25	62.5	17.21	15.05
27	6.50	65.0	16.68	14.72
28	6.75	67.5	15.99	13.95
29	7.00	70.0	14.75	12.59
30	7.25	72.5	14.85	12.67
31	7.50	75.0	14.71	12.29
32	7.75	77.5	14.49	12.04
33	8.00	80.0	14.30	11.79
34	8.25	82.5	14.77	11.85
<b>SC1</b>				
Sample #	cm	mm	Mean (µm)	Median (µm)
1	0.00	0.00	18.36	16.80
2	0.25	2.50	18.66	16.59
3	0.50	5.00	15.83	13.56

4	0.75	7.50	14.90	12.67
5	1.00	10.00	15.03	12.71
6	1.25	12.50	14.56	12.37
7	1.50	15.00	14.97	12.82
8	1.75	17.50	15.12	12.67
9	2.00	20.00	15.12	12.81
10	2.25	22.50	15.40	13.10
11	2.50	25.00	15.47	13.15
12	2.75	27.50	15.59	13.35
13	3.00	30.00	15.14	13.02
14	3.25	32.50	14.80	12.58
15	3.50	35.00	15.04	12.69
16	3.75	37.50	15.08	12.86
17	4.00	40.00	15.28	12.97
18	4.25	42.50	15.45	13.00
19	4.50	45.00	15.30	13.02
20	4.75	47.50	15.32	12.91
21	5.00	50.00	15.65	13.32
22	5.25	52.50	15.66	13.23
23	5.50	55.00	14.69	12.06
24	5.75	57.50	15.80	13.31
25	6.00	60.00	14.21	12.22
<b>SC2</b>				
Sample #	cm	mm	Mean (µm)	Median (µm)
1	0.00	0.00	23.99	21.04
2	0.25	2.50	25.64	22.77
3	0.50	5.00	27.92	24.55
4	0.75	7.50	27.29	24.28
5	1.00	10.00	26.31	23.34
6	1.25	12.50	27.08	23.90
7	1.50	15.00	26.21	22.98
8	1.75	17.50	26.86	23.63
9	2.00	20.00	28.70	25.56
10	2.25	22.50	28.59	25.90
11	2.50	25.00	30.63	27.27
12	2.75	27.50	25.19	21.84
13	3.00	30.00	20.02	16.75
14	3.25	32.50	16.73	14.02
15	3.50	35.00	16.10	13.39
16	3.75	37.50	16.60	13.71
17	4.00	40.00	16.81	14.01
18	4.25	42.50	17.43	14.71
19	4.50	45.00	18.02	15.21
20	4.75	47.50	17.28	14.66
21	5.00	50.00	15.93	13.62
22	5.25	52.50	16.06	13.67
23	5.50	55.00	15.87	13.43
24	5.75	57.50	14.90	12.43

25	6.00	60.00	14.46	12.14
26	6.25	62.50	14.10	11.98
27	6.50	65.00	13.52	11.19
28	6.75	67.50	13.77	11.38
29	7.00	70.00	13.94	11.42
30	7.25	72.50	13.76	11.18
31	7.50	75.00	13.92	11.30
32	7.75	77.50	13.40	11.12
33	8.00	80.00	13.81	11.39
<b>SC3</b>				
Sample #	cm	mm	Mean (µm)	Median (µm)
1	0.00	0.00	22.76	20.00
2	0.25	2.50	26.13	22.98
3	0.50	5.00	24.46	22.34
4	0.75	7.50	24.47	22.31
5	1.00	10.00	24.68	22.18
6	1.25	12.50	24.58	22.05
7	1.50	15.00	23.87	21.49
8	1.75	17.50	23.98	22.05
9	2.00	20.00	23.23	21.50
10	2.25	22.50	23.29	20.97
11	2.50	25.00	22.77	20.84
12	2.75	27.50	22.34	20.64
13	3.00	30.00	21.06	19.22
14	3.25	32.50	18.58	16.74
15	3.50	35.00	17.27	15.28
16	3.75	37.50	15.58	13.80
17	4.00	40.00	14.55	13.08
18	4.25	42.50	14.33	12.48
19	4.50	45.00	15.40	13.18
20	4.75	47.50	16.20	14.17
21	5.00	50.00	16.06	13.87
22	5.25	52.50	17.40	14.98
23	5.50	55.00	17.13	14.67
24	5.75	57.50	16.97	14.61
25	6.00	60.00	17.01	14.88
26	6.25	62.50	15.88	13.96
27	6.50	65.00	15.90	14.15
28	6.75	67.50	16.03	14.36
29	7.00	70.00	15.19	13.44
30	7.25	72.50	14.39	12.34
31	7.50	75.00	13.86	11.78
32	7.75	77.50	13.30	11.30
33	8.00	80.00	13.00	10.71
34	8.25	82.50	13.87	11.05
35	8.50	85.00	15.04	12.35
36	8.75	87.50	16.09	13.43
37	9.00	90.00	16.08	13.52

38	9.25	92.50	15.23	12.56
39	9.50	95.00	14.36	11.83
40	9.75	97.50	14.01	11.16
41	10.00	100.00	14.95	11.67
42	10.25	102.50	14.26	10.50
43	10.50	105.00	14.34	11.18
44	10.75	107.50	14.97	11.94
<b>D1</b>				
Sample #	cm	mm	Mean (µm)	Median (µm)
1	0.00	0.00	8.043	5.120
2	0.25	2.50	10.540	6.338
3	0.50	5.00	13.440	9.368
4	0.75	7.50	10.300	8.369
5	1.00	10.00	11.550	9.930
6	1.25	12.50	11.480	9.760
7	1.50	15.00	12.320	10.470
8	1.75	17.50	11.970	10.070
9	2.00	20.00	11.330	9.422
<b>D2</b>				
Sample #	cm	mm	Mean (µm)	Median (µm)
1	0.00	0.00	8.317	5.260
2	0.25	2.50	10.91	7.480
3	0.50	5.00	12.02	9.555
4	0.75	7.50	11.68	9.515
5	1.00	10.00	11.37	9.429
6	1.25	12.50	10.94	8.928
<b>D3</b>				
Sample #	cm	mm	Mean (µm)	Median (µm)
1	0.00	0.00	8.602	5.000
2	0.25	2.50	11.400	7.511
3	0.50	5.00	16.290	11.720
4	0.75	7.50	12.720	9.661
5	1.00	10.00	12.780	10.280
6	1.25	12.50	12.520	9.827
7	1.50	15.00	12.390	9.574
<b>D4</b>				
Sample #	cm	mm	Mean (µm)	Median (µm)
1	0.00	0.00	7.905	5.063
2	0.25	2.50	9.006	5.423
3	0.50	5.00	9.577	5.989
4	0.75	7.50	9.989	6.404
5	1.00	10.00	10.06	6.584
6	1.25	12.50	10.64	7.073
7	1.50	15.00	16.12	11.56
8	1.75	17.50	15.84	11.52
9	2.00	20.00	14.14	9.363
10	2.25	22.50	13.87	11.10
11	2.50	25.00	12.46	10.24



	12	2.75	27.50	11.67	9.353
<b>E1</b>					
Sample #	cm	mm	Mean ( $\mu\text{m}$ )	Median ( $\mu\text{m}$ )	
1	0.00	0.00	7.523	4.663	
2	0.25	2.50	9.818	6.075	
3	0.50	5.00	12.30	9.136	
4	0.75	7.50	14.44	12.43	
5	1.00	10.00	16.25	15.04	
6	1.25	12.50	16.37	15.18	
7	1.50	15.00	15.34	13.94	
8	1.75	17.50	14.56	13.02	
9	2.00	20.00	14.04	12.52	
10	2.25	22.50	13.78	12.25	
11	2.50	25.00	13.65	11.93	
12	2.75	27.50	13.42	11.63	
13	3.00	30.00	13.16	11.32	
<b>E2</b>					
Sample #	cm	mm	Mean ( $\mu\text{m}$ )	Median ( $\mu\text{m}$ )	
	0.00	0.00	9.376	5.853	
	0.25	2.50	14.38	11.98	
	0.50	5.00	16.42	14.81	
	0.75	7.50	18.34	17.25	
	1.00	10.00	18.69	17.81	
	1.25	12.50	18.78	18.00	
	1.50	15.00	18.69	17.66	
	1.75	17.50	17.85	16.62	
	2.00	20.00	16.99	15.59	
	2.25	22.50	16.63	14.96	
	2.50	25.00	15.84	14.01	
	2.75	27.50	15.12	13.34	
	3.00	30.00	14.18	12.12	
	3.25	32.50	13.74	11.52	
	3.50	35.00	13.60	11.02	
	3.75	37.50	13.34	11.00	
<b>F1</b>					
Sample #	cm	mm	Mean ( $\mu\text{m}$ )	Median ( $\mu\text{m}$ )	
1	0.00	0.00	6.742	4.242	
2	0.25	2.50	9.942	7.206	
3	0.50	5.00	11.89	10.17	
4	0.75	7.50	11.97	10.46	
5	1.00	10.00	11.29	9.747	
<b>F2</b>					
Sample #	cm	mm	Mean ( $\mu\text{m}$ )	Median ( $\mu\text{m}$ )	
1	0.00	0.00	6.72	4.309	
2	0.25	2.50	7.068	4.188	
3	0.50	5.00	8.416	5.039	
4	0.75	7.50	11.99	9.234	
5	1.00	10.00	12.84	11.37	

6	1.25	12.50	12.66	11.11
7	1.50	15.00	11.82	10.04
<b>F3</b>				
Sample #	cm	mm	Mean ( $\mu\text{m}$ )	Median ( $\mu\text{m}$ )
1	0.00	0.00	7.963	4.279
2	0.25	2.50	8.652	4.72
3	0.50	5.00	8.11	5.026
4	0.75	7.50	9.613	5.927
5	1.00	10.00	13.95	9.495
6	1.25	12.50	13.8	11.01
7	1.50	15.00	13.28	11.53
8	1.75	17.50	12.47	10.44
9	2.00	20.00	12.53	10.11
10	2.25	22.50	12.79	11.11
<b>G1</b>				
Sample #	cm	mm	Mean ( $\mu\text{m}$ )	Median ( $\mu\text{m}$ )
1	0.00	0.0	5.911	3.369
2	0.25	2.5	7.508	4.224
3	0.50	5.0	9.143	6.164
<b>G2</b>				
Sample #	cm	mm	Mean ( $\mu\text{m}$ )	Median ( $\mu\text{m}$ )
1	0.00	0.00	6.150	3.638
2	0.25	2.50	6.599	3.718
3	0.50	5.00	5.346	3.135
4	0.75	7.50	7.898	4.575
5	1.00	10.00	11.690	7.531
6	1.25	12.50	10.820	7.240
7	1.50	15.00	9.119	6.171
8	1.75	17.50	8.031	5.849
<b>G3</b>				
Sample #	cm	mm	Mean ( $\mu\text{m}$ )	Median ( $\mu\text{m}$ )
1	0.00	0.00	6.022	3.586
2	0.25	2.50	6.112	3.544
3	0.50	5.00	6.206	3.609
4	0.75	7.50	7.082	3.869
5	1.00	10.00	7.403	3.991
6	1.25	12.50	9.451	5.491
7	1.50	15.00	13.55	8.915
8	1.75	17.50	14.30	10.22
9	2.00	20.00	11.80	8.894
10	2.25	22.50	10.76	7.219
11	2.50	25.00	9.037	5.895
<b>G4</b>				
Sample #	cm	mm	Mean ( $\mu\text{m}$ )	Median ( $\mu\text{m}$ )
1	0.00	0.00	5.877	3.514
2	0.25	2.50	5.832	3.485
3	0.50	5.00	6.515	3.729
4	0.75	7.50	7.890	4.233

5	1.00	10.00	8.555	4.731
6	1.25	12.50	13.92	8.487
7	1.50	15.00	14.30	8.893
8	1.75	17.50	12.45	7.702
9	2.00	20.00	10.57	6.432
10	2.25	22.50	8.846	5.477
<b>G5</b>				
Sample #	cm	mm	Mean (µm)	Median (µm)
1	0.00	0.0	5.494	3.526
2	0.25	2.5	5.796	3.629
3	0.50	5.0	5.690	3.230
4	0.75	7.5	6.477	3.576
5	1.00	10.0	7.115	3.990
6	1.25	12.5	6.670	3.705
7	1.50	15.0	6.341	3.334
8	1.75	17.5	6.854	3.770
9	2.00	20.0	7.381	4.255
10	2.25	22.5	8.977	5.049
11	2.50	25.0	13.580	6.482
12	2.75	27.5	12.780	6.924
13	3.00	30.0	15.470	10.210
14	3.25	32.5	17.950	13.290
15	3.50	35.0	16.000	11.540
16	3.75	37.5	13.460	9.265
17	4.00	40.0	12.160	7.617
18	4.25	42.5	12.760	7.287
19	4.50	45.0	9.111	5.767

## APPENDIX C: COMPILATION OF GRAIN SIZE WINTER 2004 – SUMMER 2008

To create a graph of the past four years of grain size data all of the values needed to be put together into one document. The 2007 – 2008 and the 2004 – 2005 raw datasets were available and thus entered into Microsoft Excel. No raw data was available for the other two years so the graphs from Cobin, 2008 and Roop, 2007 were scanned and imported into Sigma Scan. The data points were then calibrated using the program and exported to a Microsoft Excel document.

All of these data are from Mooring C. All traps were sampled from the bottom. The total accumulation assumes continuous grain size analysis, however there are unconformities between all datasets.

	<u>Total Accum cm</u>	<u>Trap cm</u>	<u>Trap mm</u>	<u>Mean microns</u>	<u>Sample #</u>
<b>Megan 2007 - 2008</b>	60.7	8.25	82.5	14.77	34
	60.4	8.00	80.0	14.30	33
	60.2	7.75	77.5	14.49	32
	59.9	7.50	75.0	14.71	31
	59.7	7.25	72.5	14.85	30
	59.4	7.00	70.0	14.75	29
	59.2	6.75	67.5	15.99	28
	58.9	6.50	65.0	16.68	27
	58.7	6.25	62.5	17.21	26
	58.4	6.00	60.0	17.32	25
	58.2	5.75	57.5	17.80	24
	57.9	5.50	55.0	17.29	23
	57.7	5.25	52.5	18.18	22
	57.4	5.00	50.0	19.64	21
	57.2	4.75	47.5	22.78	20
	56.9	4.50	45.0	24.93	19
	56.7	4.25	42.5	26.93	18
	56.4	4.00	40.0	26.82	17
	56.2	3.75	37.5	25.42	16
	55.9	3.50	35.0	21.58	15
55.7	3.25	32.5	13.10	14	
55.4	3.00	30.0	14.05	13	
55.2	2.75	27.5	16.93	12	
54.9	2.50	25.0	16.62	11	
54.7	2.25	22.5	13.62	10	
54.4	2.00	20.0	11.03	9	
54.2	1.75	17.5	10.21	8	
53.9	1.50	15.0	9.52	7	

	53.7	1.25	12.5	9.25	6
	53.4	1.00	10.0	8.91	5
	53.2	0.75	7.5	8.69	4
	52.9	0.50	5.0	7.59	3
	52.7	0.25	2.5	7.49	2
<b>Megan</b>	52.4	0.00	0.0	7.37	1
<b>Patty</b>	52.4	21.8	218	12.6	71
<b>2006 - 2007</b>	51.8	21.2	212	11.4	70
	51.1	20.5	205	9.9	69
	50.7	20.1	201	9.5	68
	50.3	19.7	197	7.6	67
	49.9	19.3	193	7.6	66
	49.5	18.9	189	8.2	65
	49.4	18.8	188	9.2	64
	49.2	18.6	186	12.1	63
	48.9	18.3	183	13.4	62
	48.7	18.1	181	15.0	61
	48.5	17.9	179	16.2	60
	48.4	17.8	178	17.9	59
	48.2	17.6	176	18.0	58
	47.8	17.2	172	17.6	57
	47.5	16.9	169	18.8	56
	47.2	16.6	166	23.2	55
	47.0	16.4	164	26.3	54
	46.7	16.1	161	25.9	53
	46.4	15.8	158	26.1	52
	45.9	15.3	153	24.2	51
	45.7	15.1	151	27.7	50
	45.4	14.8	148	29.9	49
	45.0	14.4	144	32.7	48
	44.6	14.0	140	32.8	47
	44.2	13.6	136	32.6	46
	43.9	13.3	133	31.7	45
	43.4	12.8	128	32.1	44
	43.0	12.4	124	32.0	43
	42.8	12.2	122	29.2	42
	42.4	11.8	118	24.1	41
	42.2	11.6	116	21.7	40
	41.8	11.2	112	21.7	39
	41.5	10.9	109	20.0	38
	41.2	10.6	106	20.2	37

	41.1	10.5	105	21.6	36
	40.8	10.2	102	20.5	35
	40.5	9.9	99	19.4	34
	39.9	9.3	93	20.6	33
	39.8	9.2	92	21.6	32
	39.4	8.8	88	22.7	31
	39.1	8.5	85	22.9	30
	38.8	8.2	82	22.1	29
	38.6	8.0	80	19.2	28
	38.0	7.4	74	17.9	27
	37.8	7.2	72	19.1	26
	37.5	6.9	69	20.3	25
	37.3	6.7	67	22.6	24
	37.0	6.4	64	24.2	23
	36.6	6.0	60	24.3	22
	36.2	5.6	56	24.4	21
	36.0	5.4	54	24.5	20
	35.7	5.1	51	23.9	19
	35.3	4.7	47	24.0	18
	34.9	4.3	43	22.5	17
	34.5	3.9	39	19.4	16
	34.1	3.5	35	17.3	15
	33.8	3.2	32	16.4	14
	33.5	2.9	29	14.4	13
	33.4	2.8	28	11.9	12
	33.1	2.5	25	8.9	11
	32.8	2.2	22	8.5	10
	32.7	2.1	21	6.7	9
	32.5	1.9	19	5.6	8
	32.2	1.6	16	5.8	7
	32.0	1.4	14	6.2	6
	31.7	1.1	11	6.3	5
	31.4	0.8	8	6.1	4
	31.2	0.6	6	5.7	3
	31.0	0.4	4	5.5	2
<b>Patty</b>	30.8	0.20	2.0	5.14	1
<b>Heidi</b>	30.6	15.6	156	11.4	27
<b>2005 - 2006</b>	30.1	15.1	151	11.5	26
	29.8	14.8	148	11.1	25
	29.3	14.3	143	9.5	24
	28.9	13.9	139	8.8	23

	28.8	13.8	138	8.9	22
	27.9	12.9	129	9.3	21
	27.8	12.8	128	9.3	20
	26.9	11.9	119	10.4	19
	26.8	11.8	118	12.5	18
	25.9	10.9	109	12.9	17
	25.8	10.8	108	13.5	16
	25.3	10.3	103	13.0	15
	24.9	9.9	99	18.0	14
	24.4	9.4	94	36.4	13
	23.1	8.1	81	35.1	12
	22.0	7.0	70	38.4	11
	21.2	6.2	62	34.0	10
	20.2	5.2	52	37.8	9
	19.7	4.7	47	15.4	8
	19.2	4.2	42	15.3	7
	18.1	3.1	31	8.4	6
	17.1	2.1	21	6.9	5
	16.3	1.3	13	5.9	4
	15.8	0.8	8	5.9	3
	15.4	0.4	4	5.9	2
<b>Heidi</b>	15.0	0.00	0.0	10.25	1
<b>Brooks</b>	15.0	15.0	150	9.7	31
<b>2004 - 2005</b>	14.5	14.5	145	14.0	30
	14.0	14.0	140	14.7	29
	13.5	13.5	135	12.5	28
	13.0	13.0	130	10.2	27
	12.5	12.5	125	12.8	26
	12.0	12.0	120	16.5	25
	11.5	11.5	115	12.7	24
	11.0	11.0	110	11.4	23
	10.5	10.5	105	13.2	22
	10.0	10.0	100	17.8	21
	9.5	9.5	95	18.4	20
	9.0	9.0	90	17.4	19
	8.5	8.5	85	12.2	18
	8.0	8.0	80	14.6	17
	7.5	7.5	75	16.4	16
	7.0	7.0	70	16.7	15
	6.5	6.5	65	21.4	14
	6.0	6.0	60	22.9	13

**Brooks**

5.5	5.5	55	22.6	12
5.0	5.0	50	15.8	11
4.5	4.5	45	8.9	10
4.0	4.0	40	8.1	9
3.5	3.5	35	7.9	8
3.0	3.0	30	7.8	7
2.5	2.5	25	8.0	6
2.0	2.0	20	8.1	5
1.5	1.5	15	8.0	4
1.0	1.0	10	8.1	3
0.5	0.5	5	8.2	2
0.0	0.0	0	11.7	1